PB84-172469

Instrumentation, Recording, and Processing of Meteorological Data Near Portage, Wisconsin Wisconsin Power Plant Impact Study

Wisconsin Univ.-Madison

Prepared for

Environmental Research Lab.-Duluth, MN

Mar 84

U.S. Department of Commerce
National Technical Information Service
NTIS

EPA-600/3-84-053
March 1984

PB84-172469

INSTRUMENTATION, RECORDING, AND PROCESSING OF METEOROLOGICAL DATA NEAR PORTAGE, WISCONSIN

Wisconsin Power Plant Impact Study

by

Charles R. Stearns
Phillip Falconer
George Weidner
Brent Bowen
Leonard Dzamba

Water Resources Center
Institute for Environmental Studies
University of Wisconsin

Grant No. R803971

Project Officer
Gary E. Glass
Environmental Research Laboratory-Duluth
Duluth, Minnesota

This study was conducted in cooperation with
Wisconsin Power and Light Company,
Madison Gas and Electric Company,
Wisconsin Public Service Corporation,
Wisconsin Public Service Commission,
and Wisconsin Department of Natural Resources

ENVIRONMENTAL RESEARCH LABORATORY
OFFICE OF RESEARCH AND DEVELOPMENT
U.S. ENVIRONMENTAL PROTECTION AGENCY
DULUTH, MINNESOTA 55804

REPRODUCED BY
NATIONAL TECHNICAL
INFORMATION SERVICE
U.S. DEPARTMENT OF COMMERCE
SPRINGFIELD, VA. 22161

TECHNICAL REPORT DATA

(Please read Instructions on the reverse before completing)

1. REPORT NO. EPA-600/3-84-053	2.	3. RECIPIENT'S ACCESSION NO. PB84 172469
4. TITLE AND SUBTITLE Instrumentation, Recording and Processing of Meteorological Data near Portage, Wisconsin: Wisconsin Power Plant Impact Study		5. REPORT DATE March 1984 6. PERFORMING ORGANIZATION CODE
7. AUTHOR(S) Charles R. Stearns, P. Falconer, G. Weidner, B. Bowen, and L. Dzamba		8. PERFORMING ORGANIZATION REPORT NO.
9. PERFORMING ORGANIZATION NAME AND ADDRESS Department of Meteorology University of Wisconsin Madison, WI 53706		10. PROGRAM ELEMENT NO. 11. CONTRACT/GRANT NO. R803971
12. SPONSORING AGENCY NAME AND ADDRESS Environmental Research Laboratory 6201 Congdon Blvd. U.S. Environmental Protection Agency Duluth, MN 55804		13. TYPE OF REPORT AND PERIOD COVERED EPA-ORD 14. SPONSORING AGENCY CODE EPA/600/03
15. SUPPLEMENTARY NOTES		

16. ABSTRACT

As part of the Columbia Power Plant Impact Study meteorological data were collected at a network of monitoring sites from 1972 through 1977. The data were the basis for a series of studies whose purpose was to elucidate the transport of airborne pollutants and to assess the climatic impact of the power plant. In a pilot diffusion climatology survey, local wind structure was interpreted in the context of synoptic weather patterns. A significant new low wind statistic was introduced. A case study traced the movement of an elevated level of ozone from the Southern Plains across the Midwest to the East Coast. It showed that long distance transport is necessary for elevated O_3 levels to occur in most parts of the U.S. The horizontal variation of the wind field is an important factor in the transport of atmospheric pollutants from 10 to 100 km. The wind field was shown to be organized as a function of wind direction and wind speed around the Baraboo Hills. Two models for estimating concentrations of SO_2 at ground level were compared. Both used the Gaussian plume equation: one estimated the required dispersion coefficients from the Hino stability model; the other was based on data for horizontal and vertical hourly wind direction range. Overall, the climatic effects of the power plant and cooling pond appear small. Fogging, condensation, and riming may occur downwind on several days each year. Temperature increases of about 1°C may also be observed for a short distance downwind.

17. KEY WORDS AND DOCUMENT ANALYSIS

a. DESCRIPTORS	b. IDENTIFIERS/OPEN ENDED TERMS	c. COSATI Field/Group

18. DISTRIBUTION STATEMENT	19. SECURITY CLASS *(This Report)* Unclassified	21. NO. OF PAGES 160
	20. SECURITY CLASS *(This page)* Unclassified	22. PRICE

EPA Form 2220-1 (Rev. 4-77) PREVIOUS EDITION IS OBSOLETE

NOTICE

This document has been reviewed in accordance with U.S. Environmental Protection Agency policy and approved for publication. Mention of trade names or commercial products does not constitute endorsement or recommendation for use.

FOREWORD

The U.S. Environmental Protection Agency (EPA) was established to coordinate our country's efforts toward improving an defending the quality of the environment. These efforts depend greatly on reserach to monitor environmental change and to determine health standards.

One project the EPA is supporting through its Environmental Research Laboratory in Duluth, Minnesota, is the study "The Impacts of Coal-Fired Power Plants on the Environment." The Columbia Generating Station, a coal-fired power plant near Portage, Wisconsin, has been the focus of all field observations. This interdisciplinary study is conducted by the Environmental Monitoring and Data Acquisition Group of the Institute for Environmental Studies at the University of Wisconsin-Madison and involved investigators from many departments at the same university. Several utilities and state agencies also are cooperating in the study: Wisconsin Power and Light Company, Madison Gas and Electric Company, Wisconsin Public Service Corporation, Wisconsin Public Service Commission, and Wisconsin Public Service Corporation, Wisconsin Public Service Commission, and Wisconsin Department of Natural Resources.

As part of the Columbia Power Plant Impact Study, meteorological data were collected at a network of monitoring sites from 1972 through 1977. The data were the basis for a series of studies whose purpose was to elucidate the transport of airborne pollutants and to assess the climatic impact of the power plant. The Air Pollution Group, using the collected meteorological data, was responsible for assessing the transport of airborne pollutants.

Norbert A. Jaworski
Director
Environmental Research Laboratory
Duluth, Minnesota

ABSTRACT

As part of the Columbia Power Plant Impact Study meteorological data were collected at a network of monitoring sites from 1972 through 1977. The data were the basis for a series of studies whose purpose was to elucidate the transport of airborne pollutants and to assess the climatic impact of the power plant. The Air Pollution Group, using the collected meteorological data, was responsible for assessing the transport of airborne pollutants.

In a pilot diffusion climatology survey, local wind structure was interpreted in the context of synoptic weather patterns. A significant new low wind statistic was introduced: the number of crossing of the trace of a variable past its running mean during a given time interval. The low wind statistics are for wind speeds less than 4 m/sec when the speed and direction records indicate statistical non-uniformity or intermittent events in the atmosphere. The usual statistics, such as a mean value or a standard deviation, do not properly describe the record.

A case study traced the movement of an elevated level of ozone from the Southern Plains across the Midwest to the East Coast. It showed that, although the relative contributions of transport vs. local or regional formation to an episode of elevated O_3 are not clear, some degree of large scale, long distance transport is necessary in order for elevated O_3 levels to occur in most parts of the United States. A related study showed that ambient O_3 levels are reduced sharply in the presence of the plume from a coal-fired power plant.

The horizontal variation of the wind field is an important factor in the transport of atmospheric pollutants in the range of 10 to 100 km. The wind field in the study area was shown to be organized as a function of both wind direction and wind speed around the Baraboo Hills. These hills therefore have an influence on the dispersion of pollutants from the Columbia power plant due to the systematic variation in divergence and thus the vertical motion of the air.

Two models for estimating concentrations of SO_2 at ground level were compared. Both used the Gaussian plume equation, but one estimated the required dispersion coefficients from the Hino stability model, while the other was based on data for horizontal and vertical hourly wind direction range. The wind direction range model was shown to have simpler data requirements and to give results which agreed more closely with observed SO_2 values. The standard deviation of the vertical and horizontal wind direction is assumed to be the range of direction divided by 4, and when multiplied by the downwind distance yields the y and z dispersion coefficients.

Overall, the climatic effects of the power plant and cooling pond appear small. Fogging, condensation, and riming may occur downwind on several days each year. Temperature increases of about 1°C may also be observed for a short distance downwind.

CONTENTS

Foreword........ iii
Abstract........ iv
Figures........ vii
Tables........ x
Acknowledgments........ xii

1. Introduction........ 1
2. Conclusions and Recommendations........ 3
3. Meteorological Instrumentation, Recording, and Data Processing........ 5
    Introduction........ 5
    Atmospheric Diffusion Theory........ 6
    Basic Meteorology Systems and Recording........ 12
    Sites and Recording........ 17
    Data Processing........ 20
4. A Pilot Diffusion Climatology Survey for the Columbia Generating Station........ 25
    Previous Studies........ 25
    Data Processing........ 27
    Data Analysis........ 28
    Conclusions and Recommendations........ 42
5. Study of the Large-Scale Transport of Low-Level Ozone across the Central and Eastern United States........ 57
    Introduction........ 57
    Chemistry of Ozone........ 58
    Factors Affecting Local Ozone Levels........ 64
    Large-Scale Transport of Ozone........ 65
    Natural Sources of Ozone........ 67
    Data and Methodology........ 68
    Case Study........ 71
    Summary and Conclusions........ 87
6. Depletion of Ambient Ozone........ 88
    Introduction........ 88
    Siting........ 89
    Procedures........ 91
    Results and Discussion........ 91
    Summary and Conclusions........ 92
7. Topographic Influence on Surface Winds........ 97
    Introduction........ 97
    Intrumentation and Data Reduction........ 97
    Calculations of Divergence and Vorticity........ 100
    Comparative Analysis........ 103
    Conclusions........ 111

8. A Comparison between the Hino and Wind Direction Range Methods for Estimating Ground Level Sulfur Dioxide Concentrations from an Elevated Source........................ 112
    - Introduction.. 112
    - The Gaussian Model...................................... 112
    - Dispersion Coefficients................................. 113
    - Sites and Instruments................................... 116
    - Results... 119
    - Summary... 125

9. Possible Influence of the Cooling Pond on the Local Environment.. 126
    - Introduction.. 126
    - Latent and Sensible Heat Fluxes......................... 126
    - Heat Budget... 128
    - Influence on the Local Environment...................... 130

10. Intra- and Inter-Site Correlation of Wind Data................. 133

References.. 140

FIGURES

Number Page

1 Meteorological observation sites 7

2 Wind passage as a function of longitudinal eddy length 30

3 Wind passage as a function of lateral eddy length 31

4 Wind passage as a function of vertical eddy length (ξ_θ) 33

5 Wind passage as a function of vertical eddy length (ξ_w) 34

6 Frequency of occurrences of longitudinal eddy length classified according to gustiness types 36

7 Frequency of occurrences of lateral eddy length classified according to gustiness types 37

8 Frequency of occurrences of longitudinal eddy length classified according to gustiness types 39

9 Frequency of occurrences of vertical eddy length classified according to gustiness types 40

10 Dynamic response curve 41

11 Relationship of the observed mean length scale to the real gust wavelength 41

12 Surface pressure map for 1200Z, 19 October 1972 43

13 Surface pressure map for 1200Z, 27 October 1972 44

14 Surface pressure map for 1200Z, 30 October 1972 45

15 Surface pressure map for 1200Z, 31 October 1972 46

16 Surface pressure map for 1200Z, 1 November 1972 47

17 Surface pressure map for 1200Z, 9 September 1972 48

18 Surface pressure map for 1200Z, 7 October 1972 49

19 Surface pressure map for 1200Z, 9 October 1972................ 50

20 Surface pressure map for 1200Z, 19 August 1972................ 51

21 Surface pressure map for 1200Z, 24 August 1972................ 52

22 Surface pressure map for 1200Z, 25 August 1972................ 53

23 Surface pressure map for 1200Z, 29 August 1972................ 54

24 Hourly variation of selected pollutants....................... 62

25 Flow chart of O_3 photochemical cycle........................ 63

26 Distribution of O_3 monitors that supplied data for the case study... 69

27 1800Z surface analysis, 4 September 1976...................... 72

28 Ozone maximum isopleths and backward trajectories, 4 September 1976.. 72

29 1800Z surface analysis, 5 September 1976...................... 73

30 Ozone maximum isopleths and backward trajectories, 5 September 1976.. 73

31 1800Z surface analysis, 6 September 1976...................... 75

32 Ozone maximum isopleths and backward trajectories, 6 September 1976.. 75

33 1800Z surface analysis, 7 September 1976...................... 76

34 Ozone maximum isopleths and backward trajectories, 7 September 1976.. 78

35 1800Z surface analysis, 8 September 1976...................... 80

36 Ozone maximum isopleths and backward trajectories, 8 September 1976.. 80

37 1800Z surface analysis, 9 September 1976...................... 82

38 Ozone maximum isopleths and backward trajectories, 9 September 1976.. 82

39 1800Z surface analysis, 10 September 1976..................... 83

40 Ozone maximum isopleths and backward trajectories, 10 September 1976... 83

41 Graph of hourly ozone concentrations at six selected sites from 5 to 10 September 1976.......................... 85

42 Map showing locations of six selected sites.................. 86

43 Monitoring sites for meteorological data..................... 90

44 Hourly averaged concentrations of ambient O_3 and concentrations of O_3 and NO_2.................................. 93

45 Scattergram of instantaneous $[O_3]_{dep}$ versus $[SO_2]$............ 94

46 Scattergram of instantaneous $[NO_x]$ versus $[SO_2]$.............. 94

47 Scattergram of instantaneous $[NO]$ versus $[NO_x]$............... 95

48 Scattergram of instantaneous $[O_3]_{dep}$ versus $[NO_2]$............ 95

49 The dimensions of the triangle formed by the meteorological network near Portage, Wisconsin.............................. 102

50 Wind direction differences at three sites with respect to wind direction at the Wyocena site........................... 105

51 Wind speed differences for each site from the Wyocena wind speed as a function of Wyocena wind direction................ 105

52 Mean vorticity determined from the Wyocena-Dekorra-Cemetery sites as a function of the Wyocena wind direction............ 107

53 Mean divergence determined from the Wyocena-Dekorra-Cemetery sites as a function of the Wyocena wind direction............ 107

54 Vorticity as a function of the Wyocena wind speed and direction... 110

55 Divergence as a function of the Wyocena wind speed and direction... 110

56 The SO_2 ground-level concentrations obtained by using two different dispersing characteristic methods in the Gaussian Plume equation.................................... 120

57 Average annual wind speed as a function of time of day for Messer site and Truax Field for 1976......................... 138

TABLES

Number		Page
1	METEOROLOGICAL OBSERVATION AT THE MESSER SITE................	18
2	METEOROLOGICAL OBSERVATIONS AT THE CEMETERY, WYOCENA, AND DEKORRA SITES AND OTHER PROCESSED DATA.......................	21
3	DESCRIPTION OF GUSTINESS TYPES..............................	32
4	SUMMARY OF OCCURRENCES OF GUSTINESS TYPES DURING THE FALL OBSERVATION PERIOD..	35
5	MICROFORECAST CHART...	55
6	SUMMARY OF PERIODS STUDIED WHEN PLANT PLUME DEPLETED OZONE LEVELS AT PRIMARY MONITORING SITE..........................	91
7	PARAMETERS AND INSTRUMENTATION USED IN THE METEOROLOGICAL NETWORK..	98
8	LIST OF THE DATA SETS USED..................................	99
9	NUMBER OF DATA VALUES USED TO COMPUTE THE SECTOR MEANS.......	103
10	NUMBER OF 30-MIN MEAN VALUES USED IN COMPUTING CONTOUR VALUES FOR DIVERGENCE AND VORTICITY.........................	108
11	DISTANCES AND DIRECTIONS OF SO_2 MONITORING SITES FROM THE COLUMBIA GENERATING STATION................................	116
12	VARIABILITY OF σ_y and σ_z..	121
13	A TIME SERIES REPRESENTING SOME OF THE "ERRATIC" BEHAVIOR OBSERVED AT DEKORRA..	123
14	OVERALL STANDARD DEVIATIONS USING RANGE AND STABILITY METHODS...	124
15	MONTHLY AVERAGE HEAT BUDGET FOR THE COLUMBIA GENERATING STATION COOLING POND..	128
16	MONTHLY AVERAGE WATER BUDGET FOR THE COLUMBIA GENERATING STATION COOLING POND..	130

17 DAILY AVERAGES OF TEMPERATURE AND VAPOR PRESSURE ON DAYS WITH A HIGH LIKELIHOOD OF RIME FORMING DOWNWIND OF THE COOLING POND.......... 131

18 MONTHLY MEAN WIND SPEEDS AND CORRELATION BETWEEN MESSER-MESSER, MESSER-TRUAX, AND WYOCENA-TRUAX FOR 1976 AND 1977.......... 134

19 MONTHLY MEAN WIND DIRECTIONS AND CORRELATIONS BETWEEN MESSER-MESSER, MESSER-TRUAX, AND WYOCENA-TRUAX FOR 1976 AND 1977.......... 136

20 MONTHLY MEAN WIND SPEEDS AND DIRECTION CORRELATIONS BETWEEN THE MESSER SITE AND TRUAX FIELD AS A FUNCTION OF TIME OF DAY.......... 137

ACKNOWLEDGMENTS

Monitoring data and emissions were supplied by the Wisconsin Power and Light Co. The Department of Meteorology, University of Wisconsin-Madison provided most of the meteorological equipment.

Mr. Russell Johnson maintained the field installations. Susan Fiel and Steffi Law processed the data.

SECTION 1

INTRODUCTION

The meteorological sub-project objectives were:

(1) To measure the atmospheric characteristics necessary to evaluate the mass budget of chemicals transported through the atmosphere from the Columbia Generation station;
(2) To study the meso-scale airflow in the vicinity of the station;
(3) To determine possible local climatic effects of the station;
(4) To determine the influence of the cooling pond on local climate.

The meteorology sub-project began in the fall of 1972 with one site and primarily dealt with objectives 1 and 3. The operation and history of the sites is presented in Section 3, entitled "Meterorological Instrumentation, Recording and Data Processing." Included is an explanation of the measurements required for objective 1 above.

Section 4, entitled "A Pilot Diffusion Climatology Survey for the Columbia Generating Station," represents the first use of the meteorological data. Three-dimensional wind data were analyzed for wind speeds <4 m/sec to assess the length scales of the three dimensional eddies. Light wind conditions are difficult to handle in diffusion models and may result in high ground level concentrations of a scalar property from an elevated source. The synoptic conditions during which the potential for high values of ground level concentrations existed were categorized for the fall of 1972. Measurements of ground level concentrations from the station were not available at that time because the station had not begun operating. No further work was done in this area.

Material transported from other areas by the atmosphere might influence the values observed locally and possible mask the influences of the station. Section 5, entitled "Study of the Large-Scale Transport of Low Level Ozone across the Central and Eastern United States," illustrates the elevated ozone (O_3) levels which are caused by O_3 transported to the area; i.e., not generated locally. Other material is also transported by the atmosphere but O_3 serves as a good tracer because of its relatively long lifetime and an adequate number of monitoring sites.

Section 6, entitled "On the Depletion of Ambient Ozone by the Columbia Generating Station," shows that the ground level O_3 is depleted by sulfur and nitrogen oxides in the station plume.

The location of the meteorology sites in the Portage, Wisconsin area provided an opportunity to study the possible influences of the Baraboo Hills on air flow. Section 7, entitled "Topographic Influence on Surface Winds," indicate a systematic influence on the vorticity and divergence of the air flow with respect to wind direction. The divergence can result in vertical motion of the air and may influence the ground level concentration as discussed in Section 3.

The usual procedure in dispersion modeling is to use commonly measured meteorological parameters to infer the atmospheric dispersion coefficients which are not usually measured directly. Section 8, entitled "A Comparison between the Mikio-Hino and Wind Direction Range Stability Methods for Estimating Sulfur Dioxide Concentrations from an Elevated Source," compares two methods for estimating the dispersion coefficients.

Section 9 is entitled "Possible Influence of the Cooling Pond on the Local Environment" and estimates the latent and sensible heat flux from the cooling pond. The results are compared with the overall heat budget and water budget for the pond for a 1 yr period, using monthly mean values. The cooling pond's influence on the local environment was negligible.

Data from the U.S. Weather Service Station at Truax Field, Madison, Wisconsin was used for the initial environmental impact statement for the station construction. Section 10, entitled "Intra- and Inter-Site Correlation of Wind Data," presents monthly correlations between the two sites as a function of time of day.

SECTION 2

CONCLUSIONS AND RECOMMENDATIONS

The measurement instrumentation at the four meteorological sites was adequate to determine the dispersion characteristics for the atmosphere and the possible vertical motion in the area. More than 90% of the possible data was collected in 1976-77 when duplicate wind speed and direction instruments were used at each site.

Transistorized circuits were damaged by lightning and the associated electrical fields. This type of failure did not occur with vacuum tube equipment. Extensive steps should be taken to protect transistor circuits against stray electrical fields when connected to long sensor wires.

The conversion of the strip chart recordings to digital data for computer processing required more effort than initially expected. Considerable amounts of data were collected but never processed. The ideal system would have had a computer at each site processing the data and delivering it by telephone to a central location. Such systems are possible and available, but expensive. In addition, lightning and its associated strong electrical fields coupled with long wires would have damaged the computer system. Computer data collection systems, even when operating in the best of circumstances, do not operate 100% of the time for 2 yr. Any computer-based data collecting system must be backed up by systems such as strip charts in the event that a breakdown occurs.

Sections 4 and 8 are related to atmospheric dispersion and each makes use of the measured horizontal and vertical components of the wind. Section 7 estimates the horizontal divergence and the possible vertical motion in the lower atmosphere. Section 3 relates the subjects of Section 4, 7, and 8 to the concentration of a scalar property in the atmosphere. Section 8 showed that the differences between the calculated and observed ground level concentration would be significantly reduced if the measured wind characteristics had been used in the diffusion equation instead of a stability-related guess.

The questions related to atmospheric dispersion that should be looked at in the future are:

(1) Those cases where the ground level concentration was not adequately predicted using actual dispersion characteristics of the atmosphere;
(2) The role of mean vertical motion changing the height of the plume centerline with time;

(3) Possible meanders of the plume center line under inversion conditions;

(4) The dispersion process should have been looked at as a 1-hr collection of streak lines rather than diffusion.

Sections 5 and 6 deal with ozone but can also be applied to other scalar properties, such as SO_2, SO_4, and NO_x which are currently related to the problem of acid rain. The advection of material into an area from source regions remote from the site must be considered along with sources at the site and the possible interactions between scalar properties in the atmosphere.

The cooling pond did not noticeably affect the local environment when dissipating waste heat from one 527-mW unit.

The Truax Field wind speed and direction data can be highly correlated with similar observing sites at the same height above the surface. The correlation in the vertical during surface heating is fairly good, but the correlation is very low for surface cooling. Using Truax Field data to estimate the available wind energy at a height of 32 m on a 120-m hill will grossly underestimate the available wind energy.

SECTION 3

METEOROLOGICAL INSTRUMENTATION, RECORDING, AND DATA PROCESSING

INTRODUCTION

The study of environmental change related to the Columbia Generating Station was started in 1971 with a grant from the Wisconsin Power and Light Company (WPL) and was augmented by a U.S. Environmental Protection Agency (EPA) grant in July 1975.

The initial purpose of the meteorological investigation was to determine possible climatic changes associated with the station and to establish relationships between observed meteorological parameters and ground level concentrations of material from the smoke stack.

Possible climatic effects include an increase in precipitation due to introduction of condensation nuclei and water vapor into the atmosphere from the stack and modification of the local heat budget due to the station and the cooling pond. Seven years was insuficient time to determine possible climatic influences on local biota. Many of the biotic changes that have occured are due to disruption caused by station construction, thus climatic changes cannot be isolated.

Atmospheric dispersion was easily handled so the bulk of the data recording and processing was directed towards the need for determining atmospheric dispersion from an elevated point source. Dispersion of point source material is a factor in the transport and deposition of trace elements.

The site selection criteria required that at least one site be relatively free of influence by the station and that the meteorological data necessary for atmospheric dispersion measurements be valid between stack height and the plume rise. The Madison, Wisconsin wind rose shows that easterly winds are relatively infrequent and a site directly west of the station would be influenced the least by the presence of the station. The dispersion characteristics of the atmosphere between the stack top and the plume rise had to be known so atmospheric measurements needed to be made between 152 and 304 m (500 and 1000 ft) above the generating site as planned since height of the stack was 152 m (500 ft). A 152 to 304-m (100- to 1000-ft) tower on the generating site was out of the question at the time, due to station construction activity. Possible sites included a nearby AM radio antenna at a height of 137 m (450 ft) above the station site, and the Messer farm on the Baraboo Bluffs elevated about 122 m (400 ft) above the station site. The radio tower was not selected because it was AM and instruments would have been difficult to mount on the tower because the tower was isolated from the ground.

The Messer Site on the Baraboo Bluff was selected for two reasons. It provided a site relatively free of influence from the station and its 122-m (400-ft) elevation required only a 30-m (100-ft) tower to place the instruments at the same height as the stack top. The location of all sites at which meteorological measurements were made are shown in Figure 1. Cemetery, Wyocena, and Dekorra sites were available and located near roads and electrical power. Wisconsin Power and Light Company eventually equipped all sites with air monitoring equipment.

The measurements necessary for determining the climatic impact of the generating station and atmospheric dispersion are different in kind and time. Decades may be required to detect the climatic impact on plant and animal communities. The actual measurements made to support the climatic data were rainfall at each site and soil temperature at the Messer and Dekorra sites. The measurements were inadequate, but were undertaken to detect systematic differences with time between the Messer and Dekorra sites. It was hoped that these measurements could be related to the influence of the station.

The measurements needed to determine atmospheric dispersion have only a slight time displacement related to the time of travel from the stack to the sensing equipment and are relatively easy to make. The type of measurements needed can be obtained from diffusion theory.

ATMOSPHERIC DIFFUSION THEORY

Atmospheric diffusion theory starts with the equation of continuity for the density of a scalar property written as:

$$R = \frac{\partial c}{\partial t} + \frac{\partial (uc)}{\partial x} + \frac{\partial (vc)}{\partial y} + \frac{\partial (wc)}{\partial z} \qquad (1)$$

where

c is density of the scalar property

t is time

x is horizontal axis usually in the direction of the mean flow

u is speed in the x direction

y is horizontal axis perpendicular to the x axis

v is speed in the y direction

z is axis perpendicular to the xy plane

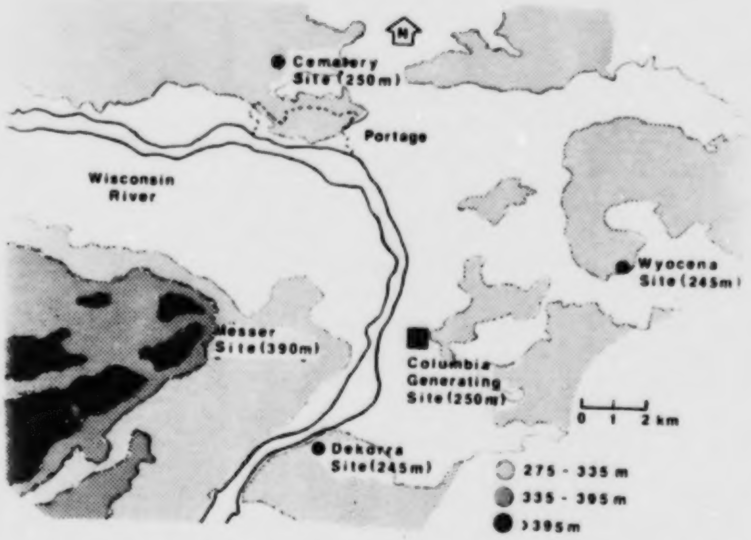
N
Cemetery Site (250m)
Portage
Wisconsin River
Wyocena Site (245m)
Messer Site (390m)
Columbia Generating Site (250m)
0 1 2 km
Dekorra Site (245m)
275 - 335 m
335 - 395 m
>395m

Figure 1. Meteorological observation sites in the vicinity of the Columbia Generating Station. The numbers in parentheses at each site are the elevations of the station above sea level.

w is speed in the z direction

R is the net addition of the scalar property per unit volume with time

$\frac{\partial c}{\partial t}$ is local change of the scalar property with time.

The terms c, u, v, and w are separated in means and fluctuations as:

$$\begin{aligned} c &= \overline{c} + c' \\ u &= \overline{u} + u' \\ v &= \overline{v} + v' \\ w &= \overline{w} + w' \end{aligned} \tag{2}$$

where the overbar refers to a time average and the prime is a fluctuation from the mean. The period of the time average is not arbitrary and should include 10 to 20 values that represent the range of the fluctuations and should also not change greatly from one averaging period to the next.

Substitution of Eq. (2) into Eq. (1) and assuming R = 0 when remote from the source of c:

$$\begin{aligned} -\frac{\partial \overline{c}}{\partial t} = \frac{\partial}{\partial x} (\overline{uc} + uc' + u'\overline{c} + u'c') + \frac{\partial}{\partial y} (\overline{vc} + \overline{v}\ c' + v'\overline{c} + v'c') \\ + \frac{\partial}{\partial z} (\overline{wc} + w'\overline{c} + \overline{w}c' + w'c') \end{aligned} \tag{3}$$

averaging over the same time period as in Eq. (2) results in u', v', w', and c' being zero.

Thus, Eq. (3) becomes:

$$\begin{aligned} -\frac{\partial \overline{c}}{\partial t} = \frac{\partial}{\partial x} (\overline{uc}) + \frac{\partial}{\partial y} (\overline{vc}) + \frac{\partial}{\partial z} (\overline{wc}) + \frac{\partial}{\partial x}\ \overline{(u'c)} \\ + \frac{\partial}{\partial z} (v'c') + \frac{\partial}{\partial z} (\overline{w'c'}). \end{aligned} \tag{4}$$

Then

$$\begin{aligned} \frac{\partial}{\partial x} (\overline{uc}) + \frac{\partial}{\partial y} (\overline{vc}) + \frac{\partial}{\partial z} (\overline{wc}) = \overline{c}\ (\frac{\partial u}{\partial x} + \frac{\partial \overline{v}}{\partial y} + \frac{\partial \overline{w}}{\partial x}) \\ + \overline{u}\ \frac{\partial \overline{c}}{\partial x} + v\ \frac{\partial \overline{c}}{\partial y} + w\ \frac{\partial \overline{c}}{\partial z}\ . \end{aligned} \tag{5}$$

The velocity divergence term is:

$$\frac{\partial \bar{u}}{\partial x} + \frac{\partial \bar{v}}{\partial y} + \frac{\partial \bar{w}}{\partial z} = 0 \qquad (6)$$

for incompressible flow, although the individual terms are not zero and can result in finite values of u, v, and w over the averaging time.

Equation (4) becomes:

$$\frac{\partial \bar{c}}{\partial t} = \bar{u}\,\frac{\partial \bar{c}}{\partial x} + \bar{v}\,\frac{\partial \bar{c}}{\partial y} + \bar{w}\,\frac{\partial \bar{c}}{\partial z} + \frac{\partial(\overline{u'c'})}{\partial x} + \frac{\partial(\overline{v'c'})}{\partial y} + \frac{\partial(\overline{w'c'})}{\partial z} \, . \qquad (7)$$

With the substitution of Eqs. (6) and (7) and the assumption that

$\bar{v} = 0, \ \bar{w} = 0, \ \dfrac{\partial \overline{u'c'}}{\partial x} = 0,$

and that

$$\frac{\partial(\overline{v'c'})}{\partial y} = - \frac{\partial}{\partial y}\left(K_y \frac{\partial \bar{c}}{\partial y}\right) \qquad (8)$$

$$\frac{\partial(\overline{w'c'})}{\partial z} = - \frac{\partial}{\partial z}\left(K_z \frac{\partial \bar{c}}{\partial z}\right) \qquad (9)$$

where K_y and K_z are the eddy diffusivities for the scalar property c in the y and z directions, respectively.

Slade (1968) and Pasquill (1962) discuss obtaining the diffusion equation of continuity in the form:

$$\frac{\partial \bar{c}}{\partial t} = \bar{u}\,\frac{\partial \bar{c}}{\partial x} - \frac{\partial}{\partial y}\left(K_y \frac{\partial \bar{c}}{\partial y}\right) - \frac{\partial}{\partial z}\left(K_z \frac{\partial \bar{c}}{\partial z}\right) \, . \qquad (10)$$

Equation (6) can be written as:

$$\frac{\partial \bar{u}}{\partial x} + \frac{\partial \bar{v}}{\partial y} = \mathrm{div}_H = - \frac{\partial \bar{w}}{\partial z} \qquad (11)$$

where div_H is the horizontal divergence. Then the mean vertical velocity at height z is:

$$\overline{w} = -\int_{0}^{z} \text{div}_{H} dz = -z \cdot \text{div}_{H}, \qquad (12)$$

assuming the divergence is constant with height. The divergence can be caused by local terrain effects and--if sufficiently large and operating for a long enough time--can significantly change the height of the plume center line. Typical short-term values of $\overline{w}$ at a height of 200 m are 0.02 to 0.2 m/sec for div_H of 10^{-4} to 10^{-3}/sec. If the div_H is primarily in the x direction then $\partial\overline{u}/\partial\overline{x} = -\partial\overline{w}/\partial z$, and if in the y direction, $\partial\overline{v}/\partial y = -\partial\overline{w}/\partial z$. In the second case $\overline{v}$ is changing away from the plume center line and can cause the plume to spread out horizontally and sink or come together horizontally and rise. This can then cause a significant change in the ground level concentration of the scalar property $\overline{c}$.

Assuming that $\frac{\partial\overline{c}}{\partial t} = 0$ away from the source, $\frac{\partial K_y}{\partial y} = 0$, and $\frac{\partial K_z}{\partial z} = 0$, Eq. (10) becomes:

$$\overline{u}\,\frac{\partial\overline{c}}{\partial x} - K_y\,\frac{\partial^2\overline{c}}{\partial y^2} - K_z\,\frac{\partial^2\overline{c}}{\partial z^2} = 0. \qquad (13)$$

A solution to Eq. (13), assuming Gaussian diffusion (Slade, 1968), is:

$$c = \frac{Q}{2\pi\overline{u}\,\sigma_y\sigma_z}\ \text{Exp}\left[-\frac{y^2}{2\sigma_y^{\,2}} - \frac{(z-h)^2}{2\sigma_z^{\,2}}\right. . \qquad (14)$$

where

Q is source strength

$\overline{u}$ is mean wind speed

h is emission height

σ_y is y dispersion coefficient

σ_z is z dispersion coefficient.

σ_y and σ_z are usually determined from stability. σ_y and σ_z are assumed to be equal to $(2\,K_y\,x/\overline{u})^{1/2}$ and $(2\,K_z\,x/\overline{u})^{1/2}$ respectively. K_y and K_z are usually not known. The dispersion coefficients also can be approximated as:

$$\sigma_y = x^a \sigma_\theta^{\,b} \qquad (15)$$

$$\sigma_z = x^d \sigma_\phi^{\,e} \qquad (16)$$

where

σ_θ is standard deviation of the horizontal wind direction

σ_ϕ is standard deviation of the vertical wind direction

a, b, d, and e are constants approximately equal to 1 and need to be determined.

Examples of this approach are given by Slade (1968) and Pasquill (1962).

σ_y and σ_z are determined commonly from atmospheric stability through a method which involves surface heating or cooling estimates based on cloud cover, wind speed, and sunshine. The method is indirect and can be used with fair success for long term (several days) averages of the surface concentration of the scalar property, c. Since σ_y and σ_z are determined using the same value of stability, it should be apparent that a unique relationship is assumed to exist between σ_y and σ_z. Ragland et al. (1980) discusses this approach.

The measurement system required to determine σ_y, σ_z and $\overline{u}$ should yield better results than Eq. (14) which uses only atmospheric stability. It is difficult to determine K_y and K_z as defined in Eqs. (8) and (9), thus the method selected was to make the measurements needed to determine σ_θ, σ_ϕ and $\overline{u}$ at the stack level on the Messer site tower and use Eqs. (15) and (16) to obtain σ_y and σ_z. The conventional approach to determining σ_y and σ_z from atmospheric stability also should be covered.

The practical measurements continuously needed at stack height are:

(1) Horizontal wind speed
(2) Horiztontal wind direction
(3) Vertical wind speed
(4) Vertical wind direction
(5) Vertical temperature gradient
(6) Solar radiation
(7) Net radiation

For the desired time period, $\overline{u}$ is obtained from the mean horizontal wind speed, σ_θ from the range of the horizontal wind direction and σ_ϕ from the range of the vertical wind direction.

Remaining problems are: (1) Are the values at the Messer tower the same as those at the stack? (2) The wind speed and direction changes with height and under some conditions the change is very large.

The other three stations at the level of the generating station are expected to help in solving problem (2) and also provide estimates of $\overline{w}$ in Eq. (12). A possible resolution to problem (1) is to estimate the wind speed at the stack from the Messer site data, which represents the release time of the observed values of $\overline{c}$ (SO_2) at the ground level stations. The time difference between the ground observations and the time of Messer site data or release of $\overline{c}$ could be as much as 3 hr. Attempts to use (simultaneously) the concentrations from the Messer site, the station, and ground level would not prove fruitful unless the conditions are such that Q, u, σ_y and, σ_z have been constant for several hours. This condition rarely exists.

BASIC METEOROLOGY SYSTEMS AND RECORDING

The meteorological measurements used equipment that was on hand along with additional items obtained from Excess Government Property and some items purchased directly from grant money starting in 1972. In general, the old recording equipment performed more reliably than new equipment. Recent advances in inking systems for writing were inadequate. Systems using transistor required expensive repairs after nearby thunderstorms while vacuum tube systems continued to operate. Duplicate systems were installed where possible in order to maximize the reliability of the recording and to provide checks between systems at the same location so that there would be some quality assurance in the data.

Anemometry

Two anemometer systems were used for the horizontal scalar wind speed. One measured the instantaneous wind speed and the second measured the wind passage.

The instantaneous wind speed system was a Beckman Whitney (BW) Type F anemometer and Wind Vane. The three cup anemometer turned a slotted disk. The slotted disk permitted light from a bulb to fall on a photo tube. The detected pulse repitition rate was measure of the rate at which the anemometer was tuning. There were 180 slots in the disk so that even in very light winds the pulse repitition rate was adequate. The pulse went to a frequency to voltage converter and the output was recorded on an Esterline-Angus Model AW 0-1 ma recorder (E-A). Full scale output was 27 $m \cdot s^{-1}$ or 60 mph. The overall system accuracy is ± 4% of full scale or ± 1.2 $m \cdot s^{-1}$. The exponential response time is about two seconds. The E-A recorder proved to be reliable as there was a reliable inking system and paper transport system. Only one of the BW systems was in operation and this was at the Messer site on the tower.

The occasional light bulb failures caused by the loss of considerable data. Bulbs were replaced on a weekly basis, so if the light bulb failed shortly after a site visit up to 7 days of data were lost.

Wind passage was measured by a Stewart four-cup anemometer with a gear set-up which made electrical contacts equivalent to 0.016 (27), 0.1 (160), 0.5 (800), and 1 mile (1600) of wind passage. The 0.5 mile contact was used to operate an event marker on an E-A recorder. Thus, the number of contacts in a 30-min period corresponded to the average wind speed in mph for the 30-min period. Direct operation of the event marker by the anemometer contact eventually failed due to dirty contacts. This problem was corrected by using a pulse amplifier to operate the even marker which considerably reduced the anemometer contact current and significantly increased the operating time before contact failure occurred. The Stewart cup anemometer cost $50 and was used for average wind speeds at 32- and 2-m heights at the Messer site and at 9-m height for the other three sites.

The contact anemometer calibration was questioned as a result of comparisons between mean monthly wind speeds at the Wyocena site (Lake George) and Truax Field. Anemometers are usually calibrated in wind tunnels which often have the following problems:

(1) The measurement of low air speeds is poor;
(2) The air speed is not uniform in the tunnel;
(3) The tunnel wall prevents the air from flowing around the anemometer as it would in an unconstrained flow.

To overcome these problems the anemometers were mounted on a 3 m-pole above a bicycle with a battery-operated recording system mounted on the bicycle. A switch operated by the rider indicated start, stop, and the passage of reference points. The bicycle was ridden at a speed of about 3 m/sec around the 1/8-mile track of the enclosed Memorial Shell at the University of Wisconsin. Each anemometer was run around the 1/8-mile track on the bicycle for 2 miles with each lap indicated on the record. The 1/60th mile contact was recorded. Five Stewart four-cup anemometers indicated 45 ± 1 contact/mile when clean and 1 contact/mile less if the anemometer was dirty. A Bendix three-cup anemometer gave 53 contacts/mile for the 1/60th mile contact. The distance that each cup must travel for each contact is the same for the Stewart and Bendix anemometers. It is also known that during rotation four-cup anemometers shield each other from the wind more than three-cup anemometers.

The nominal 0.5-mile contact on the Stewart anemometer actually is 0.667 mile. The manufacturer was unable to explain the discrepancy nor describe how the anemometer was actually calibrated. The two types of anemometers tested have been widely used for more than 40 yr.

Wind Direction

The Beckman-Whitney Type F wind vane system is a vane-positioned potentiometer with suitable amplification so that output is linear with respect to the input. The wind vane covered a range of 345° with a 15° dead zone. The system accuracy of ± 4% results in a wind direction error of ± 15° using an Esterline-Angus recorded. The unit was used only at the 32-m height at the Messer Site. The second wind direction system, a vane-positioned 1000-ohm potentiometer, was constructed by the University of Wisconsin in Mechanician Shop for another purpose and 16 units were available for use in the Portage, Wisconsin area. The output went directly to the E-A recorder and was not linear with input. Recorder resistance was 1400-ohms and with 1.4 volts of direct current (vdc) applied to the 1000-ohm potentiometer, the recorder indicated full-scale deflection for the maximum potentiometer position. The slight nonlinearity of the wind direction as a function of the recorder output is corrected in the data processing.

Initially, 1.4-vdc mercury batteries were used for the wind vane voltage. In 1975 a regulated power supply was constructed to provide the 1.4-vdc as well as the means for operating the contact anemometer. Tests showed that the power supply output voltage was constant for an input voltage range of 70 to 140 volts of alternating current (vac). The wind vane system described was used at all sites including the 32-m level at the Messer site.

The 1.4-vdc power supply included a zero and full scale switch arrangement. The purpose of the switches was to allow convenient recording of zero and full scale recorder output at the start and end of each chart. This information provided a check on the power supply output and was used as a reference point in data processing.

Initially, only the Messer site had two wind vanes with the dead zone of the potentiometers oriented 180° out of phase with respect to each other. This orientation has the advantage that when one wind vane is on the potentiometer dead zone and the recorder pen is swinging from zero to full scale the second wind vane is recording near mid-scale and the data can be recovered. In data processing the two vanes can be checked against each other to provide quality assurance for the results.

The installation of two wind vanes at one location showed that there were problems in vane orientation. The wind vane mountings were changed so that each wind vane was approximately 1 m apart and the orientation was such that the potentiometer output was zero when the vanes pointed towards each other. The direction of the zero was measured with a Brunton compass after the vanes were in position on the tower. This improved the absolute value of the wind direction, however, the vanes still indicated different values for a given time period. Part of the discrepency between the vanes may have been due to interactions between the wind and the tower structure. The most reliable wind direction value should be the average of the two vanes.

Air Temperature Gradients

The dispersion coefficients--σ_y and σ_z, which are functions of K_y and K_z--vary with the statistical vertical stability of the atmosphere. The air temperature gradient is a measure of the static stability of the atmosphere between the two measurement points.

Ventilated and shielded thermocouples with a 2-min time constant were used to measure the vertical air temperature difference at the Messer and Dekorra sites. The two junction thermocouples signal is 0.080 mv for a temperature difference of one 1°C between the junctions. Recording was on a 0 to 2.5 mv 24-point Brown recorder at Messer and a 0 to 2.5 mv Brown recorder at Dekorra. The system accuracy was ± 0.1°C, corresponding to 10-μv noise.

Bivane and Vertical Anemometer

These instruments were used at the Messer site 32-m level to estimate σ_z. The bivane anemometer system (Gill model 01002) measures the horizontal and vertical angle of the wind and the vector wind speed. The output was initially recorded on two 2-channel Daystrom recorders. Later a 3-channel recorder was purchased and used for the bivane recording but proved to be unreliable because the ink supply was inadequate. The vertical anemometer (Gill model 27100) was a propeller with the axis in the vertical which turned a generator. The output of the generator was proportional to the vertical wind component. The output was recorded on one channel of the Daystrom recorder and then on an E-A recorder when the new bivane recorder was put into operation.

The distance constant is 1.0 m for 50% recovery for the bivane anemometer system and is 0.94 m for 63% recovery for the vertical anemometer. Since the vertical wind component is fluctuating around zero, the vertical anemometer tends to underestimate the vertical component of the wind with respect to the bivane anemometer because the mean wind speed in the vertical is so much smaller than the horizontal wind speed. The comparison between the two systems is discussed in Section 4.

The winter of 1973-74 proved that the bivane anemometer system should not be used under icing conditions. Ice buildup on the propeller unbalances the propeller, and as wind speed increases the unbalanced propeller vibrates the tail and the propeller. The entire device disintigrates. The bivane alone would not be subject to the above problems. After 1974 the bivane anemometer was not operated during the winter.

The second problem was the three channel recorder specifically recommended by the bivane anemometer manufacturer. The inking system would not hold enough ink to last several days and lightning quickly put one channel of the recorder out of operation. The Daystrom 2-channel recorders obtained from Excess Government Property were superior to the newly purchased equipment.

Rain Gauges

Rainfall was recorded at each site using a tipping bucket raingauge and Weather Measure Model P521 event recorder. The raingauges had been used in other experiments and were available for the project. Each rain gauge was calibrated by slowly pouring in a known amount of water as related to the gauge area. The number of tips were recorded and used to determine the rainfall for each tip. The rain gauges were not equipped with heaters for winter use and were operated only from April through October.

The drum-type event recorder made one revolution/week. The advantage of using this method for recording rainfall is that the start and stop times can be determined. Thus, it is known fairly well when it rained and this information can be used in air pollution modeling.

Sodar (Acoustic Sounder)

An Aerovironmental Model 300 acoustic sounder was purchased in 1974 and used at the Cemetery site. A sound pulse 20 msec long is transmitted vertically in the atmosphere. Sound energy is returned from regions in the atmosphere where the air temperature is increasing with height. The presence of a signal return is detected and recorder with a vertical range of 1000 m. The pulses are transmitted every 20 sec.

The antenna shield construction was two layers of plywood separated by approximately 9 cm. The space between the two layers of plywood was filled with sand. The dimensions were those recommended by the manufacturer, except that sand was used in place of lead. The inside of the enclosure was lined with convoluted foam plastic approximately 7 cm thick.

The height of the acoustic sounder return may be related to the mixing height of the atmosphere and thus the maximum height to which stack emission can be dispersed.

Summary of Systems and Recording

The key to reliable data collection was dual systems for measuring and recording wind speed and direction. By this method one can compare the dual results and thus knows when one system is not operating properly. The second advantage in the case of wind direction is that when the two vanes are 180° out of phase with respect to the potentiometer, one of the vanes is near mid-scale when the second is crossing the potentiometer dead zone. The wind vanes on a tower should be aligned with something on the tower which can be checked for direction alignment from the ground.

The newer model recorders used on this project had poor inking and printing systems. They must have been designed with the idea that one to two people would be in constant attendance.

Transistor type circuits were vulnerable to the strong fields associated with lightning, while tube circuits continue to operate. The cost in time and money of repairing the transistor type circuits was many times greater than the tube type circuits. The damaged transistor equipment was abandoned.

SITES AND RECORDING

Each site was uniquely equipped and had different exposures to the atmosphere. The actual data periods varied as did the times when equipment was not working properly.

Messer Site

Messer was the initial site and was at an elevation that would hopefully provide a wind record valid at the station stack. To do this required a tower at least 32 m (100 ft) high. On 16 August 1972 recording began from a 40-m (128 ft) crank-up tower. On 20 September 1972 the 40-m tower blew down. Two 9-m (28-ft) masts were erected on the same site and became operational on 26 September 1972. The tower anchoring failed during heavy rains which saturated the thin layer of soil over bedrock and the anchors were dragged by the tower in a steady wind of about 30 mph. The wind vane and anemometer recorded the fall of the tower.

On 1 September 1973, recording started on a 32-m tower that was constructed from two 18-m (60-ft) towers previously used on another project at the University of Wisconsin, Madison. This time the cement anchors were tied to bedrock by drilling holes into the rock to hold pipes that extended into a concrete pad poured over the rock. The tower was equipped with two vertical tracks constructed from barn door track which were used to raise and lower the instruments by winches. At the tower top the instrument supports locked into a groove to provide lateral support to the mounting arms. This system worked well, except when the track was sheathed in ice.

The recording equipment was housed in a 7 x 9 x 7 ft hutment located near the road north of the tower. The hutment was heated electrically to keep the recorder ink from freezing and the recording equipment generally worked better at temperatures around 15°C. Summertime cooling was provided by fans. The hutment air temperature varied by several degrees (°C) during any 24-hr period without causing any apparent problems. The signal cables were brought inside the hutment to terminal strips connected to the amplifiers and recorders. Electrical power for the tower equipment--i.e., blowers--was supplied from the hutment. Amplifiers for the Beckman-Whitley wind speed and direction system were located in a weatherproof box at the tower base. Mice built nests in the circuit breaker box causing problems. Some circuit breakers also opened on several occasions. The data loss was corrected by removing the nests and plugging holes to the circuit breaker box. Table 1 gives the items measured and the time period over which one system was used.

TABLE 1. METEOROLOGICAL OBSERVATION AT THE MESSER SITE

Item	Sensor	Recorder	Height (m)	Start	Stop	Data status	Code
Wind speed	B&W instantaneous	E.A. Pen	39	8/11/72	9/20/72	Complete	31
			9	9/26/72	9/1/73		
			32	9/1/73	12/31/77		
	Stewart 0.5 mile contact	E.A. event marker	39	8/16/72	9/20/72	Complete	33
			9	9/26/72	9/1/73		
			32	9/1/73	12/31/77		
	Stewart 0.5 mile contact	E.A. event marker	2	8/16/72	9/20/72	Complete	35
			2	9/26/72	9/1/73		
			2	9/1/73	12/31/77		
Wind direction	B&W system	E.A. pen	39	8/16/78	9/20/72	Complete	32
			9	9/26/72	9/1/73		
			32	9/1/73	12/31/77		
	U.W. vane	E.A. Pen	32	March 1974	12/31/77		34
Bivane	Gill v, θ,ø	Daystrom	39	8/16/72	9/20/72	Spot processed	
			32	9/1/73	11/30/77		
				April to Nov. only			
Vertical anemometer	Gill		32	12/1/73	12/31/77	Spot processed	
Air temperature difference	Thermocouple copper-constant	0-2.5 mv Brown	39-2	8/16/72	9/20/72	1/1/76 to 4/30/77	05
			32-2	9/1/73	12/31/77		
			2-0.2	6/16/72	9/20/72	1/1/76 to 4/30/77	03
				9/26/73	12/31/77		
			8-2	11/1/75	12/31/77		09
Air to shelter temperature difference	Thermocouple copper-constant	0-2.5 mv Brown	2	8/16/72	9/20/72	1/1/76 to 4/30/77	04
				9/26/72	12/31/77		
Shelter to soil temperature	Thermocouple copper-constant	0-2.5 mv Brown	-15 cm	8/16/72	9/20/72	1/1/76 to 4/30/77	06
				9/26/72	12/31/77		
Solar radiation	10 junction Eppley	0-2.5 mv Brown	—	8/16/72	12/31/77	1/1/76 to 4/30/77	02
Net radiation	Suomi ventilated	0-2.5 mv Brown	—	8/16/72	12/31/77	1/1/76 to 4/30/77	08
Precipitation	Tipping bucket	Event recorder	—	8/16/72	12/31/77	Complete	30
				April to Oct. only			
Soil temperature	Bi-metal thermometer	Observed visually	-15 cm	8/16/72	12/31/77	Recorded each visit	— —
Shelter	Bi-metal thermometer	—	—	8/16/72	12/31/77	Recorded each visit	—

A considerable loss of data occurred in the initial year starting 11 August 1972. Some of the failures were due to cables frayed by the wind, poor recorders, and wear on equipment. The barn door track method of raising the instrumented booms worked well, but the signal cables to the boom would abrade against the tower structure in strong winds. The numerous cable breaks caused a loss of data. The problem of cable abrasion was corrected by running the cable inside the barn door track. Much of the millivolt data was lost due to a poor recorder. Replacement with a 2.5-mv Brown model 15 recorder resulted in a virtually continuous record for 3 yr.

The Beckman-Whitney anemometer used a light bulb which burned out frequently, causing a loss of instantaneous wind data. This remained a problem throughout the data collection period. The potentiometers on the wind vanes wore out in approximately 1 yr. Dual systems and a supply of extra potentiometers limited data loss. The most extensive loss of data occurred from March to April 1976, during and after an ice storm. Initially the electrical power was off, then time was required to melt the ice on the sensors so that they could start operating.

Wyocena Site

Wyocena was in operation by January 1974. The location was an open field with the only nearby obstruction being the instrument shelter and a fence. The location is shown in Figure 1. The site is sometimes referred to as the Lake George site. The basic measurements were precipitation and—at a height of 9 m—wind speed and direction. The duplicate wind speed and direction system was in operation by 1 December 1975. Recording stopped on 30 September 1977. Minimal changes were made in the systems during the operation period.

Dekorra Site

Data recording at the Dekorra site (Figure 1) began on 1 January 1974 for wind at the 9-m level. The duplicate wind system was in operation by 1 August 1975. Trees to the west of the 9 m wind mast influenced the results. The Baraboo Bluffs influenced the wind field the most in comparison to other sites in the area.

Starting May 1974 the 0.2 to 2-m air temperature difference, soil to shelter temperature difference, and shelter to air temperature differences were recorded every 5 min on a 0 to 2-mv Brown recorder. Precipitation was recorded with a tipping bucket rain gauge.

Cemetery Site

This site was operational on 1 June 1974 for precipitation and one system for wind speed and direction. Located on the north side of Portage, Wisconsin (Figure 1), the data showed a wind speed reduction for southerly winds due to the high surface roughness of the various buildings in the city. The second wind system was operational by 1 October 1975. The acoustic sounder record started in April 1975. It was first tried at the Generating Station where there was too much nearby noise and at Messer where the electric fence interferred with the record. The recording systems were in a WPL shelter. Table 2 lists the meteorological observation systems at the three sites.

DATA PROCESSING

The strip chart recording of data was used for the following reasons:

(1) A large number of strip chart recorders were available;
(2) Digital systems are not as reliable as strip charts and require capital funds and continuous maintenance;
(3) Student help is available for digitizing;
(4) A digital system would also require strip chart backup.

The data processing used two systems for translating chart position into a three-digit number on a punch card. A system was constructed by Stearns (1963) to translate the output of a digital voltmeter to punch cards on command. A potentiometer was connected to a pointer through a string-pulley arrangement so that with 1 vdc across the potentiometer the output to the digital voltmeter was linear with respect to the pointer position on the chart. Pushing a button read the chart position to a surplus IBM 020 keypunch. An extra E-A recorder was set up to transport the chart past the pointer at a rate compatible with digitizing the 1-hr mean every 4 sec. The instantaneous wind speed and direction and Messer vertical anemometers were recorded at all sites providing similar E-A records.

For processing the data, the pointer was positioned initially at the zero and full scale of the chart so that the chart calibration was known. In operation the pointer was positioned over the 1-hr mean value and the button pushed to record the data on the punch card in the position corresponding to time. The chart moved continuously with the pointer following the mean value as estimated by the operator. When the hour time line passed the tip of the pointer the record button was pushed. One chart roll recording at 3 in/hr, i.e., 2 weeks of data, is translated to punch cards in 30 min.

The second system used for digitizing strip charts was a Digi-Grid system manufactured by Computer Equipment Corporation. A cursor was placed over the point to be digitized and a button punched to record the position on a punch card through an IBM 026 key punch. The Digi-Grid system was used

TABLE 2. METEOROLOGICAL OBSERVATIONS AT THE CEMETERY, WYOCENA (LAKE GEORGE), AND DEKORRA SITES AND OTHER PROCESSED DATA

Item	Sensor	Recorder	Height (m)	Recording		Data status	Code
				Start	Stop		
Wyocena (Lake George)							
Wind speed	Stewart	E.A. event	9	Jan. 1974	9/30/77	Complete	43
	1/2 mile	marker	9	Dec. 1975	9/30/77	Not processed	
	contact						
Wind direction	U.W. Vane	E.A. pen	9	Jan. 1974	9/30/77	Complete	41
	U.W. Vane		9	Dec. 1975	9/30/77	Complete	42
Precipitation	Tipping	Event	—	Apr. 1974	Nov. 1977	Complete	40
	bucket	recorder					
Dekorra Site							
Wind speed	Stewart	E.A. event	9	Jan. 1974	12/31/77	Complete	53
	1/2 mile	marker	9	Aug. 1975	12/31/77	Not used	
	contact						
Wind direction	U.W. vane	E.A. pen	9	Jan. 1974	12/31/77	Complete	51
	U.W. vane	E.A. pen	9	Aug. 1975	12/31/77	Not used	
Precipitation	Tipping	Event	—	May 1974	Nov. 1977	Complete	50
	bucket	recorder		April to Nov.only			
Soil temperature	Thermo-	0-2.5 mv		May 1974	12/31/77	Not	
Air temperature	couple	Brown		May 1974	12/31/77	processed	
Time difference			0-0.2	May 1974	12/31/77		
Cemetery Site							
Wind speed	Stewart	E.A. event	9	June 1974	9/30/77	Complete	63
	1/2 mile	marker	9	Oct. 1975	9/30/77	Not used	
	contract						
Wind direction	U.W. vane	E.A. pen	9	June 1974	9/30/77	Complete	61
	U.W. vane	E.A. pen	9	Oct. 1975	9/30/77	Complete	
Precipitation	Tipping	Event	—	June 1974	12/31/77	Complete	60
	bucket	recorder		April to Nov.only		Complete	
Soil temperature	Aero-	included	—	Aug. 1975	12/31/77	Complete	65,66
	vironment						67,68
	system						69
Other Data							
Truax Field		Daily mean		Jan. 1974	12/31/77		27,
		3 hourly data		Jan. 1974	12/31/77		28,29
Generating Station		Gross load		Jan. 1977	Feb. 1978		80
		Inlet temperature		Jan. 1977	Feb. 1978		81
		Outlet temperature		Jan. 1977	Feb. 1978		82

for digitizing Brown recorder data point by point. The loss of operating time due to an intermittent connection amounted to several months and delayed data needed by the Air Pollution Modeling Group. One advantage of the home-built system was that it was understood and could be quickly repaired.

The E-A strip charts required 1-hr time marks on all charts and day marks every 24 hr. During the processing, the charts were checked for time discrepencies. The contact anemometer data was obtained from the strip charts by counting the number of tick marks every 30 min which corresponded to the average wind speed in mph. This data was punched manually on cards and computer-processed to obtain the 1-hr mean value of the wind speed.

The Brown recorder data (Messer site only) was read onto punch cards point by point for each item for 12 hr. Each point was 5 min apart in real time. The data was procesed to obtain 1-hr mean values in the correct scientific units.

In general the data processing involved the following steps:

(1) Timing of charts;
(2) Conversion of chart data to IBM cards;
(3) Checking the data for errors;
(4) Conversion to scientific units and averaging where necessary;
(5) Combining the data sets for the data center.

The data format was determined by the IBM card which has 80 columns. The first eight columns were used for identification and the last 72 for data.

Column	Item
1,2	Year
3,4	Month
5,6	Day
7,8	Identifier
9,10,11	Data - 1-hr mean from 00 to 01 CST
to	to
78,79,80	Data - 1-hr mean from 23 to 24 CST

With the exception of precipitation and Truax Field data, this format was followed for the initial punching of cards from the strip charts to the final card format for entry in the data bank. The precipitation data were--by their nature--intermittent so that data were recorded only when precipitation actually occurred.

Data Reduction

The digitized data set is coded with respect to time, location, and chart position. The chart position must be converted to scientific units and scanned for errors. The types of errors encountered commonly in the initial data deck were incorrect coding with respect to time or place and incorrect position of the data on the punch card. These errors were corrected easily. Calibration errors also occurred and were more difficult to correct, but the corrections were made after the initial processing of the data.

Either digitizing system is capable of punching an erroneous number or an extra punch. A listing of all original data cards also is desirable. A computer program entitled Scan was used to read the cards and calculate the difference between a data point and the one before and after. Each card is printed and if the difference exceeds 8% of full scale the differences also are printed. The differences can be examined to see if they are real or are due to an erroneous punch which then required correction.

The E-A recorder has a pen that pivots about a center point, resulting in a curved trace, and the Brown self-balancing potentiometer has a linear trace. On the E-A recorder, the linear output is the pen angle referenced to center scale and the digitizing equipment measures the cord length perpendicular to the center scale. The angular recorder output is calculated as:

$$I = 0.0005\ [\sin^{-1}\{(x-x_c)/L\}/\sin^{-1}\{(x_c-x_o)/L\} + 1] \qquad (17)$$

where

I is current through recorder in milliamps

X is digitized chart position

X_o is zero on chart

X_f is full scale on chart

$X_c = (X_o + X_f) * 0.5$ = center scale

L is length of pen arm-pivot to tip $= X_f - X_o$

Units of X, X_o, X_f, and L are the units of the chart reader. The length of the pen arm happens to be the same as the width of the recorder chart scale. The recorder full scale is 1 ma.

The data now needs to be converted to scientific units. The Beckman-Whitney wind speed at the Messer Site has full scale adjusted to 26.8 m/sec (60 mph) so that multiplying I by 26.8 gives the wind speed in m/sec. The program for wind direction data reduction included values for the full scale and zero of the recorder system as these values do not coincide necessarily with the left and right edge of the chart.

The data reduction program was tested by setting up a wind vane recorder system. The wind vane was positioned at 30° intervals from 0 to

345° while the recorder operated for 1 min at each position. The data were digitized and processed. The results were within 2° of the actual value for all points which is well within the accuracy of the recorder system. If data were in error or missing the number 999 was entered on the cards. In this manner a zero encountered on the card meant zero and not missing data.

The Messer Brown data was read at 5-min intervals for each item for 12 cards. This was done because it was easy to follow one item at a time and 12 hr of data could be positioned on the digitizing table. The Messer Brown data reduction program, reads the data cards and forms 1-hr means for each item. The output was printed in scientific units but the card output was formatted so that decimal points were not required. Since the data can be positive or negative, the three-digit data point has 500 as zero and the data are scaled so that the range is between 0 and 999. When using the output cards the data must have 500 subtracted and then properly scaled to obtain the correct units. Missing or erroneous data is coded as 999.

The acoustic sounder (Sodar) data from the Cemetery site was read manually from the charts in 1-hr mean values and coded in the same format. Again the absence of reliable or no data was coded as 999. The base and top heights of the first and second inversions and the height of the thermals are in meters with each item on a separate card with the appropriate identifier.

The rainfall data was formatted differently. The tipping bucket rain gauge and recorder system indicated the time of start and stop of the precipitation and its amount. The initial eight card columns contained year, month, day, site code, then data. The data was start time, stop time, and rainfall in inches. The start and stop times were to the nearest 30 m. This turned out to be a useful way to code the data since other users then knew the time period during which it was raining.

The monthly data--except precipitation--is arranged on a daily basis according to increasing identifier code. A computer program converts the data to scientific units where necessary and prints each day's data. These results can be entered into the data bank. The original recordings, output of Scan, the conversion to scientific units, and the final printout are preserved for all processed data for an indefinite time. The punched data set is indicated in Tables 1 and 2.

The air temperature, as determined either from the shelter temperature or the soil temperature, is not considered reliable. A detailed study of this data has not been made.

SECTION 4

A PILOT DIFFUSION CLIMATOLOGY SURVEY FOR THE COLUMBIA GENERATING STATION

In all research on air pollution dispersion and climatology it is hoped that easily measured and commonly understood meteorological parameters--which indicate the atmosphere's ability to cleanse itself--can be identified. Several objective statistical techniques have to be developed in order to arrive at a meaningful and useful climatology of surface pollution potential. Engineering solutions to atmospheric dispersion and dosage quantities often rely upon oversimplified assumptions and equations. Refined assessments of the variablility of the horizontal and vertical wind components and the vertical air temperature gradients will be presented. Where engineering solutions to air quality studies "smooth" the spectrum of hourly weather variations, an objective was to single out weather singularities, or extremes, during which adverse dispersion conditions exist. Consequently, a relationship between atmospheric dispersion characteristics and synoptic weather patterns was sought. Specifically, daily weather map types were inspected and categorized in a manner which might link periods of high pollution potential to macroscale events.

PREVIOUS STUDIES

Innumerable publications concerning air pollution or the diffusion of effluents have appeared over the years and the approaches to solving the complex questions of effluent transport number nearly as many. Reference should be made to Sutton (1953), Slade (1968), and Beals (1971). However, recent attention to the interplay between meso-macroscale meteorological phenomena, atmospheric turbulence and diffusion, and pollutant dispersion has come to the forefront (Miller 1967, Panofsky and Prasad 1967, Singer 1967). Anderson (1971), in a treatise on mesocale influences in wind fields, emphasizes that the spatial dimensions of pollutant plumes are orders of magnitude smaller than the characteristic space scales of "weather motions" and would, therefore, render conventional surface sensing techniques inappropriate for diffusion research. In his kinematic approach to pollution transport phenomena, arguments based solely on the continuity equation and potential function were employed to structure a discussion on boundary layer flow. Lettau (1959) proposed a dynamic means of couple macroscale motions with boundary layer flow by means of large scale pressure gradients. This relationship allows for turbulence elements to interact with transport processes, the consequences of which lend more realism to the mechanism of effluent dispersion.

Many studies--from the purely theoretical to the purely instrumental--have evolved over the years in the hope of deducing the nature of diffusion. Pack (1962), Munn (1964), and Shaw (1972) have each--in their own turn--looked at this problem from an instrumental aspect. Munn (1964), pointed out the need for establishing a turbulence "climatology" based upon the three-dimensional wind fluctuations over uneven terrain. Statistical reductions of the azimuthal and elevation angles from daytime and nighttime bivane observations were applied to the data. Singer (1967), in a similar approach to reduce wind variability in the planetary boundary layer into meaningful order, discussed the old meteorological evaluation techniques of wind steadiness as applied to tower wind measurements. The derived steadiness function was computed for different time periods and, by use of extreme value theory, recurrence intervals of the various mean wind direction ranges were prescribed. It should be noted, however, that the vast majority of these investigations dealt with data periods during which winds were neither calm nor even light ($\leq$ 4 m/sec). The available statistical techniques for reducing "no wind" records are seldom utilized even though there appears to be a great need for their use in these cases. Certainly one would hope to find some references to "no wind" statistics in the air pollution literature since this state of the atmosphere often deserves attention. Comprehensive treatment of plume rise and diffusion formulae (e.g., Briggs 1969) only deal with periods during which wind speeds were sufficient to spread the plume; little time was spent investigating evaluation techniques for plume dispersion in low wind situations.

With regard to weather map typing schemes, there is a scarcity of literature in the air pollution journals on the relationship of synoptic patterns to plume transport phenomena. In fact, over the years there seems to have been a tendency for researchers to classify plume behavior crudely according to wind regimes and atmospheric thermal profiles, an approach which could have been strengthened by relating plume behavior to weather type instead. Map classification schemes have been used in various ways over the past 60 yr. Bowie and Weightman (1914), Gold (1920), Flohn and Hess (1952), and Lund (1963) have each developed such techniques. However, it is surprising that these typing schemes have not been modified for use in air pollution studies as an empirical reference for plume behavior as a function of synoptic pattern. Nearly all of the synoptic mapping schemes are founded on analogues of daily surface weather circulations over time. Such procedures would seem to lend some value to classifying air pollutant levels and plume behavior according to the prevailing weather conditions, yet this relationship seldom has been pursued.

Compilation of Synoptic Parameters

Daily 1200Z synoptic weather charts for the contiguous United States were gathered from the National Oceanic and Atmospheric Administration (NOAA) State Climatologist during the August 15 to November 1 observation period. Published by the Environmental Data Service of the U.S. Department of Commerce, these daily charts provide surface and 500-mb analyses, 24-hr precipitation totals, and 24-hr maximum and minimum temperatures.

DATA PROCESSING

Wind Structure Data

Of the 78 days comprising the fall observation period, 21 days were defined as potentially poor dispersion days based upon the minimal wind speeds recorded between the hours of 1100Z and 1300Z inclusive. Rather arbitrarily, horizontal wind speeds generally < 4 m/sec (< 9 mph) were defined as an upper limit for these low wind speed occurrences. Not surprisingly, however, a small percentage of the daily traces exhibited brief periods of gustiness exceeding the 4 m/sec constraint but these traces were included in the low wind speed statistics whenever the wind speed records clearly indicated small velocities through the greater portion of the prescribed 2-hr interval. Processing the Beckman-Whitney horizontal wind speed and direction traces, the bivane elevation angle traces, and the vertical anemometer records included a similar two-fold operation. First, all records from early morning on low wind speed days were prepared for computer processing by tracing out by hand the envelope best describing the average values of the maxima and minima for each parameter (wind speed, wind direction, or elevation angle). The locus of points describing the averages of the given parameter through the 2-hr period was interpolated from the character of the previously defined envelopes.

All daily traces were marked off into 10-min intervals beginning at 1100Z and ending at 1300Z. The discrete values of the maxima, minima, and averages for each of the 13 10-min periods were processed onto punch cards using the Department of Meteorology, University of Wisconsin digitized chart reader described by Stearns (1967). No data processing of the climatological records was attempted because this was felt to be beyond the immediate scope of the project.

Map Typing Schemes

In view of the complexities of describing and classifying weather regimes, it was felt that a simplified yet expedient approach to weather pattern classifications would rely on cyclonic and anticyclonic pressure center locations in relation to Portage, Wisconsin. Consequently, what could be interpreted as a quadrant method was utilized; the parallel of latitude and line of longitude running through the power generating site (43° 30' by 89° 25') was plotted on each 1200Z daily surface map. Cursory streamline analyses were constructed for each weather map to assess the relative importance of one pressure center over another with regard to surface wind flow in the Portage region. The spatial locations of the pertinent pressure centers within the quadrants were tabulated daily and set aside if that day satisfied the requirements for being a potentially poor dispersion day.

DATA ANALYSIS

Wind Structure Data

Visual interpretations of the horizontal wind speed and direction records, as well as bivane elevation angle traces, suggested that these parameters were not normally distributed during the postulated potentially poor dispersion periods. Because these data did not appear statistically uniform, the standard deviation statistic was felt to be an inappropriate first attempt in defining wind variability. Only the vertical component of the wind vector indicated an approximate normal distribution. The standard deviations of this vector, however, were not computed in order to lend continuity to the analyses of all wind structure records.

The statistics used in the analyses were the range of the variables at prescribed 10-min intervals from 1100Z to 1300Z and the number of crossings made by the continuous trace of the given variable past the interpolated, instantaneous average value of the variable over a 10-min interval.

Determination of Range for Wind Vector Components--

The ranges of the wind speed components were calculated on a Raytheon 440 computer from data decks previously described. Thirteen range values were tabulated for consecutive 10-min periods starting at 110Z for each day under investigation. Inspection of histograms of the range of wind speed and direction revealed a characteristic positive skewness in both cases, indicating that the most frequently observed ranges fell short of the variable's mean range value. With wind speed data, ranges generally varied between 0 and 3 m/sec while wind direction records showed ranges between 0 and 80°. The bivane elevation angle ranges also exhibited a tendency for positive skewness with ranges lying between 0 and 22° limits. Vertical velocity data, however, showed a more Gaussian, or normal distribution with range; variability extended from 0.06 to 0.16 m/sec.

Number of Crossings as a Possible Test Statistics--

The number of crossings of the continuous trace across the running mean of the variable per 10-min interval was interpreted visually from the data. The information content of this statistic was felt to be pertinent as a measurement of variability although little--if any--documentation of the success of this technique has been available. The 10-min intervals--13 in total/day/chart--were centered on times corresponding to 1100Z, 1110Z, ..., 1300Z. Thus, every 10 min, a two-fold interpretation of the variability of the parameter was available. The problem of resolution of the visual traces while tolerable with chart speeds of 12 in/hr, became suspect at 3 in/hr, particularly during periods of high frequency fluctuations.

The relationship between the range of the variable and the number of crossings per 10 min, beyond a tendency for a direct dependence, bore no definable pattern; data stratification within a "range vs. crossings" framework appeared physically meaningless. A means of stratifying the relationships of these two elements as a function of the given variable was much simplified, however, by introducing the concept of a length scale, itself inversely dependent upon the number of crossings (Lettau, personal communication). Wind statistics could be reduced in such a fashion that the ratio of the total 10-min wind passage distance for each component direction to the number of crossings in the same 10-min interval yields a measure of the component eddy lengths.

A longitudinal eddy length (L) derived from wind speed data was defined as:

$$L = \frac{\overline{V} \text{ x } 600 \text{ sec}}{\text{Number of crossings/10 min}} \quad \text{in m} \qquad (18)$$

The formulation of the length scales for wind speed was made for each day under investigation. The relationship between the total wind passage length ($\overline{V}$. 600 sec) and the length scale itself (L) is shown here to be a family of straight lines corresponding to discrete values of the number of crossings made during the 10-min period (Figure 2).

For wind direction, a lateral eddy length scale (ℓ) was constructed as:

$$\ell = \frac{\overline{V} \text{ x range of direction in radians x } 600 \text{ sec}}{\text{Number of crossings/10 min}} \quad \text{in m} \qquad (19)$$

As with the longitudinal eddy length scale, ℓ plotted against the total lateral wind passage swept out over the interval exhibited a family of straight lines corresponding to discrete values of the number of crossings per 10 min. (Figure 3).

Similarly, the vertical eddy length scales (ξ) were described as:

$$\zeta_\theta = \frac{\text{V x range of elevation angle in radians x } 600 \text{ sec}}{\text{Number of crossings/10 min}} \quad \text{in cm} \qquad (20)$$

and

$$\zeta_w = \frac{\text{range of vertical and velocity x } 600 \text{ sec}}{\text{Number of crossings/10 min}} \quad \text{in cm} \qquad (21)$$

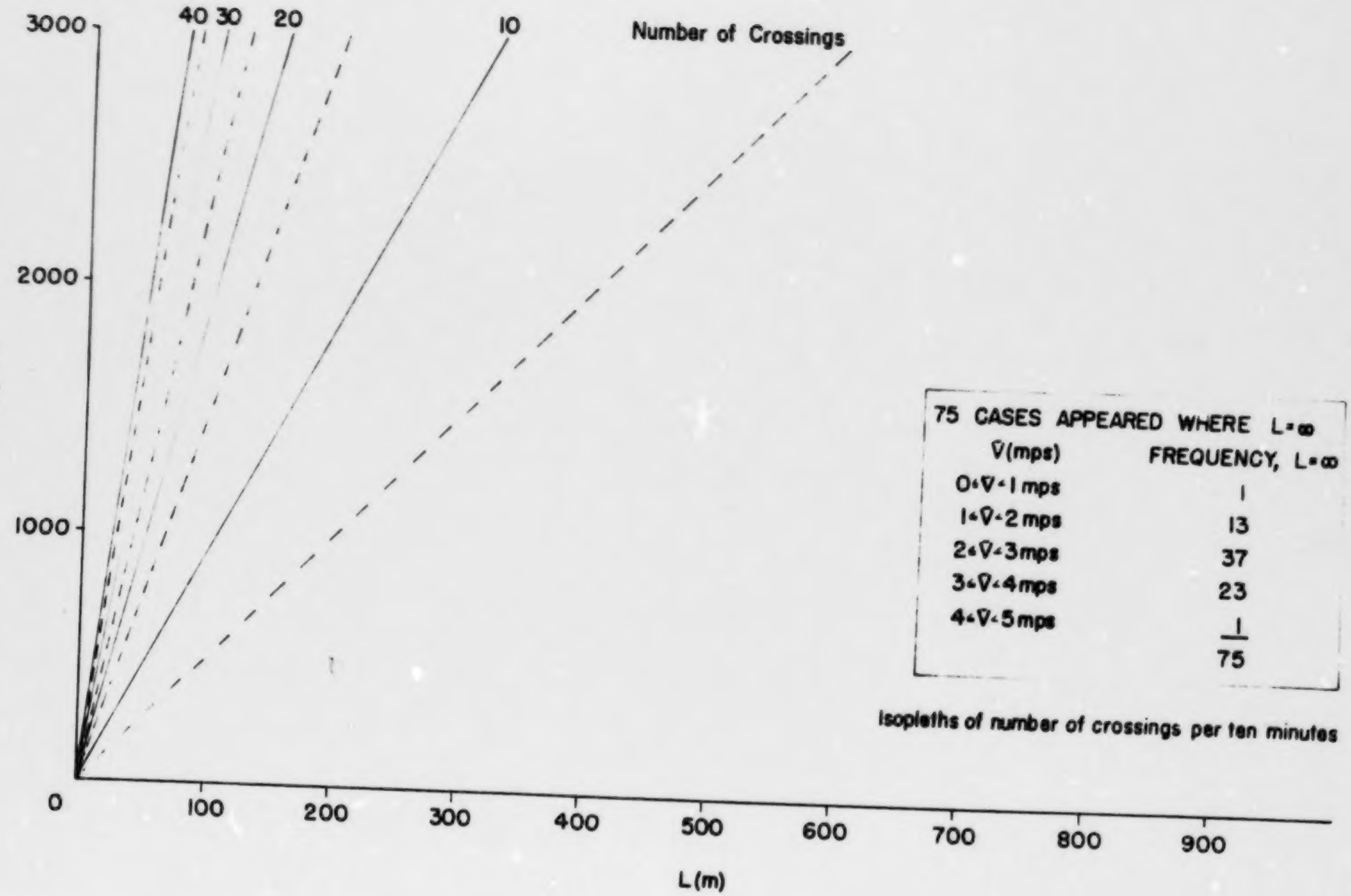

Figure 2. Wind passage in 10-min ($\bar{V}$ x 600 sec) as a function of longitudinal eddy length L (m). Isoplethed are the number of crossings of the horizontal wind speed trace past the 10-min running wind speeds.

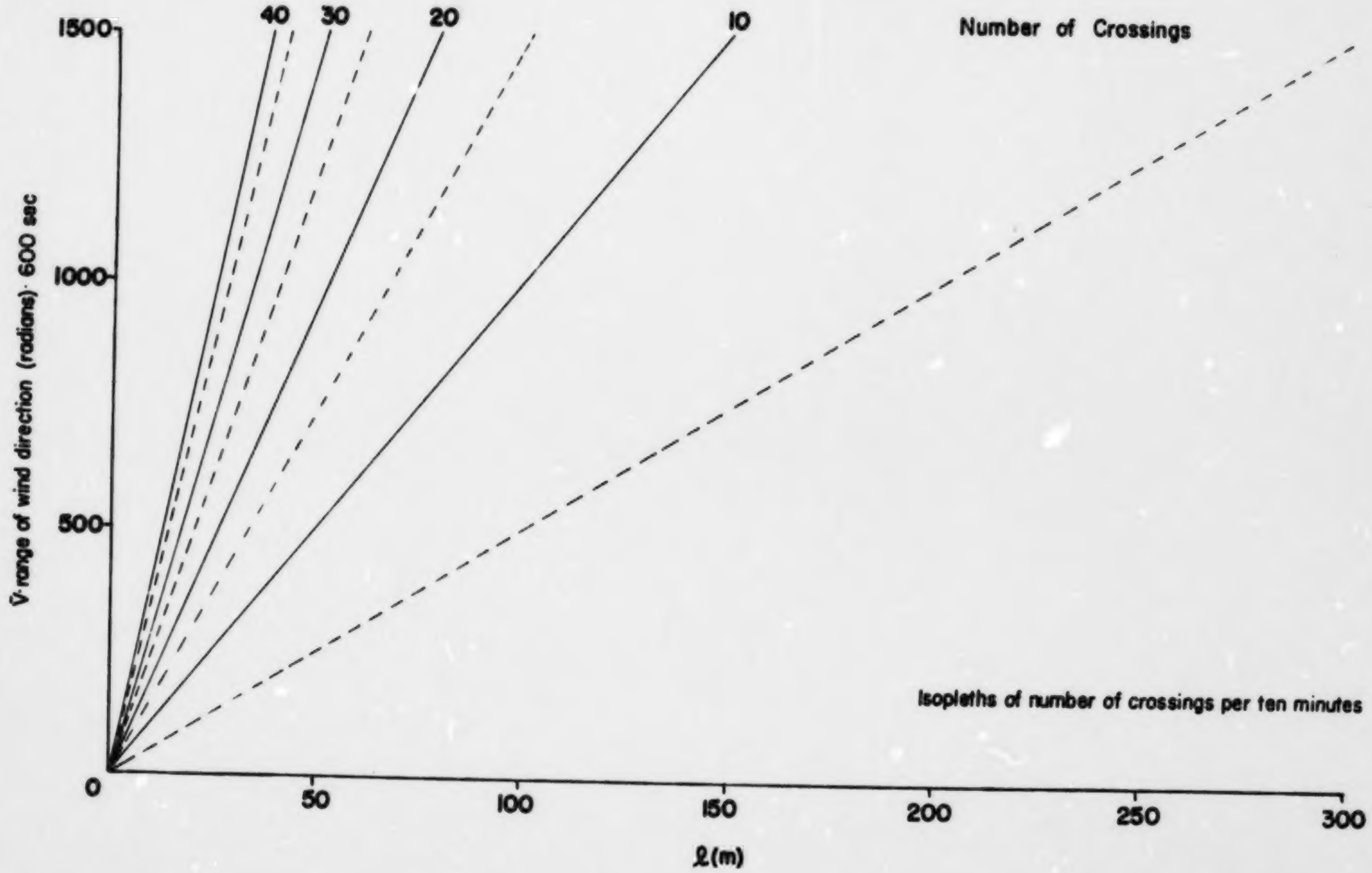

Figure 3. Wind passage in 10-min ($\bar{V}$ x range of direction in radians x 600 sec) as a function of lateral eddy length ℓ (m). Isoplethed are the number of crossings of the horizontal wind direction past the 10-min running mean wind direction.

The plots of these length scales against the total vertical distance traversed over the period also provided isoplethed families of straight lines of the number of crossings (Figures 4 and 5).

Wind Direction Traces as Indicators of Turbulence Types—

In one of the early approaches to describing the turbulence of low-level flow, Smith (1951) and Singer and Smith (1953) developed gustiness classifications implied by the horizontal wind direction traces. The gustiness of the horizontal wind was selected as the criterion for defining turbulence because gustiness, vertical temperature structure, and wind speeds all were related closely. The horizontal wind direction traces were isolated as indicators of the turbulence types because they better described convective and mechanical turbulence regimes than did wind speed trace characteristics. The classifications used in this study followed the concepts of the Smith (1951) scheme (Table 3) whereby the range and appearance of the direction traces determined the gustiness types.

TABLE 3. DESCRIPTION OF GUSTINESS TYPES (ADAPTED FROM SMITH 1951)

Type	Description	Remarks
A	Fluctuations of the wind direction exceed 90° for the given 10-min period.	Characteristic of convective turbulence. Generally strong lapse rates, weak winds.
B_1	Fluctuations confined to 15° to 45° limits.	Combination of mechanical and convectional turbulence. Brisk winds, moderate winds, moderate lapses.
B_2	Fluctuations ranging from 45° to 90°.	Combination of mechanical and convectional turbulence. Moderate winds, moderate lapses.
C	Unbroken trace showing a solid core. Straight line can be drawn for the 10-min period without touching an "open space." Fluctuations must reach 15° but no upper limit imposed.	Mechanical turbulence usually under cloudy skied with a neutral lapse condition.
D	Trace approximates a straight line. Short-term fluctuations do not exceed 15°.	Minimum turbulence implied. Generally an inversion present but may occur with an unstable lapse and cloudy skies.

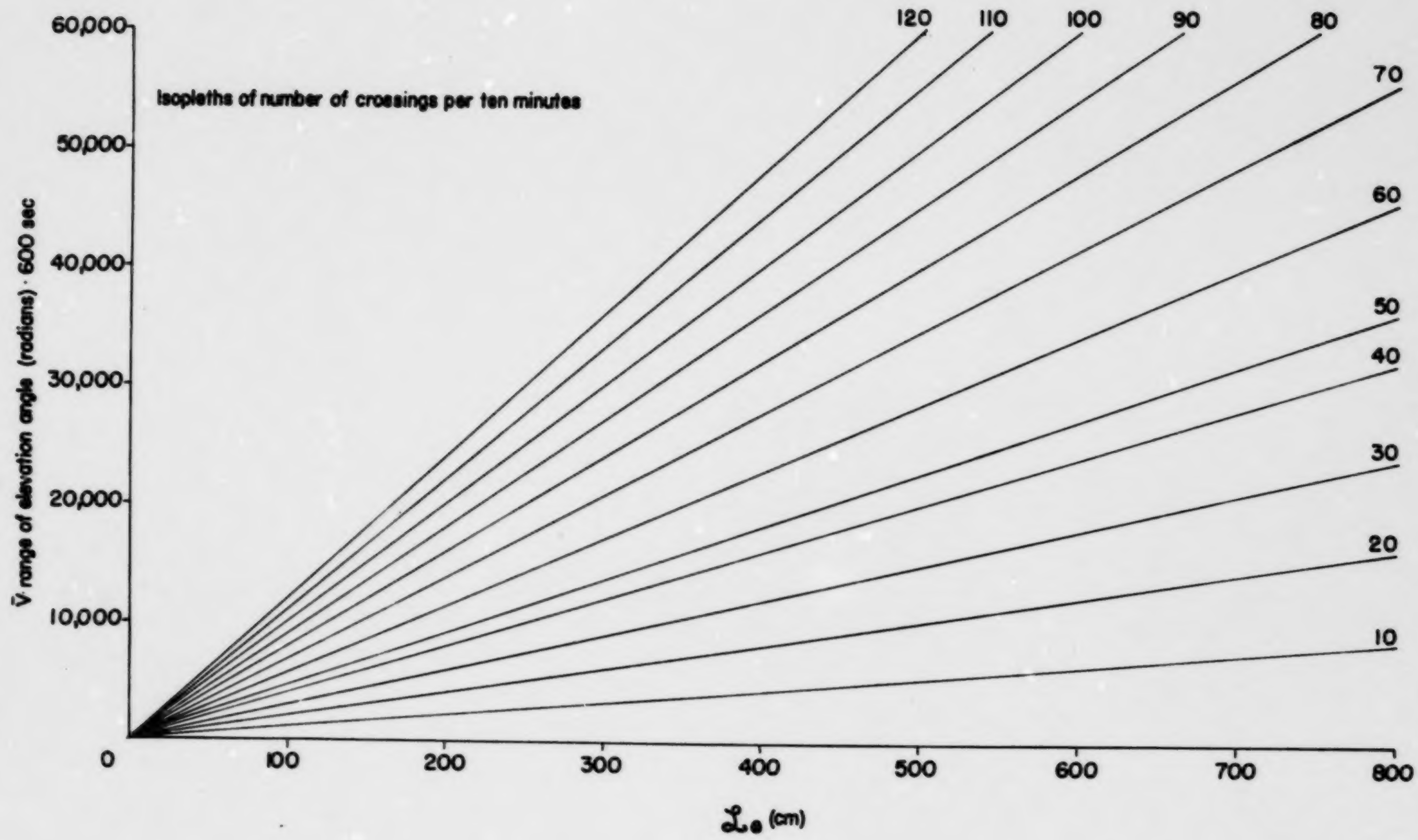

Figure 4. Wind passage in 10-min ($\bar{V}$ x range of elevation angle in radians x 600 sec) as a function of vertical eddy length ζ_e (cm). Isoplethed are the number of crossings of the elevation angle trace past the 10-min running mean elevation angles.

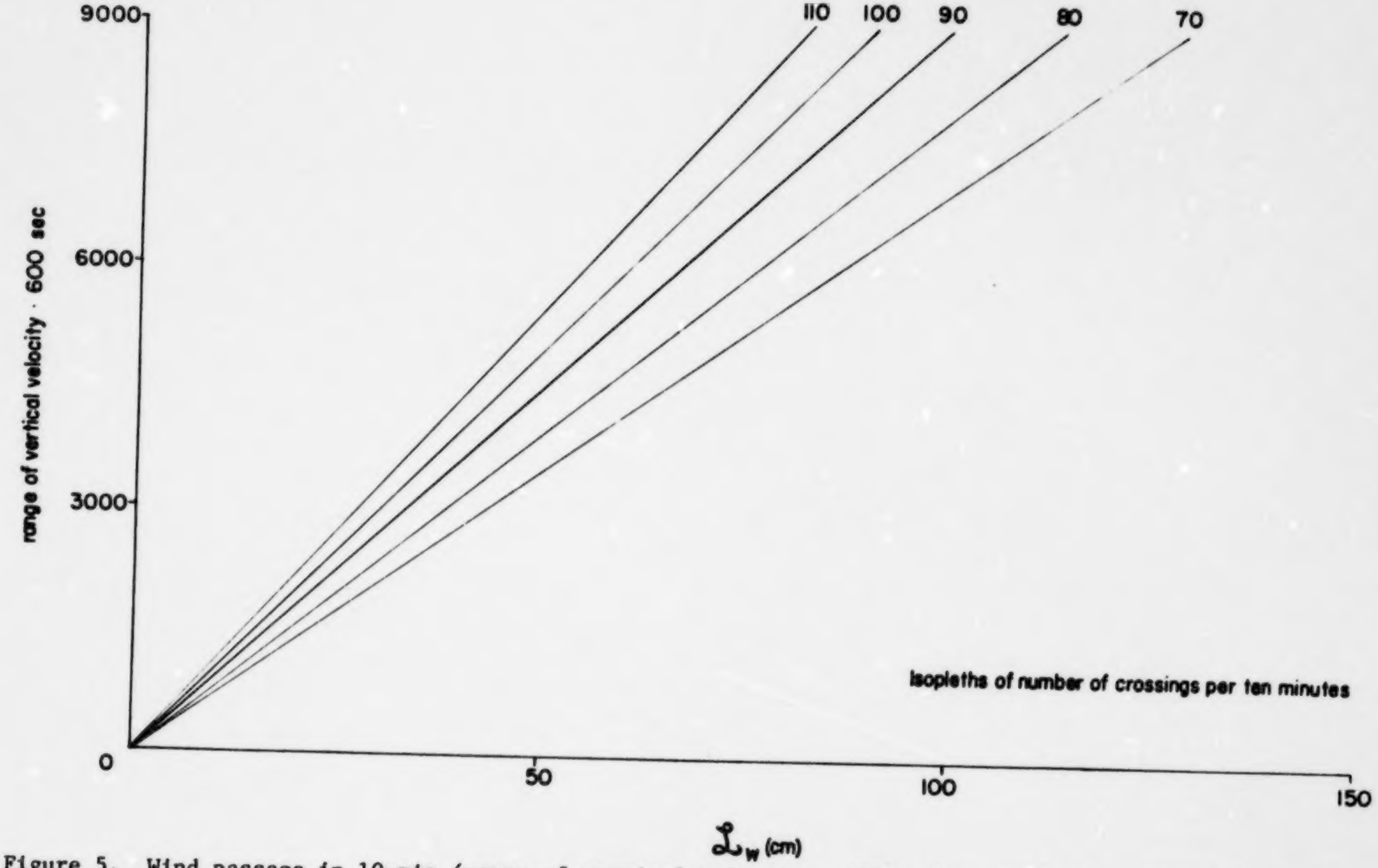

Figure 5. Wind passage in 10-min (range of vertical velocity x 600 sec) as a function of vertical eddy length ζ_e (cm). Isoplethed are the number of crossings of the vertical velocity trace past the 10-min running mean vertical velocities.

In the present pilot study, these classifications were identified with low wind speed cases despite previous indications that certain gustiness classes were associated with wind speeds of $\geq$ 5 m/sec (types B_1, B_2, and C). For each low wind speed day during which wind direction information was available, a gustiness classification was established for the 1100Z to 1200Z and 1200Z to 1300Z intervals. B_1 and D types were found to predominate (Table 4).

TABLE 4. SUMMARY OF OCCURRENCES OF GUSTINESS TYPES IN THE PORTAGE REGION DURING THE FALL OBSERVATION PERIOD, 1972

Type	Frequency	Remarks
A	1	Sunny. Apparent convective turbulence generated
B_1	10	Four cases show low level stability and scattered to no cloudiness. Remaining cases unstable with cloudiness.
B_2	3	All cases show stability and minimal cloudiness.
C	2	Broken clouds, surface layer stable.
D	9	Generally all cases stable in low levels except for two instances of moderate lapse and clouds.

Length Scales as Indicators of Dispersion Potential--

The dependence of the previously described length scales upon the number of crossings per 10-min interval has been shown to be one of inverse dependence. In order to fabricate a relationship between these eddy lengths (L) and any other independent dispersion parameters, histograms of these length scales and other elements were constructed.

Figure 6 decribes how L varies with decreased turbulence as defined by the range and appearance of the wind direction traces. Eddy lengths of the order of 75 m are associated generally with B type gustiness. However, eddy lengths between 75 and 575 m are defined exclusively as D types. The longest eddy lengths prevailed with B types, again with 2 to 4 m/sec wind speeds common.

Lateral eddy lengths (ℓ) stratified according to gustiness types (Figure 7) afforded a recognizable pattern. The shortest eddies--of lateral widths < 10 m--appeared frequently during days of minimal turbulence characteristics of the D classification. Intermediate eddy widths, from 10 to 80 m, occurred with B- and C-type traces while the few remaining eddy

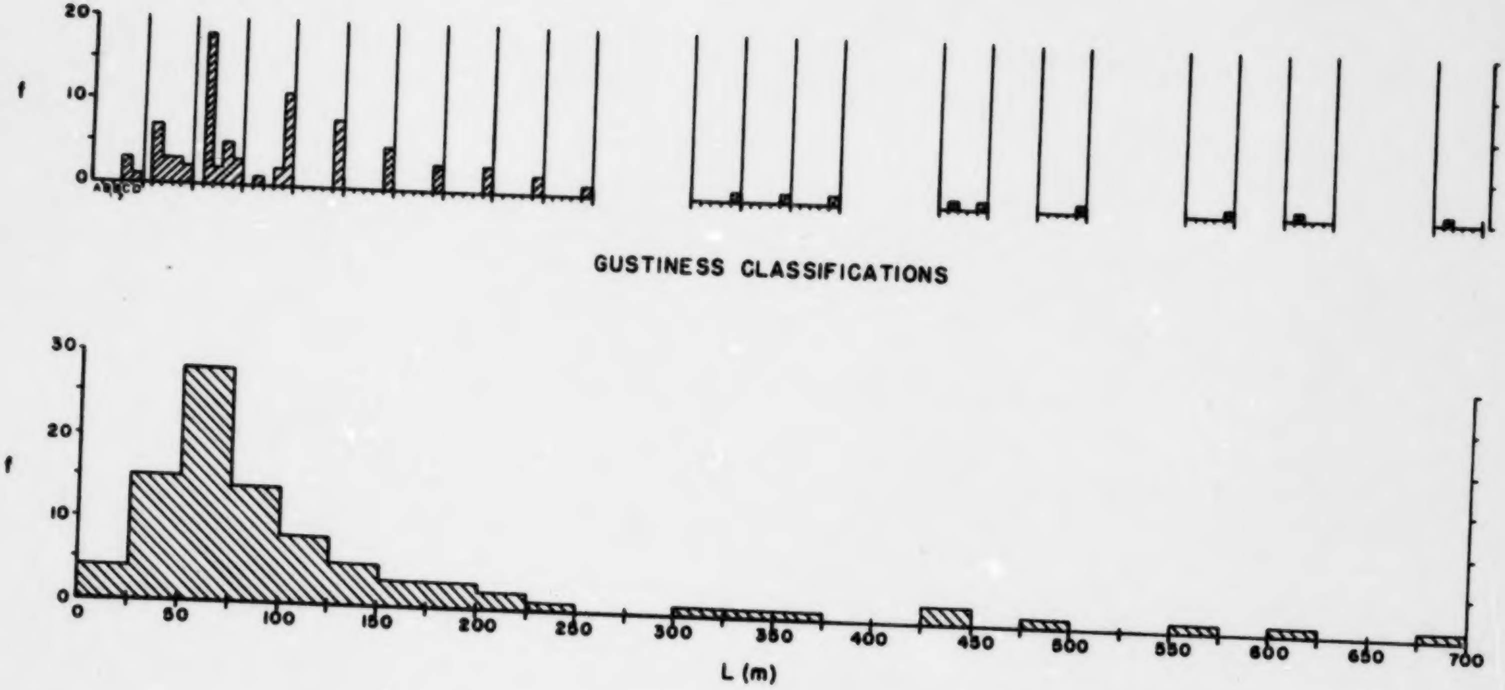

Figure 6. Frequency of occurrences of longitudinal eddy length, L, classified according to gustiness types as defined in Table 3.

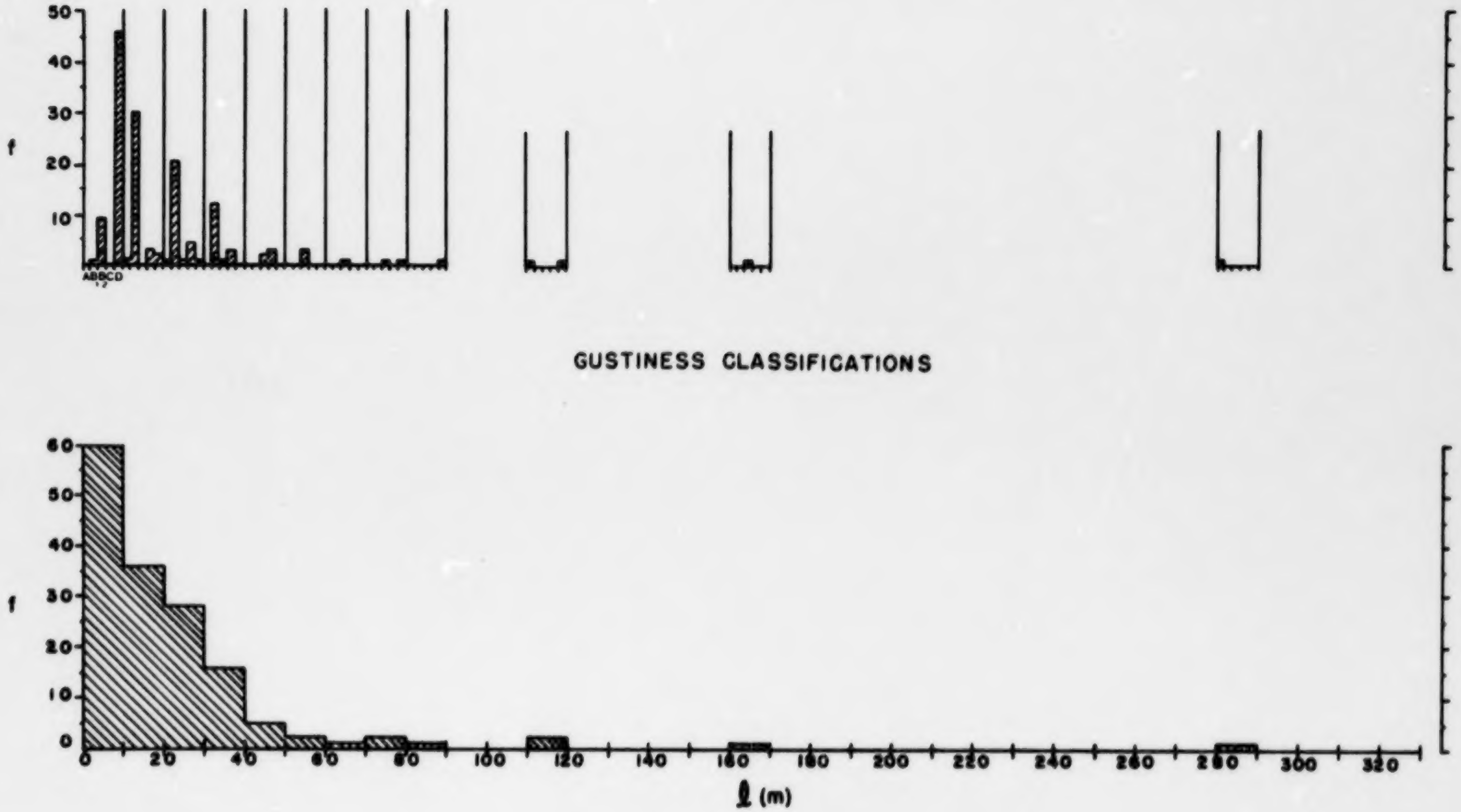

Figure 7. Frequency of occurrences of lateral eddy length, ℓ, classified according to gustiness types as defined in Table 3.

widths >80 m most frequently appeared in conjunction with B_2- and D-type gustiness classes.

Perhaps the most important indicators of potential dispersion are the vertical eddy length scales ξ_θ and σ_w). It is unfortunate that the bivane was operational for only the first month of the study because it was during this period that the majority of the days under examination displayed D-type turbulence. Figure 8 demonstrates that vertical lengths from 0 to 7.75 m generally were accounted for during time of minimum turbulence. However, of importance in contaminant transport, are the histograms of elevation angles themselves, here shown to be consistent downdrafts. It must be emphasized that the initial bivane calibrations were meticulously undertaken. The preponderance of negative elevation angles was a real feature of the flow, undoubtably related to topographic effects. Vertical eddy lengths derived from vertical anemometer records similarly displayed this consistent tendency for downdrafts (Figure 9). However, one basic difference between the bivane-derived length scales and those derived from vertical anemometer records lies in the range of the vertical eddy lengths. Figure 9 indicates that the observed ξ_w range extends from 0.3 to 1.0 m, considerably less than the range deduced from the bivane data. A response correction factor provided by the R. M. Young Company (1969) for a 19-cm (7.5 in.) propeller used with the Gill vertical anemometer (Model #27101) can be applied to the observed or filtered ξ_w values to more realistically account for the larger natural wavelengths. This assumes that the bivane senses atmospheric eddying motions more faithfully than a vertical anemometer. Literature comparing the response characteristics of the two systems was unavailable, but for the purposes of this study all bivane records were left uncorrected for response reduction. The correction factor applied to ξ_w was the response ratio defined as the observed wavelength:mean gust wavelength. This ratio was provided by the R. M. Young Company (1969) instruction manual as a graph of the dynamic response of the vertical anemometer with a 19-cm polystyrene propeller blade (Figure 10). The following equation improved the estimates of the vertical eddy lengths:

$$\xi_w\text{, real} = \frac{\xi_w\text{, observed}}{A} \quad \text{in cm} \qquad (22)$$

where A is response ratio, and ξ_w, real is mean gust wavelength. The corrected values of ξ_w are larger than those calculated initially (cf. Figure 9 with Figure 11) yet remain less than the ξ_θ values. Presumably this discrepancy is related to the poor chart resolution of the total number of crossings seen in the vertical anemometer traces.

A further difference between the ξ_θ lengths is related to the gustiness classes associated with each. All ξ_w values were computed from periods during which the B_1 type prevailed for a sample period of 3 days. It thus becomes apparent that valid inferences on the relationships of vertical length scales to gustiness classes are subject to error.

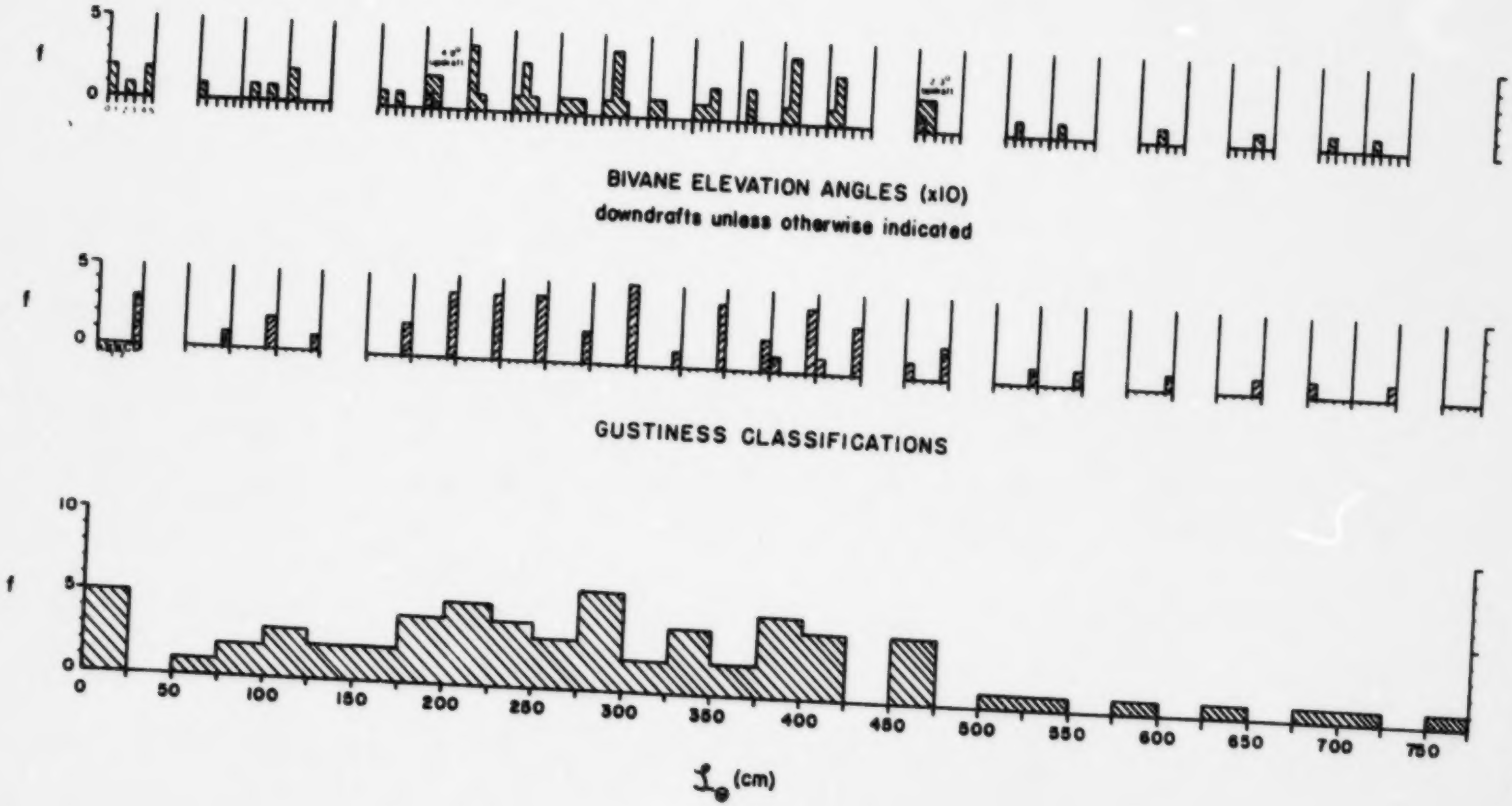

Figure 8. Frequency of occurrences of the longitudinal eddy length, ζ_θ, classified according to gustiness types.

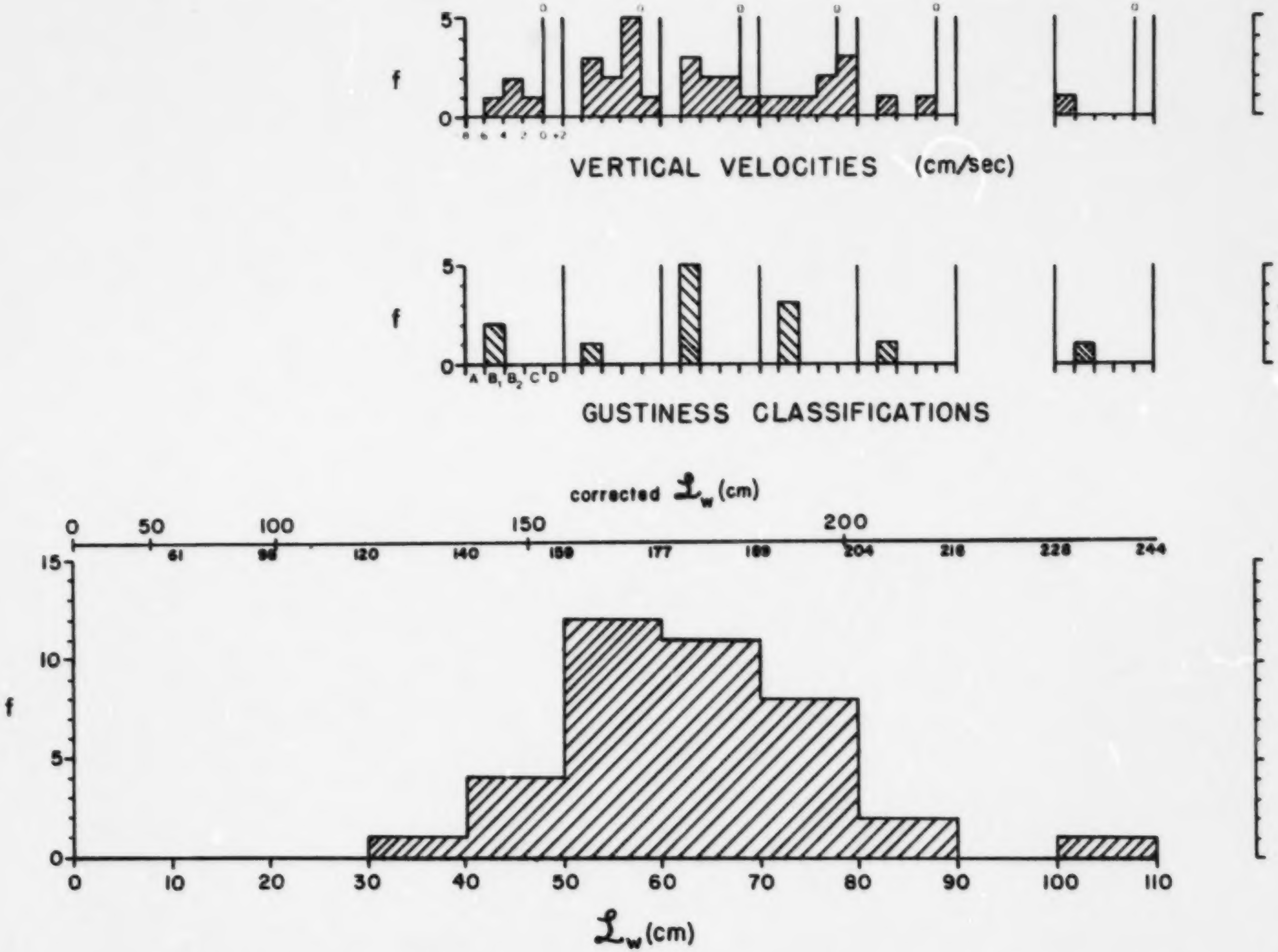

Figure 9. Frequency of occurrences of the vertical eddy length, ζ_w, classified according to gustiness types.

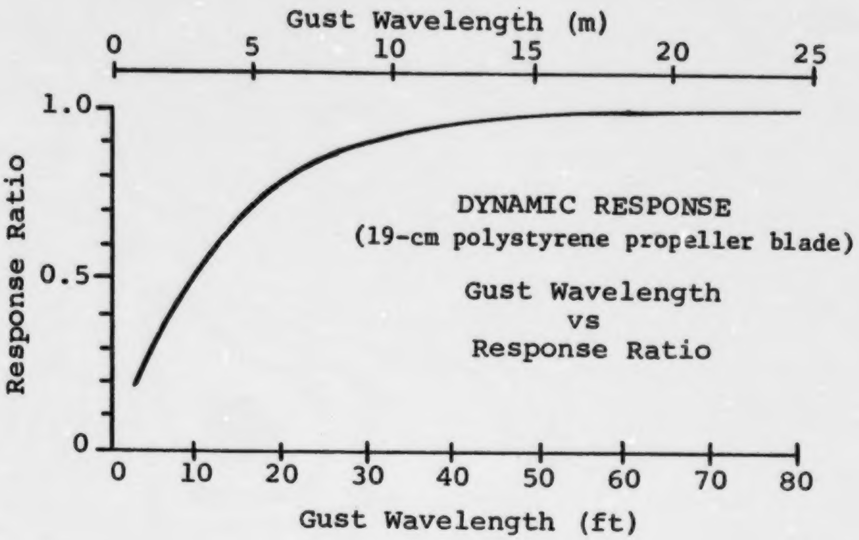

Figure 10. Dynamic response curve adapted from an original published by the R.M. Young Company (1969).

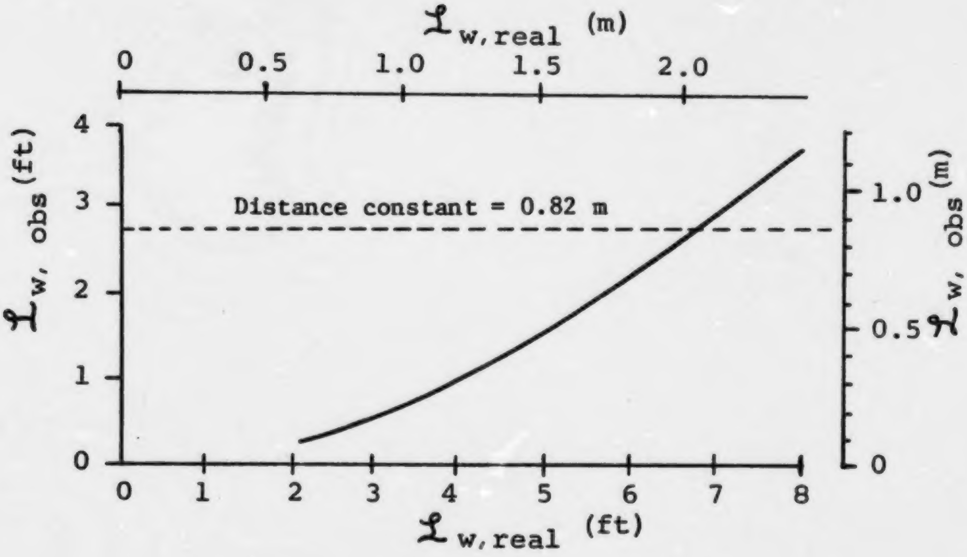

Figure 11. Relationship of the observed mean length scale ($\mathcal{L}_{w, obs}$) to the real gust wave length. Corrected according to Figure 10.

Synoptic Weather Conditions and Gustiness Types

Twelve selected weather maps (1200Z) corresponding to periods of potentially poor dispersion were analyzed (Figures 12 through 23). The wind direction traces--complete with gustiness types--are included with these maps. Table 5 is intended to present the salient characteristics of the synoptic conditions as seen with each trace. The lapse rate and air mass advection features were evaluated from morning upper air soundings provided by the National Weather Service Office at Green Bay, Wisconsin. Cloud cover was determined by surface reports and upper air surroundings.

CONCLUSIONS AND RECOMMENDATIONS

The objective of the pilot study was to investigate the wind structure for potentially poor atmospheric dispersion periods during the fall of 1972. Further, as an attempt to ease the amount of data handled in this research, only early morning hours (1100Z to 1300Z) associated with the 1200Z surface maps were considered. This particular 2-hr interval was pursued as the time when atmospheric stability underwent the transition from stable to unstable conditions. Entire days during the 1972 investigation period, however, deserved more extensive processing.

The concept of the number of crossings made by the trace of a given variable past its 10-min running mean has been shown to be a significant low wind statistic when used in formulating length scales. This is because the latter allows the observer to construct reasonable three-dimensional dispersion trajectory lengths for each 10-min period. Further, with a knowledge of the range and appearance of the wind direction traces, these length scales can be interpreted in light of the turbulence characteristics which these traces define. It was found that the longitudinal eddy lengths (L) of the longest dimensions recurred with a gustinesss type common during early morning inversions and minimal turbulence (D types). These eddy lengths--75 to 575 m—suggest early morning fanning at the stack height level. The potential for effluent drift along an extended portion of the Wisconsin River Valley is noticeably great. The shortest L values, indicating more erratic effluent behavior and less potential for hazardous surface contamination, were generally seen with B-type gustiness. Lateral eddy lengths presented a different, yet consistent, pattern. The shortest length scales--0 to 10 m—typified the class-D gustiness. In combination with the conclusions arrived at for the longitudinal length scales, the picture of a narrow, laminar type of effluent meandering during those periods of minimal turbulence and high stability emerges. Conversely, because lateral eddy lengths of the order 20 to 140 m were more typically associated with B-type turbulence, a completely different dispersion pattern is conceived. Specifically, one would interpret eddying motions in this instance to disperse effluents in a more uniform horizontal fashion. Consequently, of the two most frequent turbulence types, D-type cases stand out as potentially more hazardous. Additionally, these assessments must be viewed in terms of the vertical eddy lengths. In this study the absolute

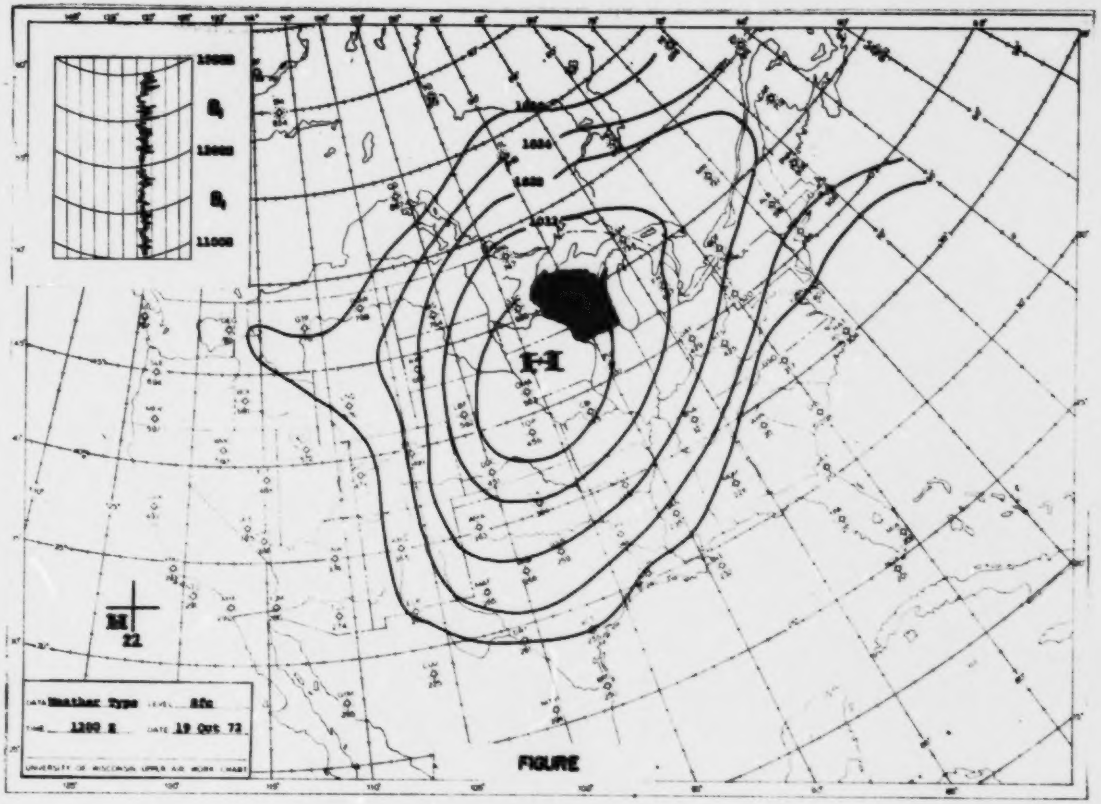
1300Z
1200Z
1100Z
H
H
22
DATA Weather Type
LEVEL Sfc
TIME 1200 Z
DATE 19 Oct 72
UNIVERSITY OF WISCONSIN UPPER AIR WORK CHART
FIGURE

Figure 12. Surface pressure map for 1200Z (0600 CST), 19 October 1972. Isobaric pattern identified as weather map type 22 (anticyclone center to southwest of Portage, Wisconsin). Insert refers to the corresponding wind direction trace for the 1100Z to 1300Z period. Recorded at the Messer site.

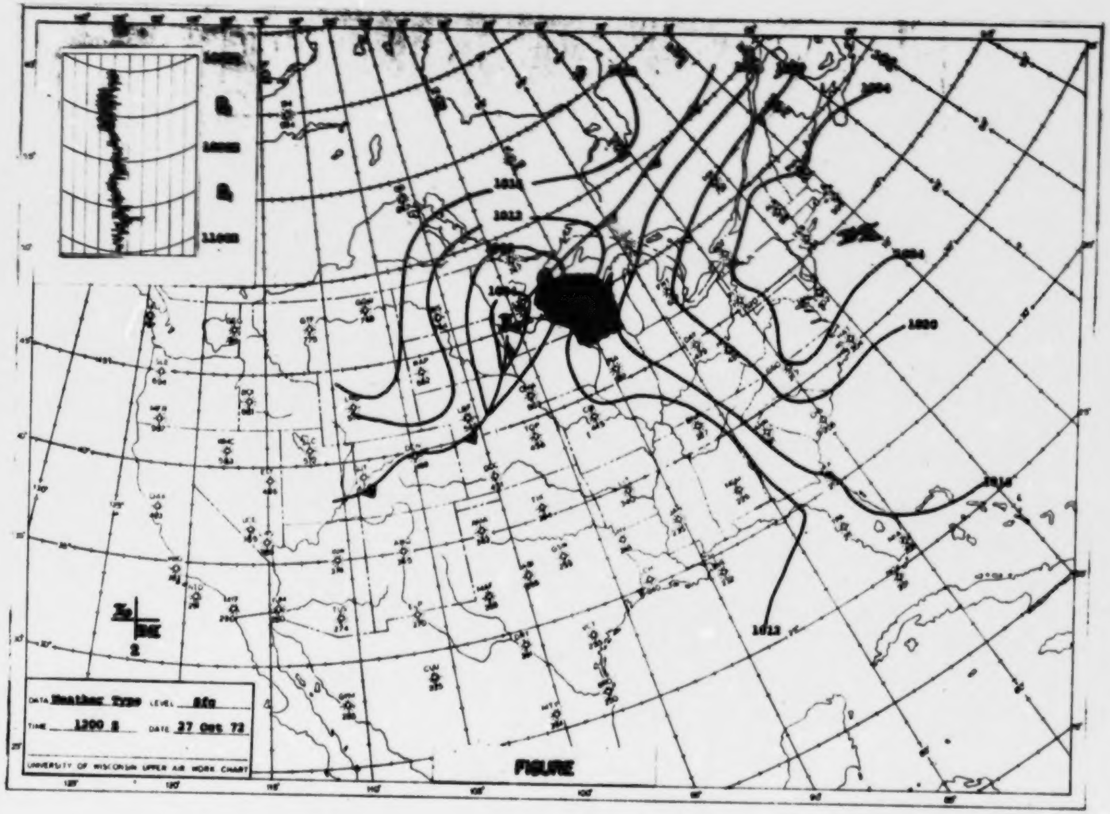

1300Z
1200Z
1100Z
1024
1020
1016
1012
DATA Weather Type LEVEL Sfc
TIME 1200 Z DATE 27 Oct 72
UNIVERSITY OF WISCONSIN UPPER AIR WORK CHART
FIGURE
2

Figure 13. Surface pressure map for 1200Z (0600 CST), 27 October 1972. Isobaric pattern identified as weather type 2 (cyclone center to the northwest of and anticyclone to the southeast of Portage, Wisconsin). Insert refers to the corresponding wind direction trace for the 1100Z to 1300Z period. Recorded at the Messer site.

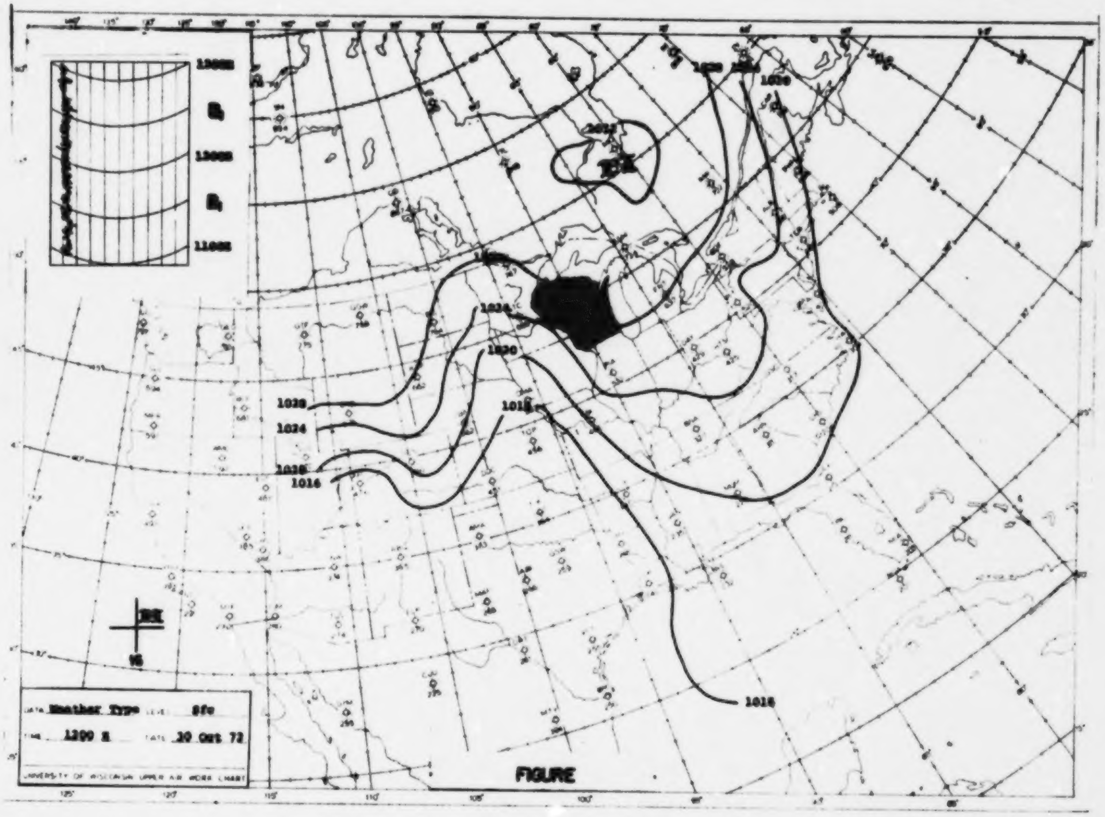

1300Z
1200Z
1100Z
1028
1024
1020
1016
1016
Weather Type
Sfc
1200 Z
30 Oct 72
UNIVERSITY OF WISCONSIN UPPER AIR WORK CHART
16
FIGURE
125°
120°
115°
110°
105°
100°
95°
90°
85°

Figure 14. Surface pressure map for 1200Z (0600 CST), 30 October 1972. Isobaric pattern identified as weather type 16 (anticyclone center to the northeast of Portage, Wisconsin). Insert refers to the corresponding wind direction trace for the 1100Z to 1300Z period. Recorded at the Messer site.

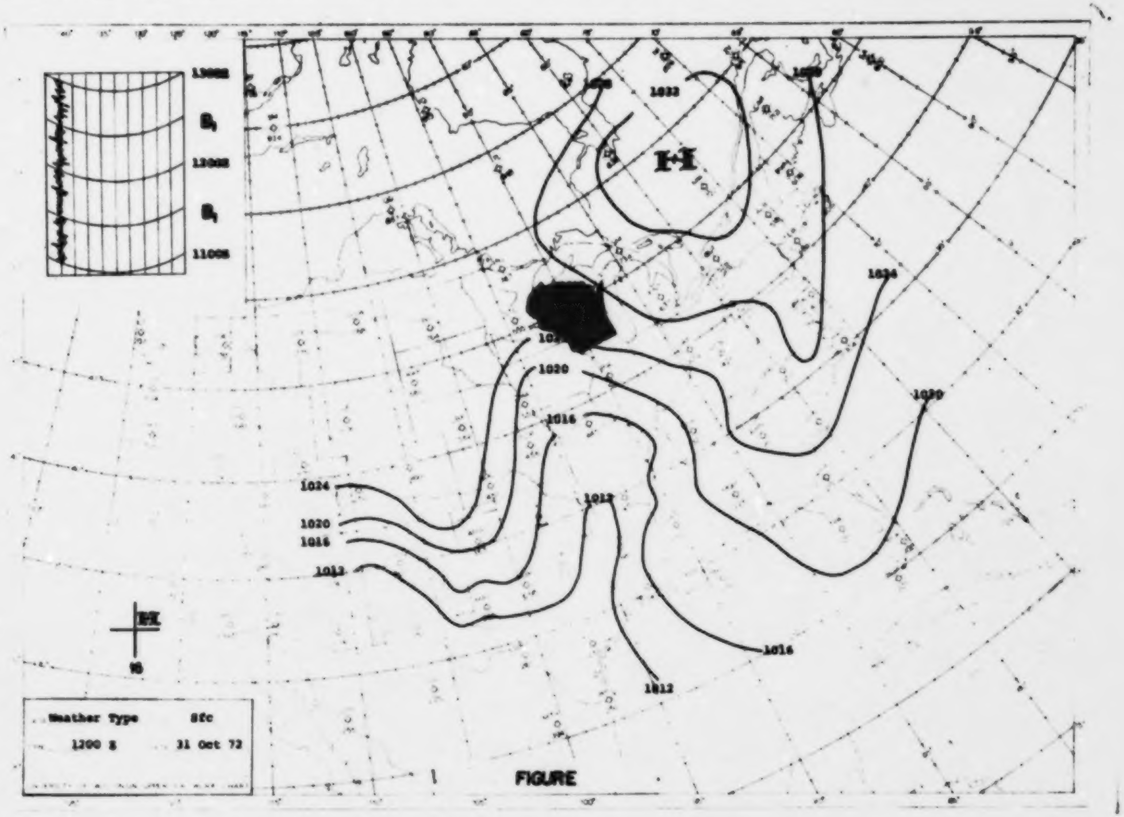
1300Z
1200Z
1100Z
1032
1028
1024
1020
1016
1012
1024
1020
1016
1012
1016
1012
1020
1024
1020
H
Weather Type
1200 Z
Sfc
31 Oct 72
FIGURE

Figure 15. Surface pressure map for 1200Z (0600 CST), 31 October 1972. Isobaric pattern identified as weather type 16 (anticyclone center to the northeast of Portage, Wisconsin). Insert refers to the corresponding wind direction trace for the 1100Z to 1300Z period. Recorded at the Messer site.

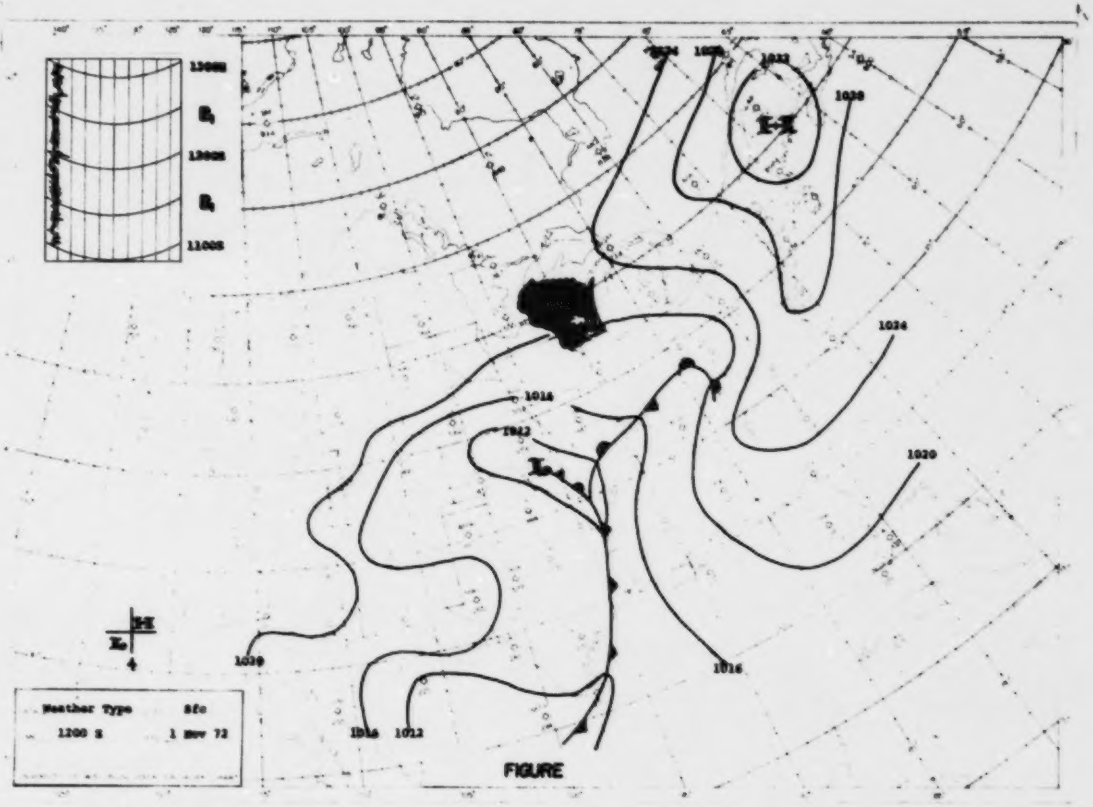
1300Z
1200Z
1100Z
H
L
4
Weather Type
Sfc
1200 Z
1 Nov 72
1024
1028
1032
1028
1024
1020
1016
1016
1012
1020
1016
1012
H
L
FIGURE

Figure 16. Surface pressure map for 1200Z (0600 CST), 1 November 1972. Isobaric pattern identified as weather type 4 (cyclone center to the southwest of and anticyclone center to the northeast of Portage, Wisconsin). Insert refers to the corresponding wind direction trace for the 1100Z to 1300Z period. Recorded at the Messer site.

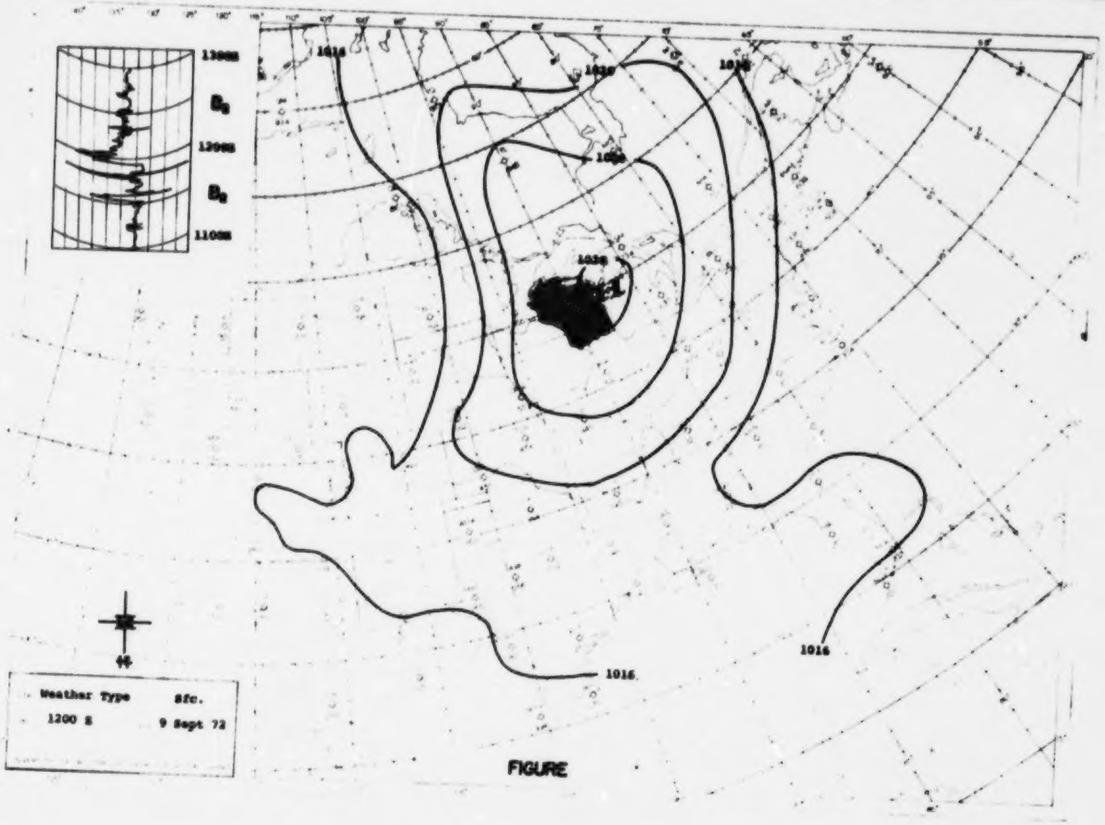
1300Z
B
1200Z
B
1100Z
1016
1020
1016
1024
1028
1016
1016
Weather Type
1200 S
Sfc.
9 Sept 72
FIGURE

Figure 17. Surface pressure map for 1200Z (0600 CST), 9 September 1972. Isobaric pattern identified as weather type 14 (anticyclone center within 5° latitude of Portage, Wisconsin). Insert refers to the corresponding wind direction trace for the 1100Z to 1300Z period. Recorded at the Messer site.

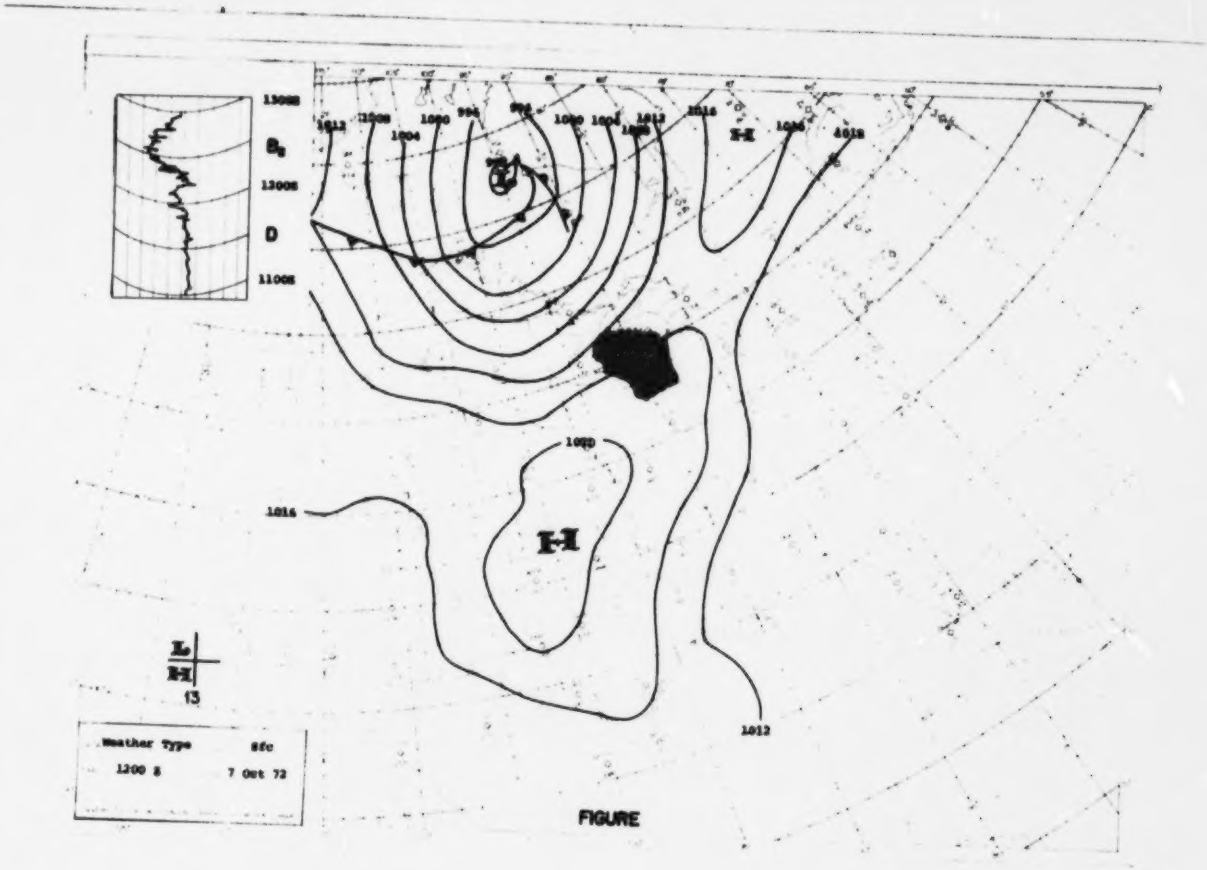
1300Z
B
1200Z
D
1100Z
1012
1008
1004
1000
996
1016
H
1020
1012
1016
L
H
13
Weather Type
Sfc
1200 Z
7 Oct 72
FIGURE

Figure 18. Surface pressure map for 1200Z (0600 CST), 7 October 1972. Isobaric pattern identified as weather type 13 (cyclone center to the northwest of and anticyclone to the southwest of Portage, Wisconsin). Insert refers to the corresponding wind direction trace for the 1100Z to 1300Z period. Recorded at the Messer site.

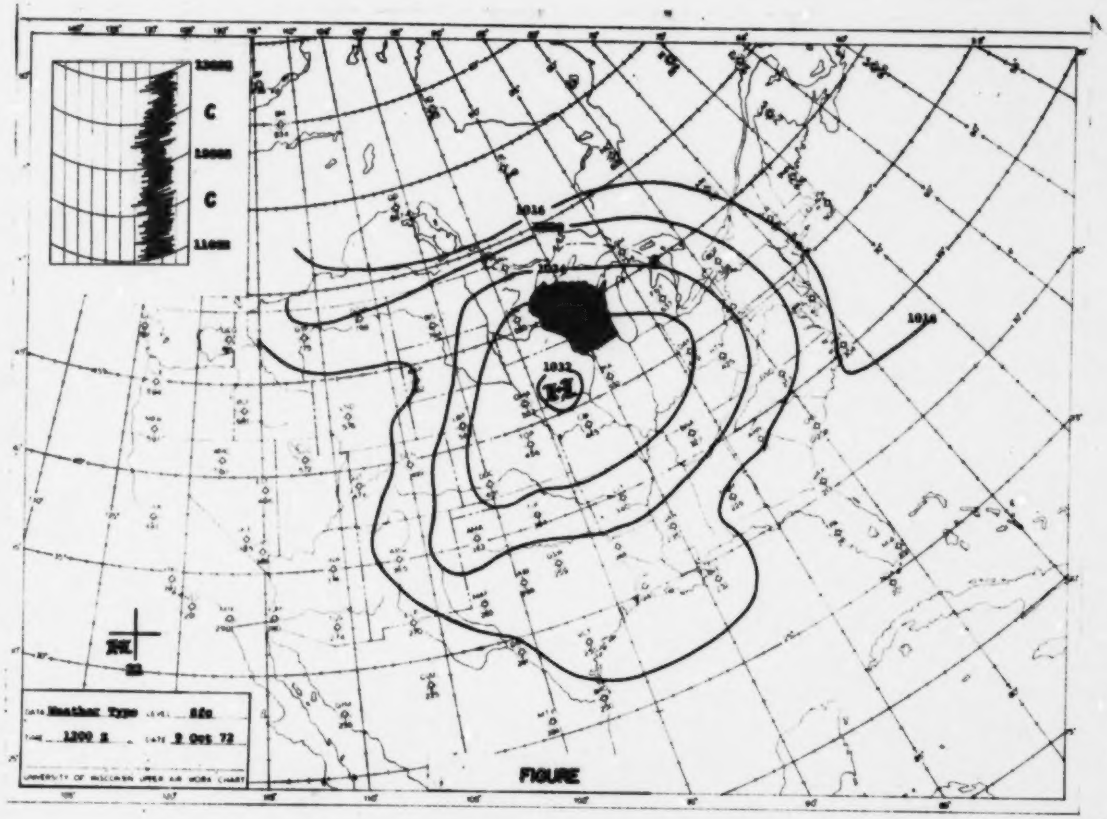
1300Z
C
1200Z
C
1100Z
1016
1024
1032
H
22
DATA Weather Type
LEVEL Sfc
TIME 1200 Z
DATE 9 Oct 72
UNIVERSITY OF WISCONSIN UPPER AIR WORK CHART
FIGURE

Figure 19. Surface pressure map for 1200Z (0600 CST), 9 October 1972. Isobaric pattern identified as weather type 22 (anticyclone center to the southwest of Portage, Wisconsin). Insert refers to the corresponding wind direction trace for the 1100Z to 1300Z period. Recorded at the Messer site.

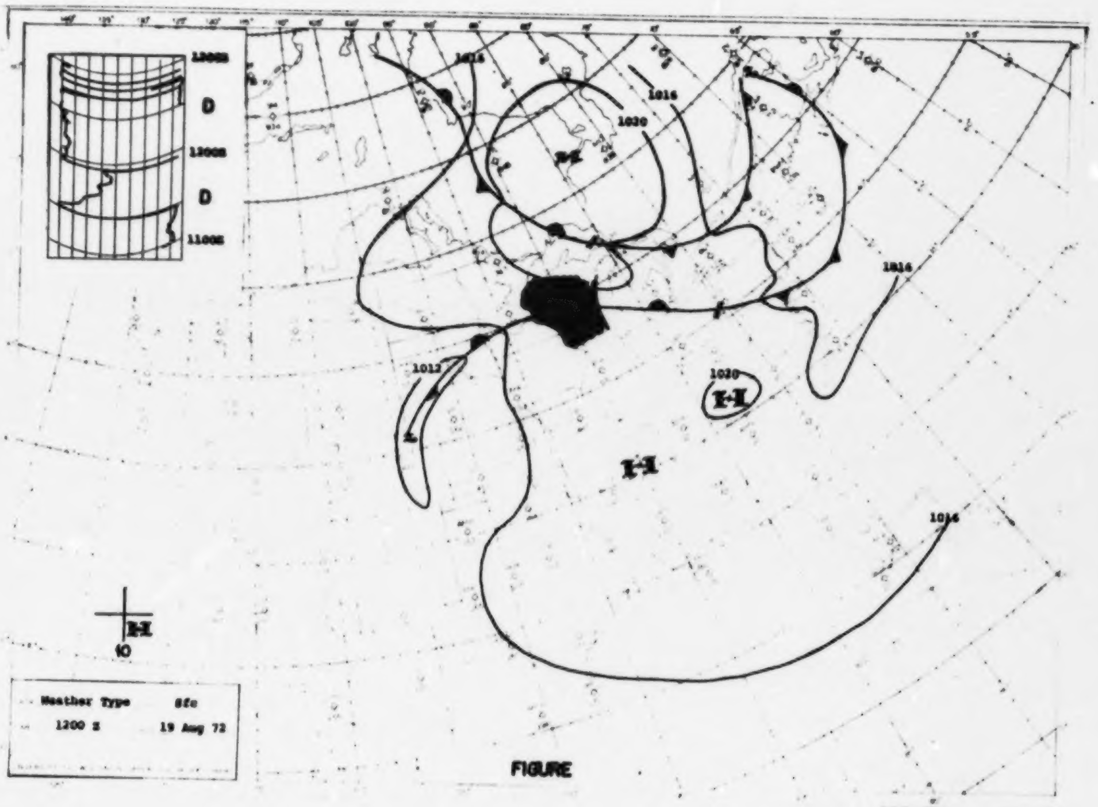
1200Z
D
1200Z
D
1100Z
1016
1016
1020
1016
1012
1030
1016
10
Weather Type
Sfc
1200 Z
19 Aug 72
FIGURE

Figure 20. Surface pressure map for 1200Z (0600 CST), 19 August 1972. Isobaric pattern identified as weather type 10 (anticyclone center to the southeast of Portage, Wisconsin). Insert refers to the corresponding wind direction trace for the 1100Z to 1300Z period. Recorded at the Messer site.

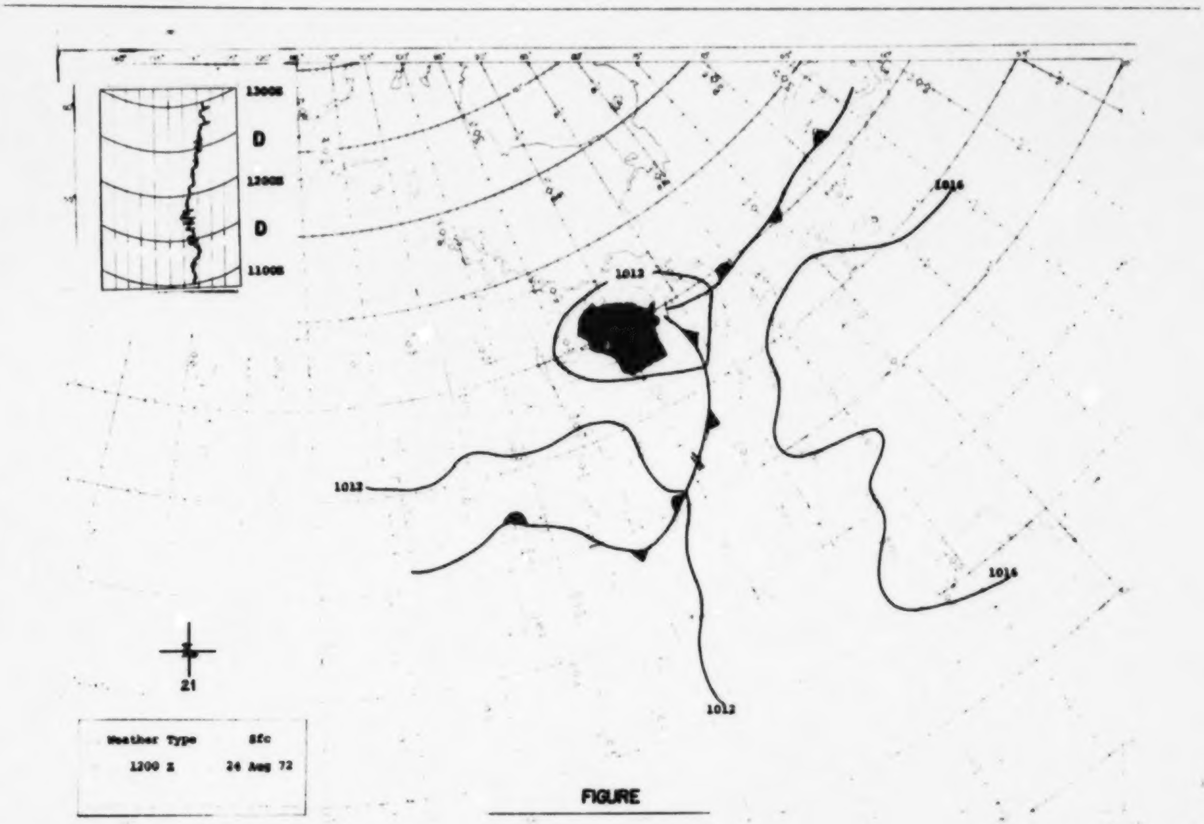
1300Z
D
1200Z
D
1100Z
1012
1016
1012
1016
1012
21
Weather Type
Sfc
1200 Z
24 Aug 72
FIGURE

Figure 21. Surface pressure map for 1200Z (0600 CST), 24 August 1972. Isobaric pattern identified as weather type 2 (cyclone center within 5° latitude of Portage, Wisconsin). Insert refers to the corresponding wind direction trace for the 1100Z to 1300Z period. Recorded at the Messer site.

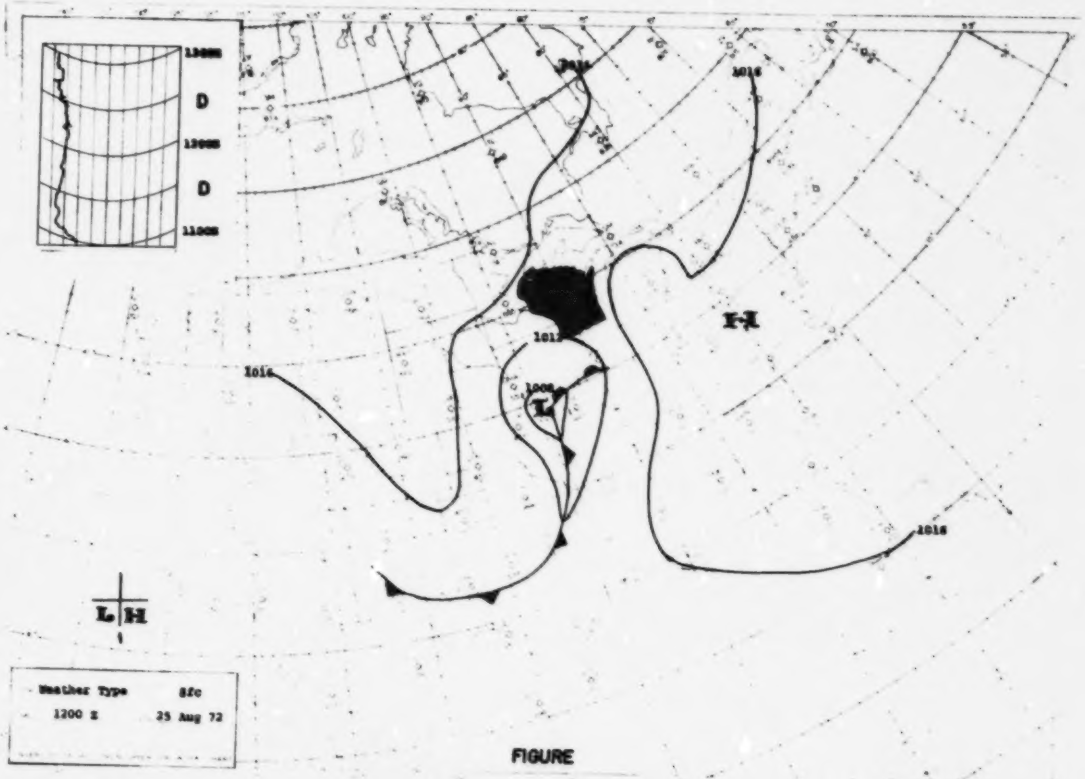
1300Z
D
1200Z
D
1100Z
1016
1012
1008
L
H
L
H
Weather Type
Sfc
1200 Z
25 Aug 72
FIGURE

Figure 22. Surface pressure map for 1200Z (0600 CST), 25 August 1972. Isobaric pattern identified as weather type 1 (cyclone center to the southwest of and anticylone to the southeast of Portage, Wisconsin). Insert refers to the corresponding wind direction trace for the 1100Z to 1300Z period. Recorded at the Messer site.

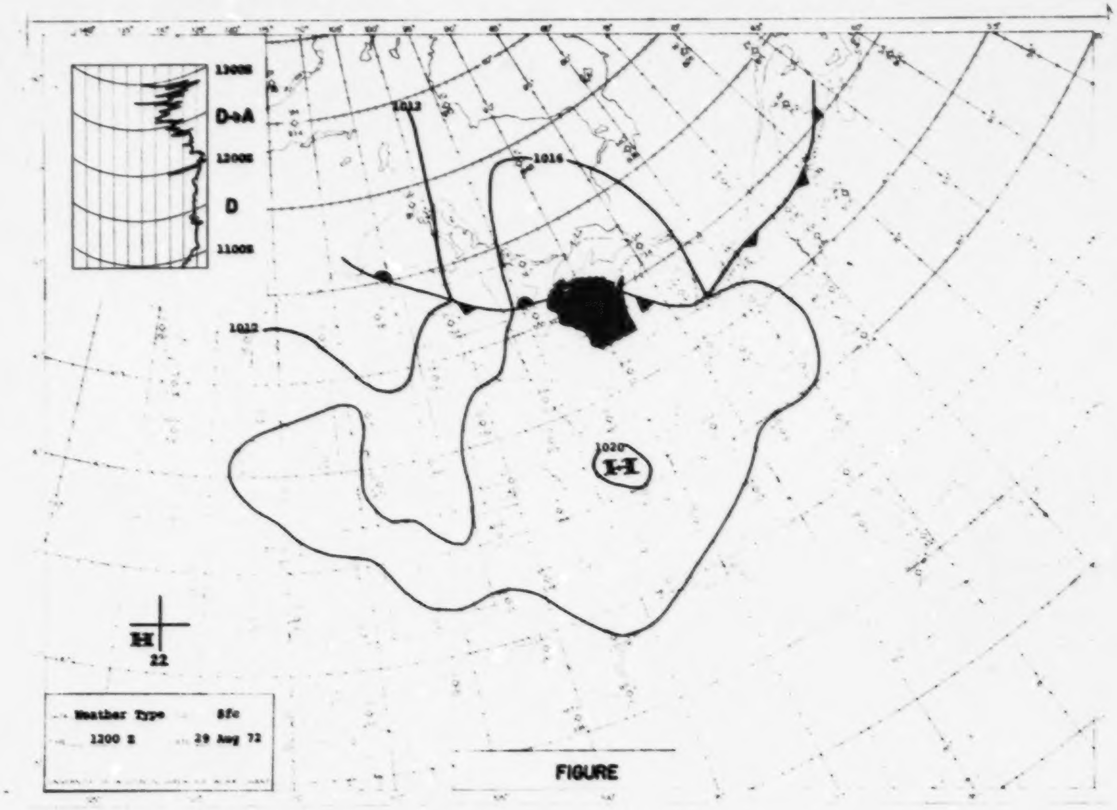
1300Z
D→A
1200Z
D
1100Z
1012
1016
1012
1020
H
H
22
Weather Type
Sfc
1200 Z
29 Aug 72
FIGURE

Figure 23. Surface pressure map for 1200Z (0600 CST), 29 August 1972. Isobaric pattern identified as weather type 22 (anticyclone center to the southwest of Portage, Wisconsin). Insert refers to the corresponding wind direction trace for the 1100Z to 1300Z period. Recorded at the Messer site.

TABLE 5. MICROFORECAST CHART BASED ON RECORDS FOR AUGUST THROUGH SEPTEMBER 1972

Expected gustiness class	Preferred months	Cloud cover[a]	Advection characteristics	General air mass lapse	Low level lapse $\frac{\Delta T}{300\ m}$ (^{0}C)	Remarks on the wind traces
A	Aug.-Sept.	○ to ◔	Low level cool air influx with neutral advection aloft	Conditionally unstable	Slight lapse	Typical under sunny skies after early morning inversion dissipation.
B_1	Oct.	◔	Warm to neutral	Conditionally unstable	Stable +1.0 to 2.0	Often seen with moderate winds during an early monring inversion followed by an increased post-sunrise convective turbulence.
	Oct.	◕ to ●	Cool advection favorable	Conditionally unstable	Generally neutral	Common with 3 to 5 m/sec wind speeds in advance of an approaching cyclone.
B_2	Sept.	○ to ◔	Warm influx through most layers aloft	Conditionally unstable	Stable +1.5 to 2.0	Similar to the first instance of the B_1 type except wind speeds less, stability large.
C	Any	◕	Weak low level warm advection with strong cold advection at a higher level	Stable	Stable +0.0 to 0.5	Traces typical of a fall day on the northern portions of an expansive anticyclone. Wind speeds generally of moderate intensity.
D	Aug.-Oct.	○ to ◔	Generally warm advection aloft	Stable	Stable +1.0 to 1.5	Common with light winds and clear skies during early morning inversion conditions.
	Aug.-Oct.	○ to ●	Generally cold advection aloft	Conditionally unstable	Lapse or stable -2.0 to +1.0	Found during rapidly changing lapse rates before a cyclone passage.

[a] ○ clear; ◔< 50% cloudiness; ◕> 50% cloudiness; ● overcast.

values of ξ_θ and ξ_w were not as consequential as was the persistence of downdrafts, regardless of turbulence character. The topography of the Baraboo Bluff becomes an overriding feature in wind flow across the valley because it disrupts cross-valley horizontal flow. However, it is not clear what effects bluff topography have on effluent dispersion, but westerly winds would be subject to impressed mountain-valley circulations. This situation commands attention, particularly during morning hours when fumigation could be enhanced with substantially increased ground level contaminant concentrations.

With regard to the synoptic conditions as indicators of dispersion, only intuitively satisfying results emerged (Table 5). A more complete inventory would be fruitful and would undoubtably result in minor alterations for each synoptic indicator; the basic framework of such a table appears sound. A distinguishing pattern of weather map types as dispersion indices did not appear, and logically so for such a short sampling interval. Based on this limited sample, two conclusions can be reached. First, it is evident that poor contaminant dilution conditions--especially D-type cases--appear during periods of weak, or eroding, horizontal pressure gradients. This is not surprising but there are indications that the isobaric analyses on the daily surface weather maps are of sufficiently poor resolution to preclude a true picture of local pressure gradients and mesoscale flow. Thus, regardless of the large-scale distribution of the cyclonic and anticyclonic pressure centers and the macroscale pressure gradients, local dispersion character remains a function of generally undetected local pressure variations. For an observer in the field, one would be forced to conclude that either (1) the researcher is familiar with the local mountain-valley circulations under a variety of synoptic conditions, or (2) the local pressure gradients need to be evaluated as a function of larger scale weather conditions with a suitable microbarograph network. The alternative appears to be to continue the procedures outlines in this study over a number of similar observation periods.

The possibility that a meaningful examination of dispersion characteristics for a region representative of the Columbia Electric Power Generating Site remains. Perhaps at a later date confirmation of the quality of a local "diffusion climatology" can be arrived at through photographic surveys or tracer analyses. The efforts of this research should not be looked on with disenchantment because regional environmental impact statements should continue to search for and encourage understandable and comprehensive meteorological inputs.

SECTION 5

STUDY OF THE LARGE-SCALE TRANSPORT OF LOW LEVEL OZONE ACROSS THE CENTRAL AND EASTERN UNITED STATES

INTRODUCTION

Photochemical oxidants (primarily ozone--O_3) were first recognized as urban air pollutants around Los Angeles in the early 1950s. By 1962, high O_3 levels were measured in several other large U.S. cities. Later, O_3 was found to be a problem in most of the 33 cities (Fankhauser 1976).

Further monitoring by state and local agencies in the 1970s indicated that high O_3 levels were present in rural areas, remote from urban areas. Levels of O_3 exceeding the national standard of 80 ppb have been documented in rural Maryland and West Virginia by Johnson et al. (1973) in rural New York by Stasiuk and Coffey (1974), and in rural Wisconsin by the Wisconsin Department of Natural Resources (1974).

Recent evidence shows that O_3 can be transported over long distances. Wolff et al. (1976) demonstrated that high O_3 levels formed in the Midwest and were advected to the Northeast. In addition, areas of restricted visibility due to haze coincided with areas of elevated O_3. An O_3 transport study of the Midwest by Samson and Ragland (1978) indicated that high O_3 levels occurred in regions of reported haze and that these haze areas had definite bounds which could be followed across the country.

This is a case history study of the distribution and transport of low-level O_3 east of the Rockies from 4 to 10 September 1976. Ozone data obtained from various state and federal agencies are used to construct daily maximum O_3 maps. Various meteorological analyses are presented in order to investigate possible relationships between high O_3 levels and weather conditions such as visibility. Backward trajectories are constructed to trace air movements in the boundary layer.

CHEMISTRY OF ZONE

Photochemical Production

Formation of Ozone Precursors: Nitrogen--

Oxides--The photochemical production of O_3 occurs in the presence of nitrogen oxides (NO_x) and sunlight. The two primary nitrogen oxides in the lower atmosphere are NO and NO_2. High-temperature combustion processes (i.e., automobiles, fossil power plants, etc.) form them. Nitric oxide is formed initially under high temperatures by two coincident reactions known as the Zeldovich mechanism (Schuck and Stephens 1969):

$$N + O_2 = NO + O \tag{23}$$

$$O + N_2 = NO + N. \tag{24}$$

The overall reaction is summarized:

$$N_2 + O_2 = 2NO. \tag{25}$$

The newly formed NO can be reconverted to O_2 and N_2 if the effluent is cooled slowly. However, NO and other exhaust products are cooled quickly as they are emitted into the atmosphere, thereby "fixing" the NO concentration.

As NO begins to mix with O_2 in the atmosphere. NO_2 is formed by oxidation of NO (Schuck and Stephenson 1969):

$$2NO + O_2 = 2NO_2 \tag{26}$$

However, the bulk of the NO is not oxidized quickly in this manner, since the three-body reaction in Eq. (26) depends heavily on the NO and O_2 concentrations. When the NO-laden plume enters the atmosphere, O_2 levels in the plume are low, preventing a large amount of oxidation. Conversely, when the plume has dispersed and entrained much O_2, NO levels become relatively small preventing significant oxidation.

NO_2-NO-O_3 Cycle--

Ozone is photochemically produced in the presence of NO_2 and sunlight. Nitrogen dioxide is a brownish gas which derives its color from selective absorption of sunlight of wavelengths 0.60 to 0.38 μ. With absorption of wavelengths < 0.40 μ (E), NO_2 dissociates into NO and atomic oxygen (Schuck and Stephens 1969):

$$NO_2 + E = NO + O^{\bullet} \quad (27)$$

where the dot signifies an unshared valence electron. The unstable $O^{\bullet}$ combines with O_2 to form O_3:

$$O^{\bullet} + O_2 + M = O_3 + M. \quad (28)$$

In this equation M represents any molecule which absorbs the excess energy created in the reaction. The absorbing molecule usually is N_2. The third reaction is the oxidation of NO to NO_2 (Stephens 1969):

$$NO + O_3 = NO_2 + O_2. \quad (29)$$

When Eqs. (4 through 6) are analyzed and solved with their rate constants, the O_3 concentration can be predicted by:

$$[O_3] = kI \frac{[NO_2]}{[NO]} , \quad (30)$$

where I is intensity of sunlight and K is a constant dependent on the absorption characteristics of NO_2 and the rate constant for Eq. (2). Leighton (1961) indicates that Eq. (30) must control the concentrations of O_3 since the reactions in Eqs. (27 through 29) proceed faster than any other known reactions taking place in the lower atmosphere.

In reality, O_3 levels in urban areas exceed levels predicted by the NO_2-NO-O_3 cycle. For example, O_3 levels in the Los Angeles area were sometimes as much as 10 times higher than predicted. Therefore, this cycle alone is not capable of explaining elevated O_3 levels in urban areas and another mechanism must exist.

Role of Hydrocarbons--

The presence of various reactive hydrocarbons (RHCs) emitted in the urban atmosphere alters the NO_2-NO-O_3 equilibrium, allowing build-up of O_3 levels. The primary source of RHCs in most cities is automobile exhaust (Perkins 1970). Industrial processes using solvents also are important contributors.

This section briefly describes the most important processes involving RHC and O_3 formation. Williamson (1973) and Perkins (1974) provide a more rigorous and complete explanation.

An atom of oxygen formed by the photodissociation of NO_2 in Eq. (27) can attack a RHCs; e.g., an olefin (a hydrocarbon with one or more C=C) is split easily into two organic molecules by an oxygen atom. Olefins are highly reactive because their double bonds are easily broken to form highly reactive free radicals. This olefin-oxygen atom reaction can be represented by:

$$O + \text{Olefin} = R^{\bullet} + R'O^{\bullet} \;. \qquad (31)$$

where R and R' are organic radicals. The dots signify an unshared valence electron, making the end products reactive free radicals. Organic free radicals can react with O_2 to form peroxy radicals (species ending in $OO^{\bullet}$):

$$R + O_2 = ROO^{\bullet} \qquad (32)$$

It is the peroxy radicals which allow elevated O_3 levels in the urban atmosphere. They accomplish this by competing with O_3 in reacting with NO. A peroxy radical reacts with NO to yield NO_2 and forms another free radical:

$$ROO^{\bullet} + NO = RO^{\bullet} + NO_2 \;. \qquad (33)$$

Although one less potential O_3 molecule is formed due to the involvement of an $O^{\bullet}$ with an RHC, more than one NO molecule is depleted for each RHC an $O^{\bullet}$ attacks. This explains the buildup of O_3 due to RHCs.

The reaction rates of RHCs and their products are much smaller when compared to the rates of reaction in the NO_2-NO-O_3 cycle. However, the equilibrium in the NO_2-NO-O_3 cycle is delicate and is disturbed by the presence of RHCs. The time needed to allow for maximum concentration of O_3 in the air has been estimated to be from 0.5 to 3 hr (Ripperton et al. 1971, and Leighton 1961), depending on meteorological conditions.

The effect of reactive RHCs on the NO_2-NO-O_3 cycle is shown in Figure 24. As can be seen, sunlight and NO_2 are necessary for the production of O_3. In addition, RHCs play the important role of slowly building up O_3 levels by competing with O_3 for NO.

Based on calculations made by Friedlander and Seinfeld (1969), RHCs, NO, NO_2, and O_3 levels in urban atmospheres can be predicted by a dynamic model. It was found that the variation in time of these chemicals in the model was similar to the variation found in cities. This dynamic aspect of the pollutant level is illustrated in Figure 25 (U.S. Department of Health, Education and Welfare 1970). For the day in question in Philadelphia, NO, NO_2, oxidant (mostly O_3), and non-methane RHC levels are plotted against time of day. It should be noted that the O_3 peak occurred at 10:00 a.m. while the NO_2 peak occurred at 7:00 a.m. This lag is due to the importance of the photodecomposition of NO_2 by sunlight, which produces O_3. The effect of the RHCs is also demonstrated by the low levels of NO encountered by 9:00 a.m. while O_3 and RHC levels simultaneously increased.

Meteorological Effects

The rate of O_3 formation depends on the intensity of sunlight since the rate of NO_2 photodecomposition is directly proportional to sunlight intensity. The reactions of RHCs are also important in the buildup of O_3 because of their independence on sunlight intensity. This means that less O_3 is produced in winter than in summer because of the decreased intensity and frequency of sunlight. Cloudy conditions also restrict O_3 formation and O_3 is not produced at night.

Temperature is another important variable in O_3 formation. Air temperature determines the ground state energy of all chemical species, including the reactants important in O_3 formation. Higher temperatures encourage greater and faster O_3 production (e.g., Pitts et al. 1961). It has been demonstrated that NO_2 can be photodecomposed at slightly longer wavelengths of sunlight as air temperatures increase (Pitts et al. 1961). As previously mentioned, NO_2 is decomposed by sunlight with wavelengths $< 0.4\ \mu$. Since an increasing amount of sunlight is attenuated with wavelengths $< 0.4\ \mu$ the effect of higher temperature can be important in the formation of O_3 by the breakdown of NO_2. Bufalini and Altshuller (1963) indicated that a temperature increase of 22°C doubles the rate of NO and RHC oxidants. Also, Alley and Ribberton (1961) demonstrated that with a 20°C temperature increase, the production rate of O_3 was increased fourfold in some systems.

The most favorable time for high O_3 levels is in summer when sunlight is intense and air temperatures are high. The effect of other meteorological factors on O_3 levels are considered in later sections.

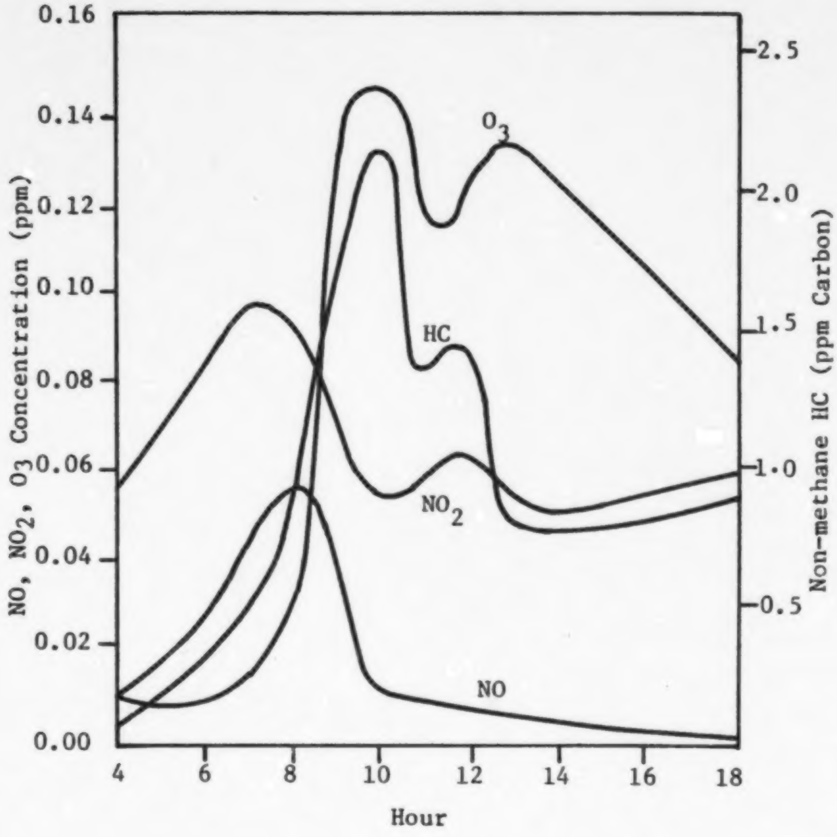

Figure 24. Hourly variation of selected pollutants in Philadelphia on Tuesday, 18 July 1967 (U.S. Department of Health, Education and Welfare 1970).

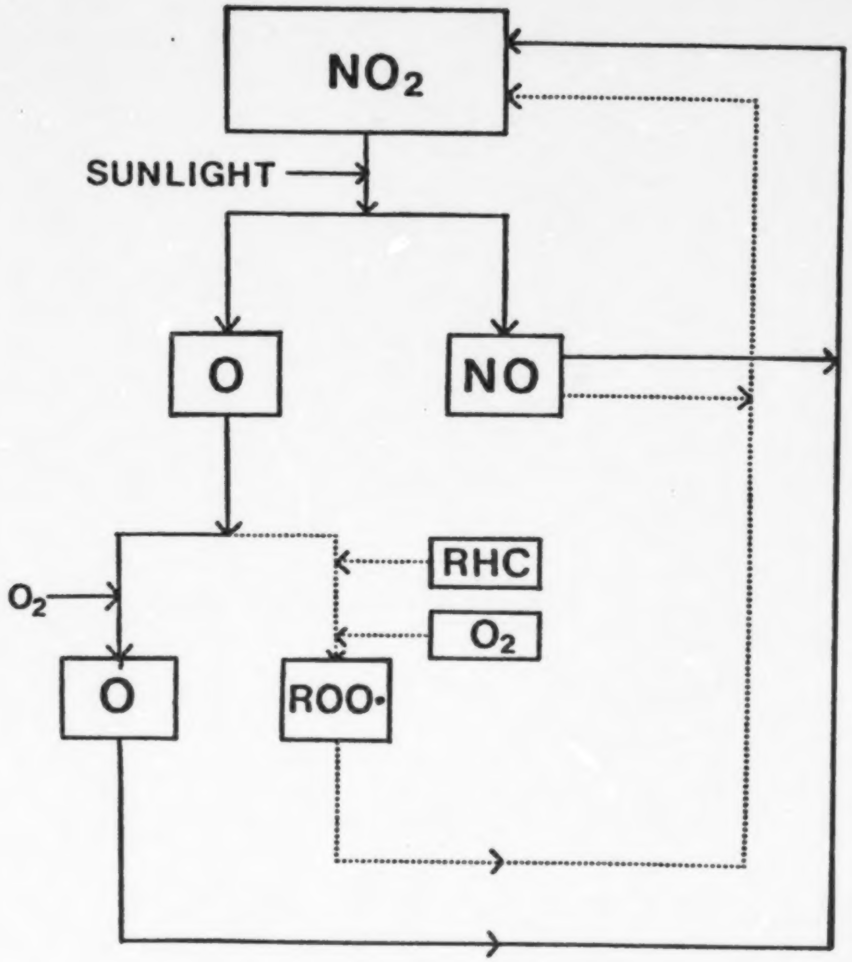
NO2
SUNLIGHT
O
NO
RHC
O2
O2
O
ROO·

Figure 25. Flow chart of O_3 photochemical cycle. Solid lines indicate fast reactions and dashed lines indicate slow reactions.

Destruction of Ozone

As pointed out earlier, NO reacts with O_3 to form NO_2. Therefore, as O_3-laden air is injected with fresh emissions of NO, O_3 levels decrease. It has been shown that a rural coal-fired power plant can appreciably reduce ambient O_3 levels in the plume up to 10 km downwind from the plant (see Section 6). The addition of NO to the air by the power plant causes this. Similarly, O_3 levels are often lower in cities than upwind from them since fresh emissions of NO deplete the O_3 levels in the cities.

Furthermore, O_3 can be depleted by contact with the ground, vegetation, and other objects. Kroening and Ney (1962) and van Dop et al. (1977) have demonstrated the importance of the ground as a sink for O_3. Galbally (1969) showed that during conditions of strong vertical mixing in a rural setting O_3 levels often decreased 2 ppb at 16 to 1 m above the ground. Galbally (1968) described a nocturnal surface inversion in a rural area in which the O_3 level increased from 5 ppb at 1 m, to 12 ppb at 3 m, and to 25 ppb at 200 m above the surface.

FACTORS AFFECTING LOCAL OZONE LEVELS

Quantity of Primary Pollutants

As previously discussed, O_3 production depends on the concentration of NO_x and RHCs. The abundance of these O_3 precursors in and downwind of cities and industrial areas accounts for the large O_3 concentrations in these areas.

The ratio of RHCs to NO_x also is an important factor determining O_3 formation. Allwind and Westberg (1977) showed that a RHC:NO_x ratio of 14 optimizes O_3 production as determined by spiking in bags of air samples collected in southeastern Wisconsin with NO_x.

Meteorological Effects

Two meteorological variables--sunlight and temperature--help determine the amount of O_3 produced. More O_3 is formed with greater solar radiation and higher temperatures.

Two other meteorological variables affect the ground levels of O_3 by determining its distribution in the lower atmosphere. These variables--mixing height and wind speed--determine the volume of air that "loads up" with O_3 and its precursors. The mixing height is the height below which air is mixed thoroughly by turbulence. Surface heating by the sun drives the afternoon mixed layer. Above the mixing height an inversion exists which acts as a lid to pollutants, preventing them from reaching higher levels. A low mixing height can cause high levels of O_3 and other pollutants in and downwind of populated areas; e.g., the coast of California is subject to sea breezes and winds from the relatively cool Pacific Ocean and frequently experiences marine inversions. It has been shown that high O_3 levels generally occur on days with a marine inversion (Sandberg and Thuiller 1970, Angell et al. 1970, Kauper 1960, and Stephens 1968). Similarly, flows off the Great Lakes can create high O_3 levels. Regions along the western shore of Lake Michigan experienced high O_3 levels, especially on days with lake breezes or onshore large-scale winds (Lyons and Cole 1973, 1976). The Chicago-Gary area was cited as the source.

Light winds also encourage high concentrations of pollutants. One reason is that light winds result in pollutant release to only a relatively small volume of air. In addition, less mechanical turbulence occurs with light winds which--in turn--limits vertical and horizontal dispersion of the pollutants.

LARGE-SCALE TRANSPORT OF OZONE

In recent years, because of more intensive O_3 monitoring, high O_3 levels have been discovered in many rural areas remote from large cities or other sources of obvious pollution. Levels of O_3 exceeding the national standard of 80 ppb have been documented in rural Wisconsin by the Wisconsin Department of Natural Resources (1975) and in rural New York by Stasiuk and Coffey (1974).

These reports and others indicate that elevated O_3 levels ocur typically in rural and urban areas when a high pressure system is over or east of the affected region. Since warmer air is advected northward on the west side of the ridge, high O_3 levels coincide generally with high air temperatures. The O_3 levels invariably drop after the passage of a cold front.

Several recent case studies support the idea of large-scale O_3 transport. Wolff et al. (1976), in a case study during April 1976, revealed that elevated O_3 levels developed initially in Indiana and Ohio near the center of a high pressure system. Over the next few days this area expanded and extended from Wisconsin and Illinois to the Atlantic coast. Trajectory analyses agreed with the movement of high O_3 levels from the Midwest to the East Coast.

It is evident that widespread O_3 episodes occur near or west of surface high pressure systems. This can be understood by studying the characteristic weather conditions associated with a high pressure system. High pressure systems frequently originate in Canada and migrate across the Midwest and the southeastern U.S. Many times they become stagnant and remain over the southeastern U.S. or over the Atlantic Ocean.

For example, as a high pressure system approaches the Midwest, it typically brings cool, clear, breezy conditions. Since the air originated in Canada it is low in O_3 and other pollutants. When the system moves over the Midwest, winds become light and daytime levels of O_3 and other pollutants can become high over heavily populated areas. At night a strong radiation surface inversion forms, encouraging high levels of most pollutants, but limiting levels of O_3. The reason is that the O_3 formed earlier in the day is depleted by NO and by contact with the ground.

The most widespread cases of elevated O_3 levels occur when the high passes to the east or south of a region. One reason for the elevated levels is that O_3 is formed locally. This is true because as a high passes a region, sunny conditions continue while winds remain rather light. In addition, warmer air is advected into the region from the south. As mentioned earlier, O_3 can be formed more readily in warm air.

Ozone can be transported along with warm air over great distances. During the day, winds on the western side of an anticyclone can pass several cities, causing the entire mixed layer below the subsidence inversion to become O_3-laden. At sunset a radiation inversion forms near the ground, which decouples the air above the inversion from the ground. Since the O_3-laden air above the surface inversion is not subjected to large emissions of NO from below or contact with the ground, it can be conserved partially as it is advected. After traveling hundreds of miles overnight, the O_3 fumigates to the ground after sunrise when the surface inversion has disappeared. The surface O_3 levels typically reach a maximum in mid-afternoon when low-level mixing is at a maximum. Coffey and Stasiuk (1975) showed that for several sites in New York state, the maximum O_3 concentrations usually occurred near the times of a maximum surface temperature and windspeed.

The transport of O_3 by the boundary layer during the day and night is indicated by aerial O_3 monitoring conducted by the Wisconsin Department of Natural Resources from 1974 to 1976. Many of these flights revealed that high O_3 levels (80 ppb) were quite uniform horizontally and vertically over rural areas of Wisconsin and northern Illinois during O_3 episodes. More importantly, several evening and early morning flights revealed that high levels of O_3 existed above a surface-based inversion, with much lower levels prevalent near the ground.

Comparing O_3 levels on several rural mountainsites (over 1000 m) in New York with other rural and urban sites (Stasivk and Coffey 1974) further evidences O_3 transport. It was shown that a strong correlation existed between all the sites with high levels common to all sites. Most importantly, very little diurnal variation was found at the mountain site where a nocturnal radiation inversion is not expected. On the other hand, the lower sites displayed a strong diurnal cycle, with O_3 levels approaching those of the mountain sites in mid-afternoon and falling to lower values overnight.

The importance of large-scale O_3 transport depends on the lifetime of O_3. Based on vertical profiles of O_3, Ripperton (1976) estimated the O_3 half-life above the nocturnal inversion layer to be approximately 29 hr. This long lifetime allows O_3 to be efficiently transported during nighttime hours. During the day, when it comes in contact with the ground, its half-life is shorter. However, more O_3 is formed during the day.

NATURAL SOURCES OF OZONE

Stratospheric Ozone

Ozone is formed naturally in the stratosphere. Sunlight with wavelengths < 0.24 μ can split O_2 into two unstable atoms. The atoms are then free to combine with O_2 to form O_3.

Average maximum density of stratospheric O_3 is approximately 4.86×10^{18} molecules/m^3 or 4000 ppb at a height of 22 km at 4° N latitude (U.S. Standard Atmosphere 1976). However, this concentration is equivalent to 200 ppb O_3 and essentially decreases exponentially above and below 22 km, decreasing by an order of magnitude near 41 and 6 km height.

The O_3 from the stratosphere undeniably contributes to ground level concentrations of O_3. Except for areas affected by photochemical air pollution, ambient ground levels of O_3 in the northern hemisphere are consistently near 20 ppb (Junge 1963). However, there is overwhelming evidence that stratospheric O_3 is not the principle cause of elevated O_3 levels (80 ppb) common in the United States. Extensive aerial monitoring of O_3 by the Wisconsin Department of Natural Resources (1975 to 1976) indicates that O_3 levels decreased markedly in Wisconsin at altitudes 1500 to 7500 m above the ground. This demonstrates that the stratosphere is not a primary contributor of the high surface O_3 levels. Furthermore, high O_3 levels are usually found on the western side of a high pressure systems. Strong downwind air motion from the stratosphere is not expected in this portion of a high.

Hydrocarbons from Forests

Another possible source of O_3 arises from photochemical synthesis by RHCs emitted from trees. The fraction of O_3 produced by this process is believed to be small. Lyons and Cole (1976) point out that O_3 levels in Wisconsin generally are greater south or upwind of the heavily forested areas of northern Wisconsin, casting doubt on the importance of trees in O_3 formation. Furthermore, no cases of high O_3 levels can be attributed to forests.

DATA AND METHODOLOGY

Ozone Data

Available O_3 data for states east of the Rocky Mountains is used in the case study. Hourly O_3 data was obtained for most of states in which O_3 is monitored. In addition, daily maximum O_3 concentrations were supplied by the Interstate Commerce Commission. The vast majority of O_3 data was measured by chemiluminescent O_3 monitors approved by the EPA.

Figure 26 shows the network of O_3 monitors which supplied data. The numbers in the figure represent the populations of cities. It does not show all of the monitors in some of the cities where multiple monitoring stations are located.

The technique of constructing daily O_3 isopleth maps was first used by Wolff et al. (1978). Daily O_3 maxima exceeding 70 and 100 ppb are analyzed for the central and eastern U.S. Very little smoothing of the data was undertaken.

Several types of errors are probably present in the analyses. One possible source for error is that calibration of the monitors may differ from state to state and within states. Another problem is related to the fact that many of the monitors are located in downtown areas of cities where there are especially large NO emissions. Therefore, O_3 data from some cities may not represent the air mass levels of O_3 representative of areas upwind from the city. This problem may be particularly acute in areas of the country where O_3 is only measured inside large cities. Finally, several parts of the country have only a few O_3 monitors. In these areas, scarcity of O_3 data may preclude an accurate and reliable O_3 analysis.

Weather Data

All meteorological data presented in the case study were derived from the National Weather Service data. The specific sources included facsimile products and the Services A and C teletype circuits.

Three 18Z (12:00 CST) surface maps depicting sea level pressure and surface winds, visibility, and dew point are presented for each day. In addition, a 24Z (18:00 CST) 850-mb contour map and a maximum surface temperature map are presented daily.

Trajectory Analyses

Backward trajectories were computed at several selected sites during the study. The trajectories were calculated by a computerized post-facto

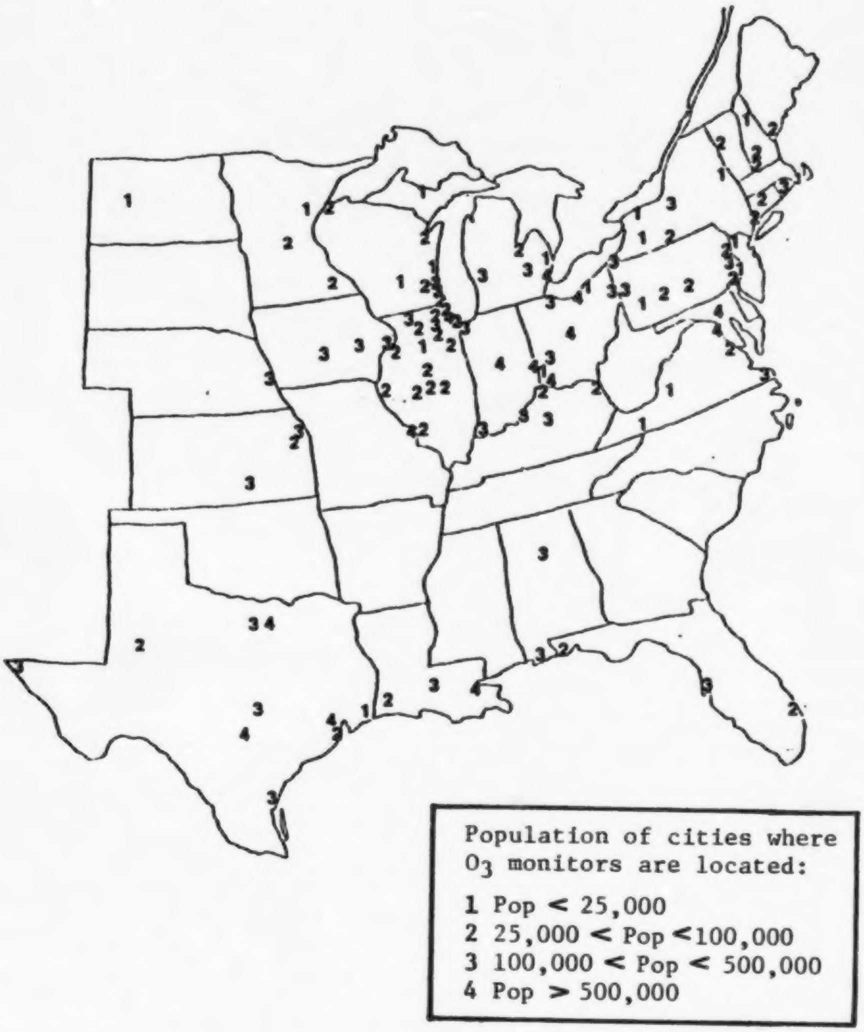
Population of cities where O_3 monitors are located:
1 Pop < 25,000
2 25,000 < Pop <100,000
3 100,000 < Pop < 500,000
4 Pop > 500,000

Figure 26. Distribution of O_3 monitors that supplied data for the case study. Numbers 1-4 represent populations of cities in which monitor is located (see key).

trajectory model (Heffter and Taylor 1975). The observed winds used in the model are available on magnetic tapes (USAF-ETAC). These tapes include surface and upper air wind reports for all reporting stations in theworld.

Each backward trajectory is a series of segments of length $\overline{u}\ \Delta t$, where Δt is 3 hr and $\overline{u}$ is the vector wind. The segment is calculated for a specific site by consideration of winds within a 300-nautical mile radius. The winds are weighted by the inverse squares of the distances from the observation sites to the end of the last trajectory segment. An additional weighting factor is employed to consider the alignment of the reported winds with respect to a specific site (i.e., observations directly upwind and downwind receive the greatest weight). Wind trajectory segments are computed only when the following criteria are met:

(1) At least two reporting stations are within 300 nautical miles or one station is within 150 nautical miles;
(2) At least two reporting wind levels are available at a reporting station to average the wind in the chosen layer.

In this study, the layer between 300 and 2000-m is considered for the trajectories. The 2000-m altitude was chosen as the representative top of the afternoon mixing layer (Heffter and Taylor 1975). A subsidence inversion was common over much of the country during the case study period. However, there were many instances in which no detectable subsidence inversion was present. Winds in the layer below 300 m were not considered because the winds were retarded by the earth's surface.

The backward trajectories are intended to approximate actual transport of air in the mixing layer. However, several errors are possible with trajectory analyses:

(1) Errors in wind observations;
(2) Errors in temporal and spatial interpolation of observed winds;
(3) Vertical motion is ignored by the model;
(4) Horizontal diffusion is ignored by the model.

Of all the errors, the neglect of horizontal diffusion is probably the most crucial. It should be emphasized that the trajectories represent the average horizontal path of all air parcels and not the absolute path of all parcels. Furthermore, the discrepancy between actual air motions and a trajectory increase as the length of time increases (i.e., as the trajectory becomes longer). Vertical motion of the air is important near low pressure systems and fronts. Therefore, great care must be used in interpreting trajectories in areas of strong vertical motion.

4 September 1976

On the first day of the study a surface high pressure system is located over the north central part of the country (Figure 27). A cold front extends from Lake Erie to southwestern Missouri where it turns into a warm front. A very weak low is situated in southwestern Kansas. At the 850-mb level an extensive ridge is located over the central part of the country, causing light winds with warm conditions over the Plains and southern Midwest.

Figure 28 shows two large areas with O_3 levels exceeding 70 ppb, one in the Plains and western Midwest and the other in the eastern Midwest. Another area is located along the East Coast megalopolis. Levels also exceed 70 ppb in the El Paso, Texas area. Included in Figure 28 are 24-hr backward trajectories.

Much of the eastern U.S. has visibilities < 10 km, the threshold used to report haze. The elevated O_3 area in the central U.S. (Figure 28) is not accompanied by an area of restricted visibility.

5 September 1976

The high pressure system over the Midwest has intensified slightly and is now located over northeastern Wisconsin (Figure 29). A low pressure system is centered north of Maine with a cold front trailing to the south and west into Arkansas. A strong warm front extends from Arkansas to southwestern Nebraska where a very weak low is present. A ridge with light winds extends from Texas into the Great Lakes. The Plains had the highest temperatures with cool conditions present over the Great Lakes.

Figure 30 shows that elevated O_3 levels persist over the Central Plains. Another area with O_3 levels exceeding 70 ppb is located over the East Coast. Trajectories indicate that high O_3 levels may have been advected into the East Coast. The trajectory ending at Richmond, Virginia shows that the 300 to 2000-m air layer was advected from southern Ohio in the past day, where high O_3 levels were previously common. The trajectories at Omaha, Nebraska and Wichita, Kansas show that the air has traveled within the area of high O_3 levels. The trajectory at Dallas-Fort Worth indicates very light winds.

The area most favorable for high O_3 level production covers Oklahoma, parts of Texas, and Arkansas. This area is under a high pressure ridge, and therefore has light winds; sunny skies and high temperatures also are common. The high O_3 levels in the Plains are not accompanied by low visibilities.

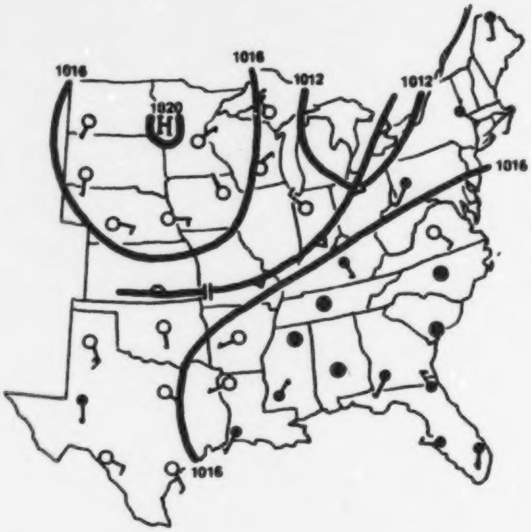
1016
1016
1012
1012
1020
H
1016
1016

Figure 27. 1800Z surface analysis for 4 September 1976. Full barb represents 5 m/sec wind speed. Circle around station indicates calm winds.

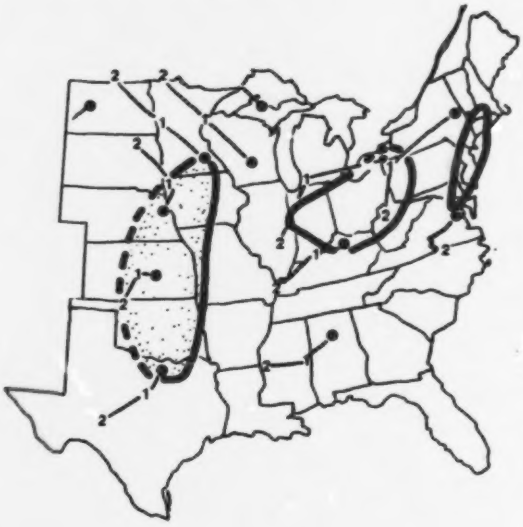
2
2
1
2
1
1
2
2
1
2
2
2
2
1
1
2

Figure 28. Ozone maximum isopleths and backward trajectories for 4 September 1976. Light hatching represents O_3 levels exceeding 100 ppb. All trajectories end at 1800Z.

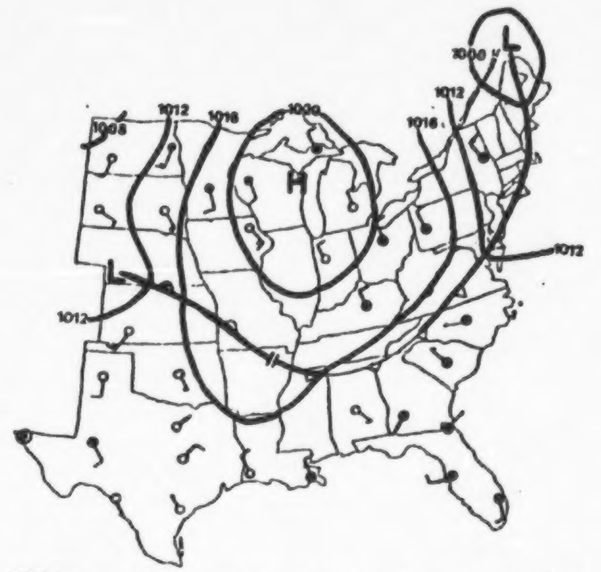
1008
1012
1016
1000
1016
1012
1000
H
L
1012
1012
L

Figure 29. 1800Z surface analysis for 5 September 1976. Full barb represents 5 m/sec wind speed. Circle around station indicates calm winds.

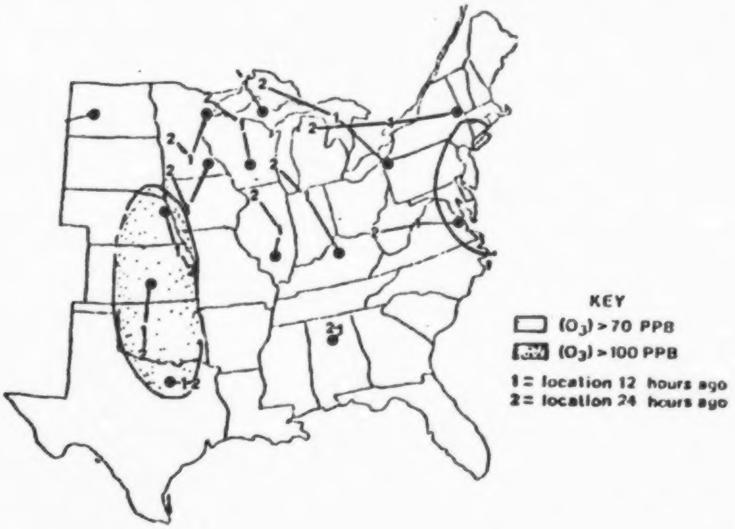
KEY
(O3)>70 PPB
(O3)>100 PPB
1= location 12 hours ago
2= location 24 hours ago

Figure 30. Ozone maximum isopleths and backward trajectories for 5 September 1976. Light hatching represents O_3 levels exceeding 70 ppb. Darker hatching represents O_3 levels exceeding 100 ppb. All trajectories end at 1800Z.

6 September 1976

The high pressure system has intensified further and is now centered over Ohio (Figure 31). Most of the country is experiencing sunny skies. An area of light winds is east of the line from Texas to Lake Huron, with strong winds in the northern Plains and northern Midwest. The warmest air is located over the northern Plains, with cooler conditions in the Northeast.

The area of elevated O_3 levels in the central U.S. has now drastically enlarged (Figure 32). Strong winds at 850 mb have helped to bring high O_3 levels as far north as the Canadian Border and as far east as the western Great Lakes. In this large area a smaller area with O_3 levels exceeding 100 ppb extends across southeastern Minnesota and central Wisconsin. Levels exceeding 100 ppb also are occurring along the western shores of Lake Michigan in northeastern Illinois and southeastern Wisconsin. The Birmingham, Alabama vicinity reports levels of O_3 exceeding 100 ppb.

Trajectory analysis shows the rapid northeastward movement of the 300 to 2000-m air in the north-central U.S. The lengths and direction of the trajectories account for the movement of the elevated O_3 area. The Northeast--still on the eastern side of the high--is under a northwesterly flow. The trajectory ending at Birmingham, Alabama indicates light winds which may explain the high O_3 levels.

Optimal conditions for the creation of high O_3 levels continue in the southern Plains. Sunny skies accompanied by light winds and high temperatures in the mixing layer continue to exist in this area. Strong winds--especially at 850 mb--in the north-central U.S. are unfavorable for the formation of high O_3 levels. These winds, however, are transporting O_3 from favorable regions (the southern Plains) into this area. Note that the elevated O_3 levels have spread northeastward into the upper Midwest by the averaged mixing layer winds. At the same time, surface winds are southeasterly. It is clear that large-scale transport of O_3 is not necessarily in the direction of the surface winds. Another important fact is that the region directly under the high center is protected from transport of high O_3 levels; transport cocurs on the western and northern perimeters of the high.

The southeastern U.S., under the effect of a cold front, has restricted visibilities. There are no large areas of elevated O_3 levels in this region.

7 September 1976

The center of the surface high pressure system has intensified slightly and moved to Virginia (Figure 33). The associated 850-mb high center also has intensified and is now located over the panhandle of Virginia. A distinct temperature maxima is present at the 850-mb surface level over

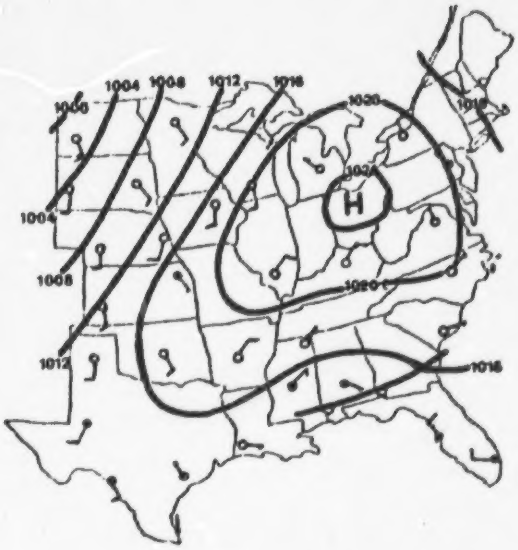
1000
1004
1008
1012
1016
1020
1024
H
1004
1008
1012
1020
1016
1016

Figure 31. 1800Z surface analysis for 6 September 1976. Full barb represents 5 m/sec wind speed. circle around station indicates calm winds.

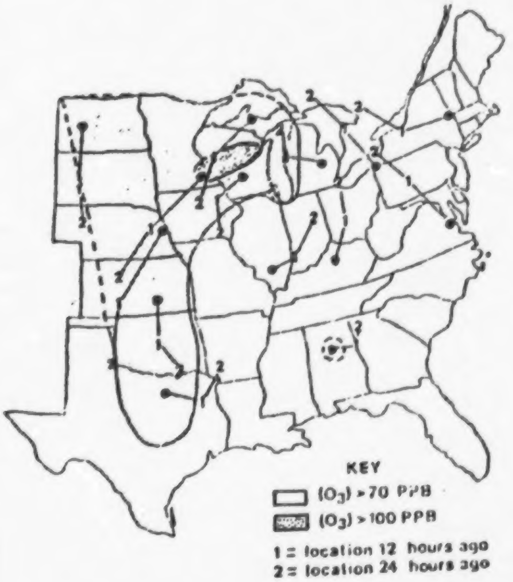
KEY
$(O_3) > 70$ PPB
$(O_3) > 100$ PPB
1 = location 12 hours ago
2 = location 24 hours ago

Figure 32. Ozone maximum isopleths and backward trajectories for 6 September 1976. Lighter hatching represents O_3 levels exceeding 70 ppb. Darker hatching represents O_3 levels exceeding 100 ppb. All trajectories end at 100 ppb.

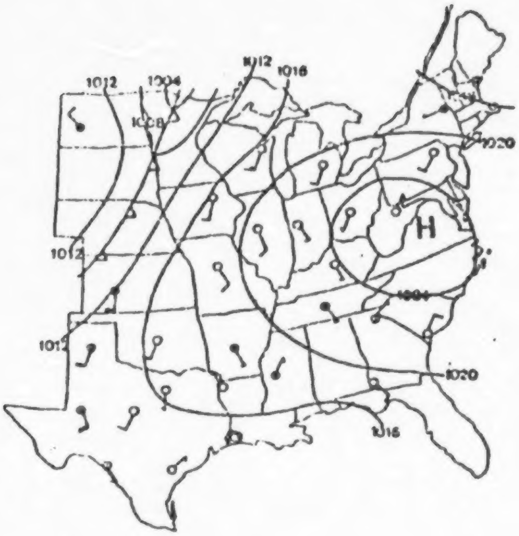
1012
1004
1012
1016
1008
1020
1012
H
1024
1012
1020
1016

Figure 33. 1800Z surface analysis for 7 September 1976. Full barb represents 5 m/sec wind speed. Circle around station indicates calm winds.

Wisconsin and Lake Superior, while the highest surface temperatures were recorded over parts of Minnesota, Wisconsin, and Iowa.

On this day, the large area with O_3 concentrations > 70 ppb has expanded further. It now extends in a band from the Texas and Louisiana shores of the Gulf of Mexico into the Midwest, and as far east as eastern New York. In this area, a region with concentrations > 100 ppb extends from northeastern Iowa and southeastern Minnesota to northern Michigan. Also, an area with concentrations of O_3 > 70 ppb has formed over the lower Ohio River Valley. In addition, three urban plumes with O_3 concentrations > 70 ppb are apparent downwind of St. Louis, Chicago, and New York City.

Trajectories ending on this day lend credence to the concept of large-scale O_3 transport (Figure 34). For example, the trajectory ending at Marquette, Michigan shows that the incoming air originated from Kansas--a distance of more than 1500 km--where elevated O_3 levels were common the day before. Trajectories also show the slow movement of the air in the southern Plains, encouraging formation of high O_3 levels there. The trajectory ending at Dallas-Fort Worth indicates that the 300 to 2000-m air has only travelled 300 km in the past 24 hr. Similarly, light windspeeds are evident over the Ohio River Valley. The trajectory ending at Lexington, Kentucky shows the slow, looping air movement during the passage of the high pressure center through the area. With light winds common over this heavily populated and industrialized area, O_3 levels are > 70 ppb. The trajectories show clearly that these elevated O_3 levels were not advected in, but more likely were formed regionally.

The weather conditions most favorable for formation of high O_3 levels were predominant on this day in the southern Plains and the Ohio River Valley. Once again, sunny skies, high temperatures, and light winds throughout the mixed layer were common in the southern Plains. These same conditions were prevalent for the first full day in the Ohio Valley Region. This explained the elevated O_3 levels formed there. Following the passage of a cold front, the high O_3 levels in the Dakotas have dissipated. Behind this front, northwest winds are bringing cold, clean air from Canada.

One important question remains to be answered: Why do O_3 levels begin to exceed 100 ppb in the Midwest but not in the Plains? One explanation may be that the air in the mixing layer accumulates more and more O_3 on its journey into the Midwest. Another possibility is that the O_3 monitors in the Plains are all located in rather large cities where fresh emissions of NO are large. The presence of high NO levels might lower the O_3 levels in the cities, thereby misrepresenting the actual higher O_3 levels that may exist in the rural areas. In the Midwest, several O_3 monitors are located in smaller cities where local NO emissions are too small to appreciably effect ambient O_3 levels.

Limited visibility is not a reliable indicator of high O_3 levels. Reduced visibility coincides with elevated O_3 levels only in southern Ohio.

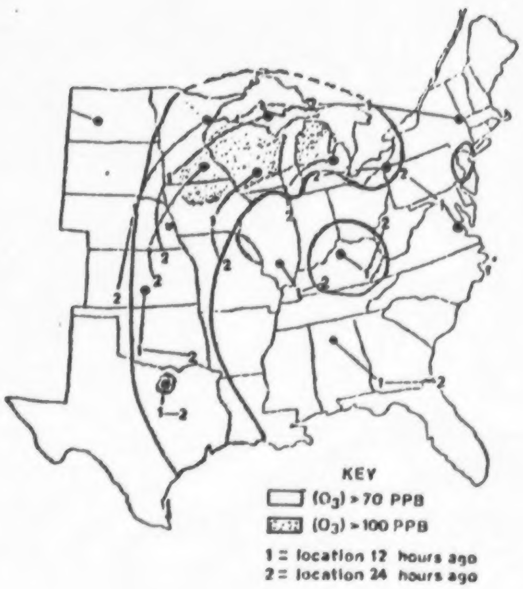
KEY
$(O_3) > 70$ PPB
$(O_3) > 100$ PPB
1 = location 12 hours ago
2 = location 24 hours ago

Figure 34. Ozone maximum isopleths and backward trajectories for 7 September 1976. Light hatching represents O_3 levels exceeding 70 ppb. Darker hatching represents O_3 levels exceeding 100 ppb. All trajectories end at 1800Z.

8 September 1976

The cold front located across the northern Plains on the previous day now extends from Wisconsin to the Texas Panhandle (Figure 35). A stationary front is present across southern New York. A high pressure system continues to dominate the eastern half of the country at the surface and 850-mb levels. The 850-mb temperature maximum has moved eastward to Lake Huron, while the area of highest surface temperatures--exceeding 30°C--now bulges northward over lower Michigan and Lake Huron. Cloudy skies are keeping temperatures slightly lower over an area centered over Tennessee, Alabama, and Mississippi.

The areas of elevated O_3 levels now differ greatly from the previous areas (Figure 36). The area with O_3 concentrations > 70 ppb located from the Texas and Louisiana Gulf to areas to the Great Lakes has now split, with the northern branch combining with the newly formed area over the Ohio Valley. The area with O_3 concentrations > 100 ppb over the Great Lakes area has retained its size from the previous day and is now entering western New York and northwestern Pennsylvania. Another area with O_3 concentrations $>$ 100 ppb has formed in the Washington D.C.-Philadelphia-New York City corridor. An area with O_3 concentrations > 70 ppb remains over Louisiana and western Texas.

A striking feature on this day is the coincidence between the location of the fronts and the boundaries of elevated O_3 areas. Behind the cold front in the central U.S., O_3 levels have dropped dramatically from the previous day. Also, O_3 levels are remaining < 70 ppb north of the stationary front lying across New York.

Trajectories ending on this day imply that elevated O_3 levels have been advected into the mid-Atlantic states in the past day. The trajectories ending at Albany, New York and Richmond, Virginia suggest that high O_3 levels over the western Midwest on the previous day have been advected to the East Coast. Looping trajectories ending at Indianapolis, Indiana and Lexington, Kentucky indicate that the high O_3 levels in this region are a result of regional O_3 production, not large-scale transport. Again, the trajectory ending at Dallas-Fort Worth shows little air movement, explaining the maintenance of elevated O_3 levels there.

Examination of the weather conditions on this day shows that optimal conditions for producing high O_3 levels are common in the west Texas and Louisiana area and in an area covering the eastern Midwest and mid-Atlantic states. In both areas, sunny skies along with light winds and high temperatures in the mixed layer are prevalent. The panhandle of Florida and the Birmingham, Alabama area had levels of ozone < 70 ppb, where an overcast of clouds was present.

A large area with visibilities < 15 km extends from the Gulf of Mexico to the eastern Midwest and into Canada. In this area is a rather large area with visibilities < 10 km (i.e., haze). The restricted visibilities are not due to showers or small dew point depressions (except for the Gulf states

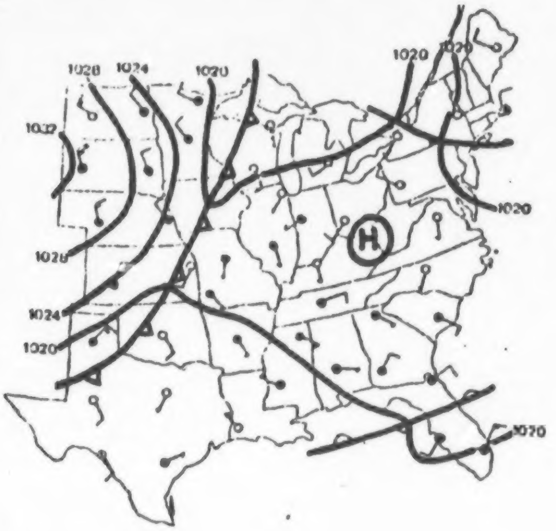
1028
1024
1020
1020
1020
1032
1028
1024
1020
H
1020
1020

Figure 35. 1800Z surface analysis for 8 September 1976. Full barb represents 5 m/sec wind speed. Circle around station indicates calm winds.

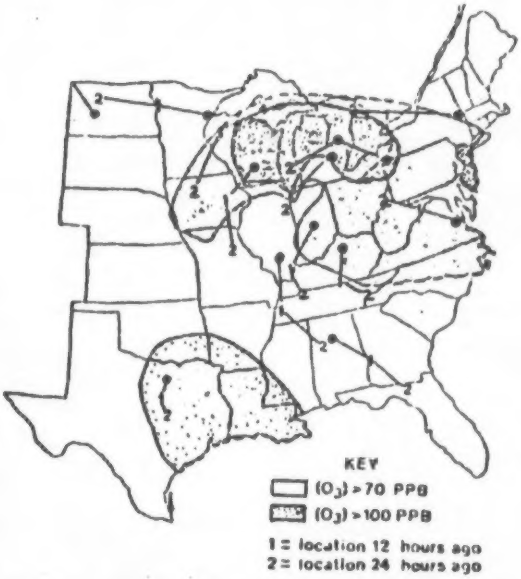
KEY
(O3) >70 PPB
(O3) >100 PPB
1 = location 12 hours ago
2 = location 24 hours ago

Figure 36. Ozone maximum isopleths and backward trajectories for 8 September 1976. Light hatching represents O_3 levels exceeding 70 ppb. Darker hatching represents O_3 levels exceeding 100 ppb. All trajectories end at 1800Z.

where showers are occurring). Showers also are present in parts of Minnesota and Wisconsin where there is a small area with visibilities < 15 km.

It is again evident that areas with high O_3 levels do not necessarily have restricted visibility. For example, most of Illinois has levels of O_3 < 70 ppb; however, most of the state has hazy conditions. Furthermore, the mid-Atlantic states have O_3 levels > 70 ppb, while the area has visibilities > 15 km.

9 September 1976

The high pressure system located over the eastern part of the country on the previous day has now broken down. A vigorous cold front and low pressure trough extends from Lake Huron to Texas (Figure 37). Along this front clouds and some showers are present. Another area of clouds and showers is situated over the southeastern states.

With the passage of the cold front across the central U.S., O_3 levels are < 70 ppb (Figure 38). An extensive area with O_3 levels > 70 ppb is present over the northeastern states, including a smaller area with O_3 levels > 100 ppb. Another area with elevated O_3 levels is present along the Gulf of Mexico.

Trajectories in Figure 38 indicate the eastward movement of the mixing layer air at Erie, Pennsylvania and Richmond, Virginia. However, at Albany, New York, which is located north of the stationary front, a northwesterly flow is apparent. This northerly flow is advecting "cleaner" air into northern New York.

The areas with the most favorable conditions for producing O_3 are in the northeastern states and the Gulf Coast. Sunny skies along with light winds and high temperatures prevail in these areas.

10 September 1976

A storm center has moved to a position north of Lake Ontario, with a trailing cold front extending along the East Coast into the Gulf of Mexico (Figure 39). A large high pressure system, with the center located in Oklahoma, dominates the central U.S. Temperatures are lower in the Midwest and northeastern U.S., while there are warmer conditions in the Southeast and northern Plains areas of the country.

The area of elevated O_3 levels in the Northeast (Figure 40) has moved north and east, extending into New England. A small area with O_3 > 100 ppb is located in parts of New York and Pennsylvania. Another area of elevated O_3 levels covers most of Texas, with the highest levels present in the Odessa region of western Texas.

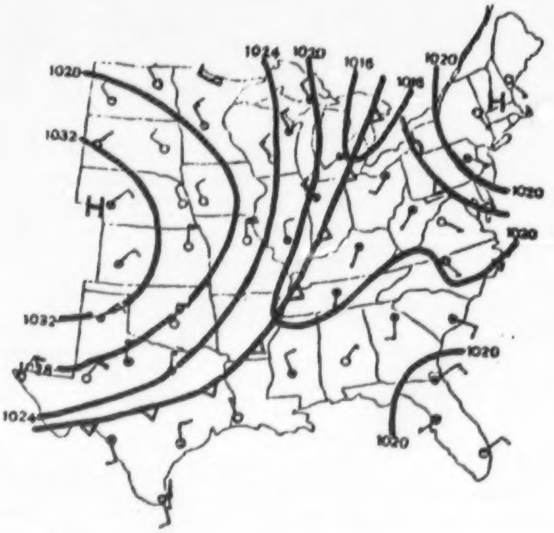

1028
1032
1024
1020
1016
1016
1020
H
H
1020
1020
1032
1020
1024
1024
1020

Figure 37. 1800Z surface analysis for 9 September 1976. Full barb represents 5 m/sec wind speed. Circle around station indicates calm winds.

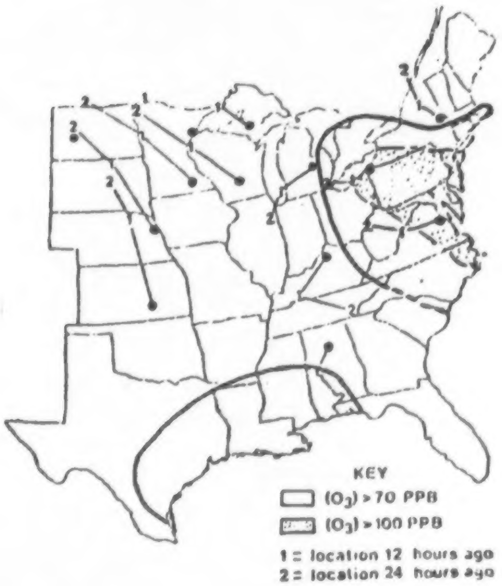

KEY
☐ $(O_3) > 70$ PPB
▨ $(O_3) > 100$ PPB
1 = location 12 hours ago
2 = location 24 hours ago

Figure 38. Ozone maximum isopleths and backward trajectories for 9 September 1976. Light hatching represents O_3 levels exceeding 70 ppb. Darker hatching represents O_3 levels exceeding 100 ppb. all trajectories end at 1800Z.

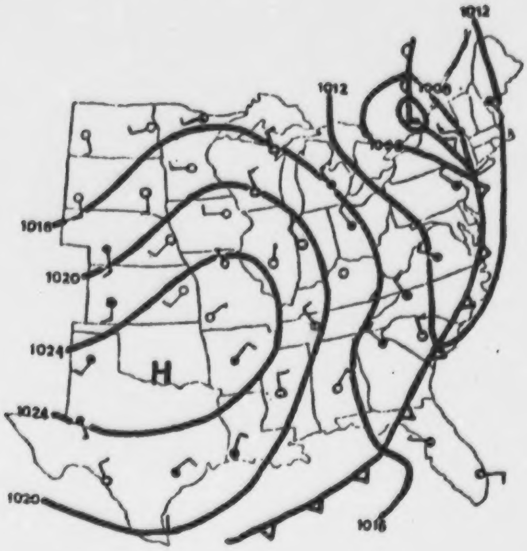
1012
1012
1008
1008
1016
1020
1024
H
1024
1020
1016

Figure 39. 1800Z surface analysis for 10 September 1976. Full barb represents 5 m/sec wind speed. Circle around station indicates calm winds.

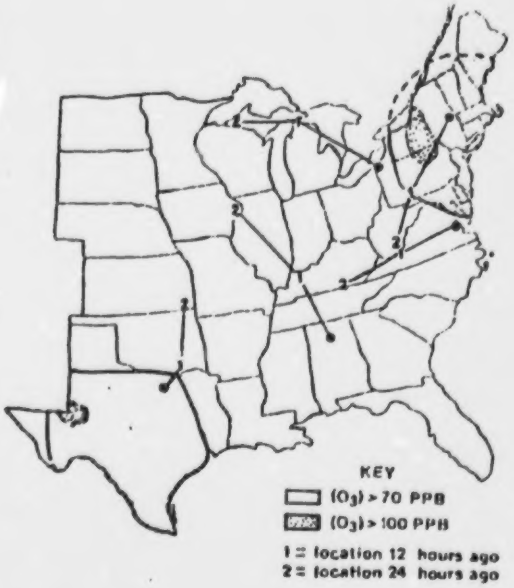
2
2
2
2
2
KEY
(O3) > 70 PPB
(O3) > 100 PPB
1 = location 12 hours ago
2 = location 24 hours ago

Figure 40. Ozone maximum isopleths and backward trajectories for 10 September 1976. Light hatching represents O_3 levels exceeding 70 ppb. Darker hatching represents O_3 levels exceeding 100 ppb. All trajectories end at 1800Z.

The trajectory ending in Albany, New York indicates that the 300 to 2000-m air movement has been northeastward in the past 24 hr. This agrees well with the actual northeastward movement of the elevated O_3 area. The trajectory ending at Richmond, Virginia shows a more eastward movement in the past day. The eastward displacement of this trajectory has nearly matched the movement of the westward edge of the elevated O_3 area in the past day. The trajectory ending at Dallas-Fort Worth indicates a transport of air from southeastern Kansas in the past day. An important feature of this trajectory is that it is much shorter in the first backward 12 hr period than in the second, indicating a decrease of windspeeds in the area. These light winds are due to the presence of a ridge over Texas at 850 mb, with its light winds which coincide with the elevated O_3 area over Texas.

Review of Ozone Episode

Figure 41 shows the hourly O_3 levels in six cities affected by this O_3 episode. The graph includes the time from 5 to 10 September 1976. The hours in the graph represent local standard time. Figure 42 shows the location of these six sites.

One noticeable quality of the O_3 levels is the shift of days with maximum values from top to bottom (west to east). This represents the eastward advance of higher O_3 levels throughout this period. Also note that the maximum O_3 level differs from site to site. The actual hourly advance of high O_3 levels can be seen at several of the sites. Increasing levels can be seen at Marquetee, Michigan on the night of 6 September 1976 and on the morning of 7 September 1976. Levels in Erie, Pennsylvania rose from 0 ppb at 2100 EST to 40 ppb by 0300 EST on 5 to 6 September 1976. In these examples, high O_3 levels were not common on the previous day. This clearly indicates transport of O_3 into these sites since O_3 is not formed without sunshine.

Figure 41 also shows the different qualities of the diurnal change of O_3 levels at the six sites. Portage and Marquette show the least diurnal variation. This is because the monitors are located in rural areas, free from large levels of NO_x. The other sites show a much larger diurnal variation. St. Clair county, located north of Detroit, exhibits a very sharp diurnal pattern.

Also apparent are the differences in maximum O_3 levels for the period from site to site. The highest level of 130 ppb was reached at Green Bay; the lowest maximum level of 78 ppb occurred at Cedar Rapids. The significance of these differences cannot be determined since local emissions may interfere with the monitors located in cities.

Figure 41 also shows the time of a frontal passage at each site. Note the dramatic falloff of O_3 passage at each site; not the dramatic falloff of O_3 levels shortly after the cold front passes. The cleansing action of a cold front is very apparent.

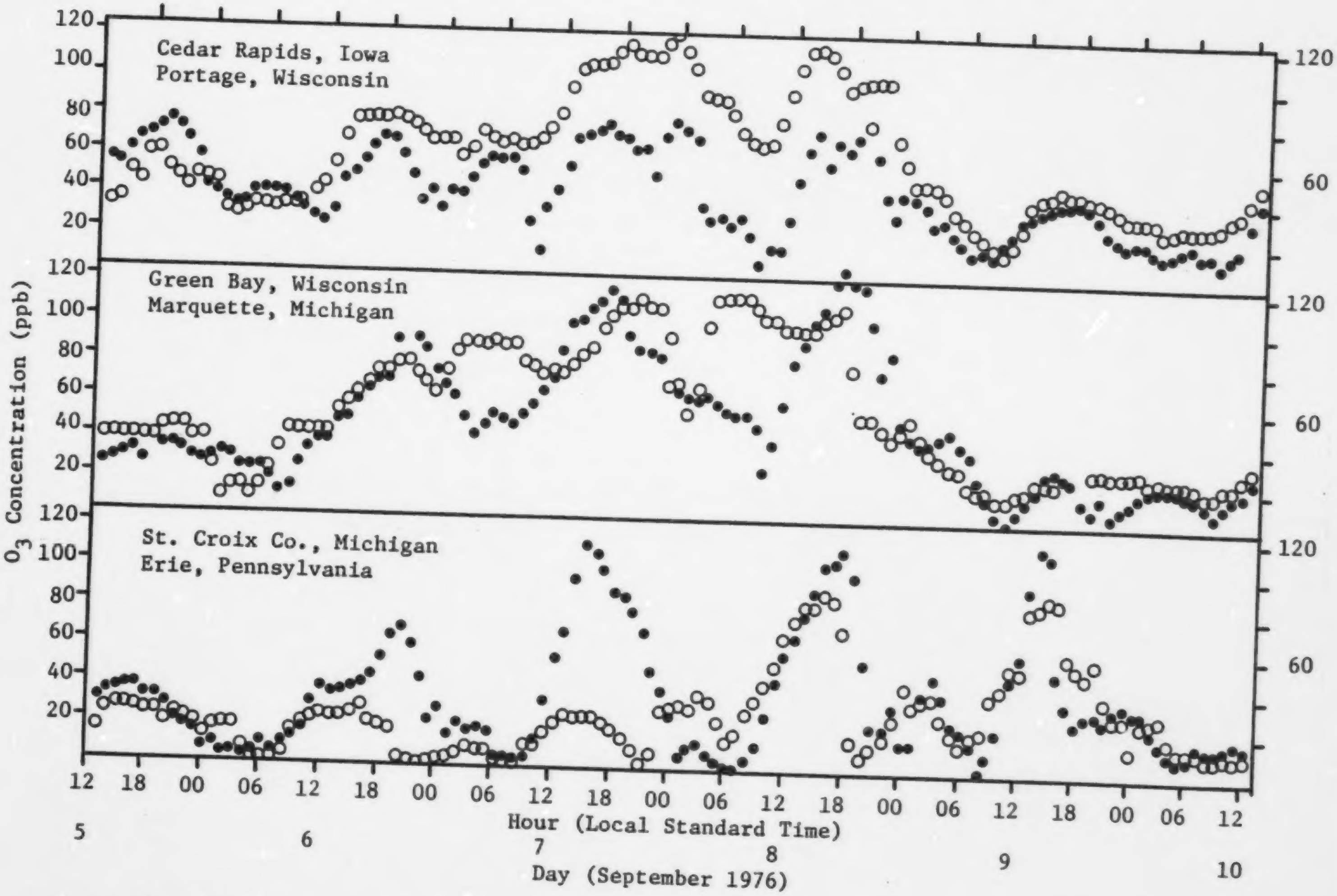

Figure 41. Graph of hourly ozone concentrations at six selected sites from 5 to 10 September 1976. Hours are in Local Standard Time.

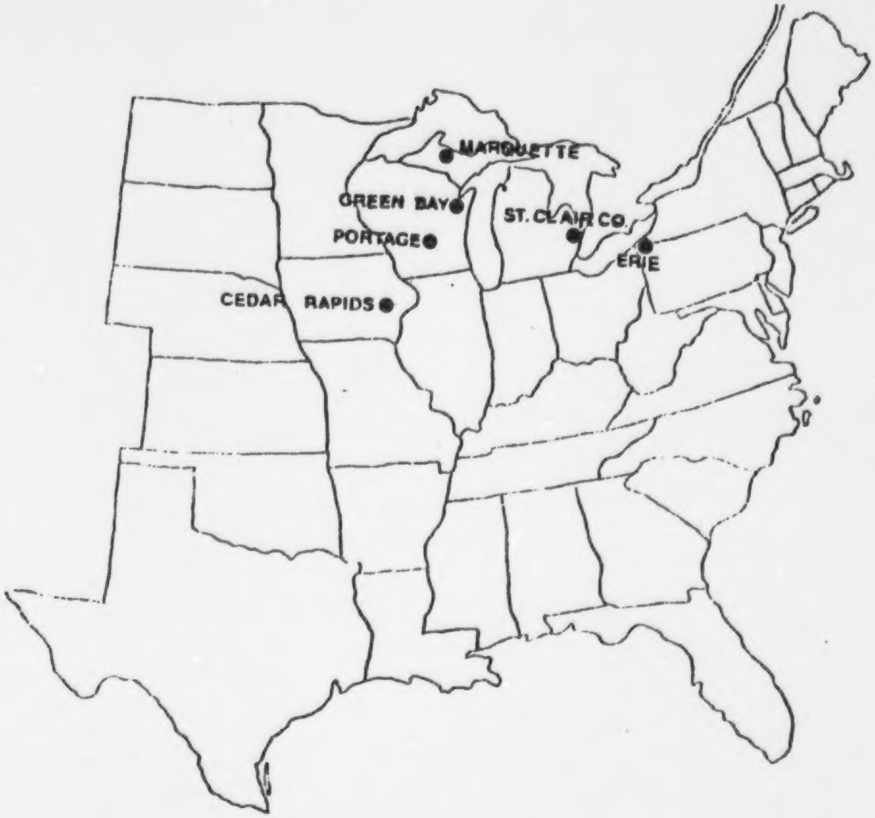
MARQUETTE
GREEN BAY
ST. CLAIR CO.
PORTAGE
ERIE
CEDAR RAPIDS

Figure 42. Map showing locations of six selected sites (see Figure 41).

SUMMARY AND CONCLUSIONS

Large-scale transport of low-level O_3 is demonstrated to be important in determining regional O_3 levels across the central and eastern U.S. A large area with O_3 levels $>$ 70 ppb formed under an 850-mb ridge in the southern Plains at the onset of the case study. This area spread northward into the northern Plains and then spread eastward across the northern Midwest as the 850-mb ridge moved to the East Coast. A smaller area with O_3 levels $>$ 100 ppb developed within the larger area over the northern Midwest. Another area with O_3 levels $>$ 70 ppb formed over the Ohio Valley and merged with the advancing area of elevated O_3 levels over the Great Lakes. Elevated O_3 levels then spread to the East Coast. The O_3 levels dramatically subsided as a cold front swept eastward across the United States.

Trajectories averaged through the 300 to 2000-m layer agreed with the direction and speed of movement of the elevated zone areas. However, surface winds were not necessarily in the same direction as that of O_3 transport.

The relative importance of transport of O_3 versus the regional or local formation of O_3 remains unclear. However, the evidence is overwhelming that large-scale transport of O_3 is important in causing elevated ozone levels in the United States. In addition, large areas of elevated O_3 levels maintained distinct boundaries as they moved across the United States.

Another important finding is that high O_3 levels do not imply restricted visibilities. Areas of restricted visibility (e.g., haze) with sunny conditions generally were found to be associated with areas of high dew points. This is due to the scattering of light by aerosols. Regions with elevated O_3 levels often experienced unrestricted visibilities.

In order to better understand the problem of large-scale O_3 transport, ozone should be monitored more extensively and strategically. Much of the United States has little or no O_3 monitoring. Also, more O_3 monitors should be placed in rural areas or in sites upwind of cities to avoid O_3 decay by NO_x. Aerial monitoring of O_3 also would be helpful in learning about the importance of large-scale O_3 transport. Ozone cannot be controlled at the local level as many states and cities in the United States are attempting to do. The lack of O_3 monitors at rural sites downwind of the power plant and the questionable O_3 values obtained at the local monitoring sites made it impossible to determine the actual contribution of O_3 by the power plant as compared to what was advected into the area.

SECTION 6

DEPLETION OF AMBIENT OZONE

INTRODUCTION

The depletion of ambient ozone by NO in the plume of the Columbia Generating Station was studied in the summer of 1976. Ozone, SO_2, NO, and NO_2 were monitored continuously at a ground level site 10 km north of the plant. The O_3 levels were sharply reduced when the plume was present at the site. The plume's presence was indicated by high levels of NO_x ($NO + NO_2$) and SO_2 associated with a southerly wind. For at least 1-hr time period the O_3 concentration met the federal standard of 80 ppb due to the presence of the plume. The analyses indicate that the amount of O_3 depletion depends on the ambient O_3 levels and the levels of SO_2 and NO_x associated with the plume. The NO_2 levels from the plume were found to be proportional to the amount of O_3 removed from the ambient air.

It is well understood that coal-fired power plants contribute SO_2, NO_x (primarily nitric oxide) and a host of other chemicals to the atmosphere. However, these same power plants do have a beneficial aspect--they deplete O_3 primarily via the quick reaction (Stephens 1969):

$$O_3 + NO \rightarrow NO_2 + O_2 . \tag{34}$$

Therefore as a plant plume disperses into O_3-laden air, the NO is quickly converted to NO_2, while the O_3 is depleted. The NO_2 in turn will be photodecomposed in the presence of ultraviolet light (UV) from the sun:

$$NO_2 \xrightarrow{UV} NO + O . \tag{35}$$

The lone reactive oxygen atom will then quickly react with another oxygen atom:

$$O + O_2 + M \rightarrow O_3 + M . \tag{36}$$

where M is a molecule of air absorbing excess energy, usually N_2. Under the restraints of these reactions, O_3, NO, and NO_2 will reach an equilibrium level depending on the initial concentrations of O_3 and NO_x, and the amount of solar radiation. In addition, the total amount of NO_x remains constant:

$$[NO] + [NO_2] = [NO_x] = \text{constant}, \tag{37}$$

while the amount of oxydizing species is conserved (Meteorology Research 1975):

$$[NO_2] + [O_3] + [O] = \text{constant}. \tag{38}$$

Since [O] has a very short lifetime, Eq. (38) can be simplified to:

$$[NO_2] + [O_3] = \text{constant}. \tag{39}$$

Meteorology Research (1975) and Davis et al. (1974) have shown that power plants deplete O_3 levels up to 15 km or more downwind.

The presence of hydrocarbons and other organic molecules interferes with the cycle of reactions in Eqs. (34, 35, 36); this allows a buildup of NO_2 and O_3 levels and a decrease of NO levels. A recent study of Allwine et al. (1974) shows that a HC/NO_x ratio of 14 allows the greatest production and highest levels of O_3.

Our study during the summer of 1976 illustrates the depletion of ambient ozone by the Columbia Generating Station. The tracer gases NO, NO_2, and SO_2 in the plume were compared with the amount of O_3 depleted $[O_3]_{dep}$.

SITING

The primary monitoring site, located 10 km north of the Columbia Generating Station (Figure 43), is in the midst of low, flat farmland. Sulfur dioxide, O_3, NO, and NO_2 levels were continously monitored throughout the study period. A Phillips PW-9700 and a Meloy OA 300 monitor were used to measure SO_2 and O_3 levels, respectively. A Monitor Labs 8440 measured the NO and NO_2 levels. All chemical concentrations were measured at a height of approximately 5 m and were recorded on strip charts.

Two other sites were used to supply meteorological data. One, located 10 km west of the power plant, gave wind direction and speed at the smoke stack height. An Epply pyranometer located here supplied solar radiation data for this study. The other site, situated 6.5 km northeast of the plant, supplied wind direction and speed at a height of 9 m.

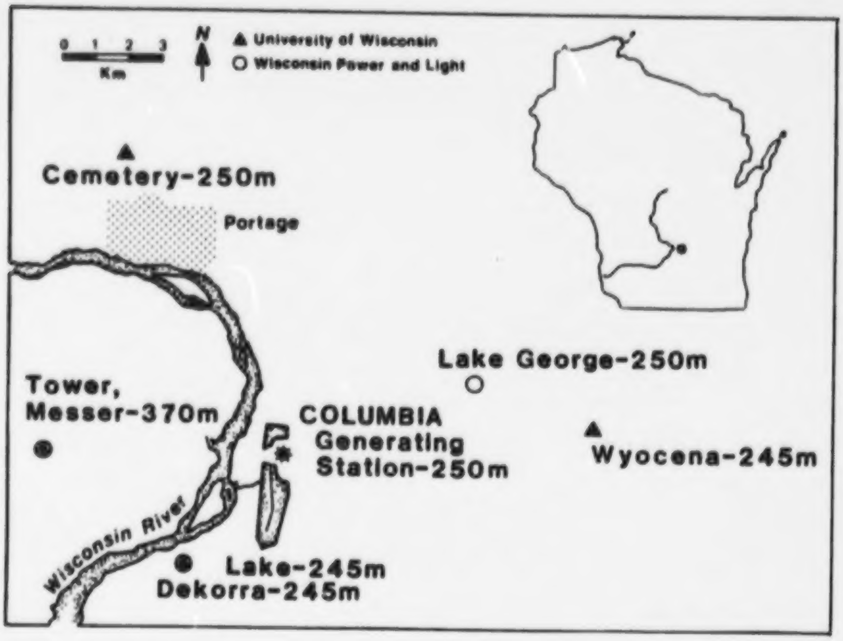
0 1 2 3
Km
N
▲ University of Wisconsin
○ Wisconsin Power and Light
Cemetery-250m
Portage
Lake George-250m
Tower, Messer-370m
COLUMBIA Generating Station-250m
Wyocena-245m
Wisconsin River
Lake-245m
Dekorra-245m

Figure 43. Monitoring sites for meteorological data.

A total of five sites in the vicinity of the plant were equipped with Phillips PW-9700 SO_2 monitors. The SO_2 levels from these sites were averaged to determine an ambient level.

PROCEDURES

High hourly averages of SO_2, NO_x ($NO + NO_2$), and O_3 were used to indicate the times when the plant plume was drifting over the primary site. Inspection of the strip chart records revealed that these hours were characterized by rapid and frequent fluctuations of O_3, SO_2, and NO_x levels. The simultaneous, instantaneous extremes of the levels of these gases were then determined and analyzed.

Since this study focuses on the effect of the plant on ambient O_3 levels, ambient levels of SO_2, NO, and NO_2 were to be subtracted from the total levels in the plume. However, this usually was not necessary for SO_2 and NO because ambient levels were consistently near 0 ppb. Since ambient NO_2 levels were appreciable at times (up to 12 ppb), they were subtracted from the total levels measured during plume presence. Ambient levels of NO_2 were determined at moments when the plume was temporarily absent (i.e., when both $[SO_2]$ and $[NO] \simeq 0$ ppb). Ambient O_3 levels were determined identically.

RESULTS AND DISCUSSION

Eight periods were studied when the plume depleted O_3 levels at the primary site (Table 6). South-southeasterly to south-southwesterly winds prevailed during these periods.

TABLE 6. SUMMARY OF PERIODS STUDIED WHEN PLANT PLUME DEPLETED OZONE LEVELS AT PRIMARY MONITORING SITE DURING SUMMER OF 1976

Day	Time (CST)	Ambient $[O_3]$ (ppb)	Wind speed (m/sec) Stack level, 150 m	Stack level, 9 m	Solar insolation, (ly/min)
13 July	0818-1035	42-77	4	3	0.6 - 0.8
19 July	0618-0700	50	6	3	0.1 - 0.2
19 July	1811-2140	50-57	7	4	0.0 - 0.04
9 Aug.	0958-1026	60	3	1	~ 1.00
16 Aug.	1312-1509	45-52	3	1	~ 0.90
30 Aug.	1114-1516	72-88	5	4	0.8 - 1.0
6 Sept.	0826-1136	38-61	5	3	0.5 - 1.0
12 Sept.	0940-1202	36-44	6	3	0.7 - 1.0

We found that O_3 levels were reduced in every case when the plume was present. On an isolated day, this O_3 reduction prevented O_3 levels from exceeding the National and Wisconsin 1-hr standard of 80 ppb O_3 for 2 consectuive hr (14 and 15 CST) on 30 Aug. 1976 (Figure 44). In addition, Figure 44 exhibits the coincidence between depressed O_3 levels and increased NO_2 and SO_2 levels attributed to the presence of the plant plume.

The amount of O_3 depleted--$[O_3]_{dep}$--is demonstrated to be strongly correlated with $[SO_2]$ in Figure 45. It must be emphasized that nearly all of the SO_2 originated from the power plant since the background levels were very small. Although this relationship is linearly correlated for $[SO_2] <$ 200 ppb, $[O_3]_{dep}$ becomes less dependent on $[SO_2]$ as total depletion of O_3 is approached (i.e., for increasing values of $[SO_2]$).

The levels of NO_x also determine the amount of O_3 depleted. This is logical since this plant is fired by coal with a fairly invariant concentration ($\sim$0.8%) of S (Ragland et al. 1976). A strong linear correlation was found between $[NO_x]$ and $[SO_2]$ (Figure 46). The average $[SO_2]/[NO_x]$ ratio was nearly 2.25.

Although elevated SO_2 and NO_x levels resulting from the plant can predict the amount of ozone depletion surprisingly well, it must be stressed that $[O_3]_{dep}$ is also dependent on (1) ambient ozone levels - $[O_3]_{amb}$ - and (2) solar radiation intensity. Figure 47 shows the importance of these variables. It is evident from this scatterplot that at constant $[NO_x]$, the absence of appreciable solar radiation (nighttime conditions) or relatively high $[O_3]_{amb}$ ($>$ 70 ppb) displaces $[NO]/[NO_x]$ ratios to lower values. According to Eqs. (37 and 39), a lower $[NO]/[NO_x]$ ratio implies lower O_3 concentrations (i.e., greater O_3 depletion). Since the occurrences with little sunlight or high O_3 levels were few, the linear regression line fits the points well.

The amount of NO_2 present in the plume seems to be the most accurate method for determining the amount of O_3 depletion. When ambient levels were subtracted from total NO_2 levels, $[NO_2]$ was found to have a nearly one-to-one ratio with $[O_3]_{dep}$, as evident from Figure 48. This ratio is expected from Eq. (39). Unlike the previous correlations of $[O_3]_{dep}$ $[SO_2]$ and $[NO_x]$, $[O_3]_{dep}$ is dependent on $[NO_2]$ alone. Another advantage of the $[NO_2]$ - $[O_3]$ relationship is that it has nearly the same ratio when mass concentrations ($\mu g/m^3$) are used: NO_2 has nearly the same gram molecular weight as O_3.

SUMMARY AND CONCLUSIONS

The results of our study further prove that coal-fired power plants are important in depleting ozone. This is shown to be true at ground level 10 km down-wind in a rural area.

The amount of O_3 depleted is shown to be linearly dependent on SO_2 and NO_x concentrations due to a plant plume. The amount of ambient ozone and solar radiation intensity also affects the amount of O_3 depleted.

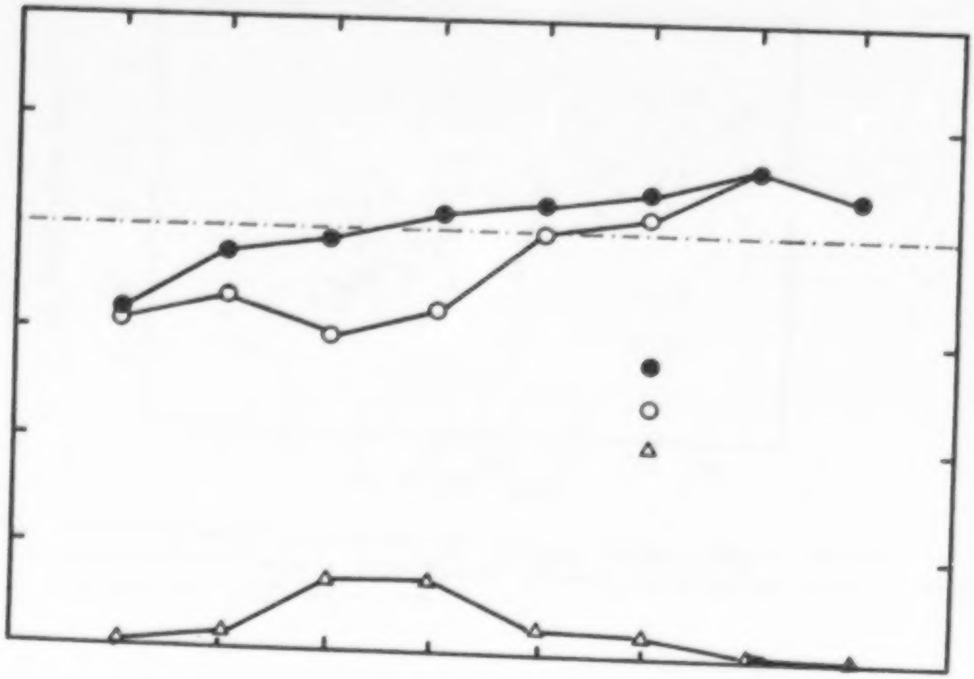

Figure 44. Hourly averaged concentrations of ambient O_3 and concentrations of O_3 and NO_2 at the primary site during plume presence on 30 August 1976.

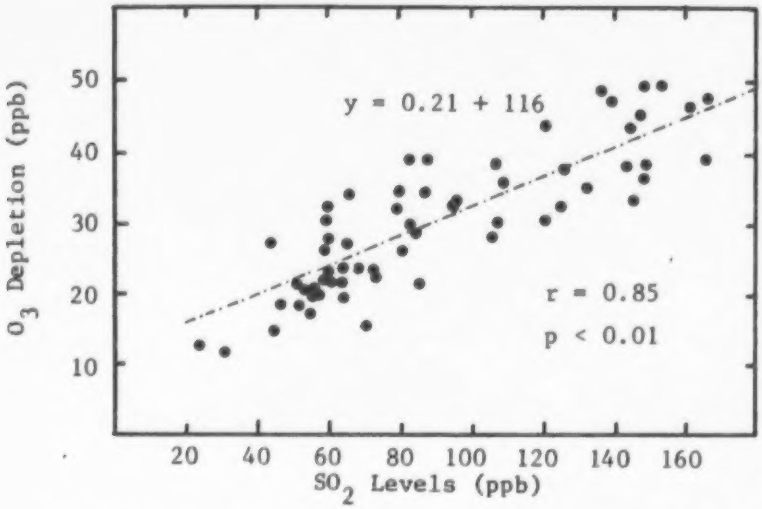

Figure 45. Scattergram of instantaneous $[O_3]_{dep}$ versus $[SO_2]$. The 61 observations have a significant linear correlation with $r = 0.85$ at the 99% confidence level.

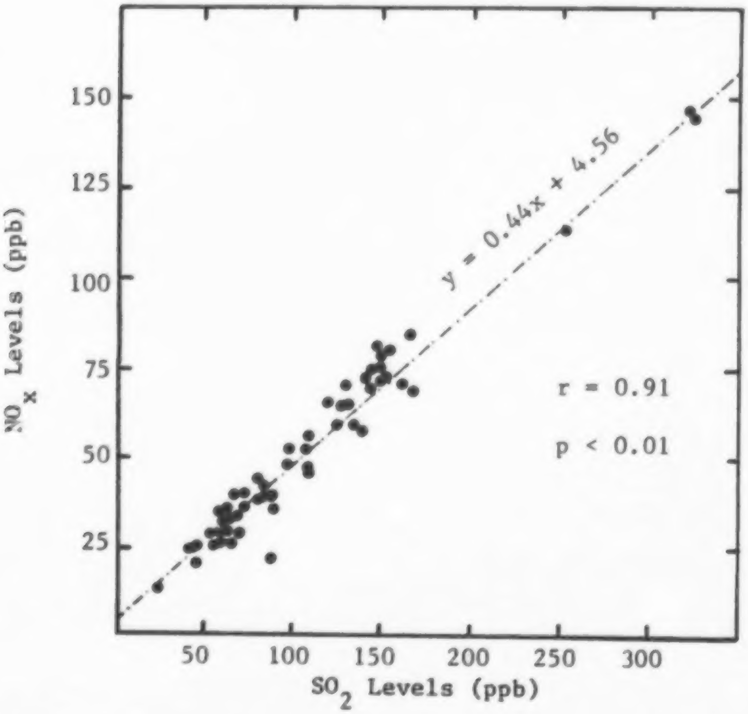

Figure 46. Scattergram of instantaneous $[NO_x]$ versus $[SO_2]$. The 61 observations have a significant linear correlation with $r = 0.91$ at the 99% confidence level.

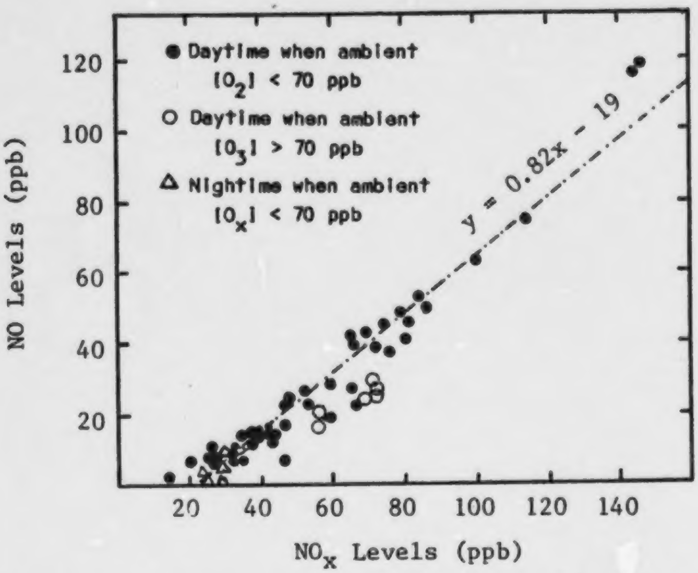

Figure 47. Scattergram of instantaneous [NO] versus [NO_x]. The 64 observations have a significant linear correlation with r = 0.96 at the 99% confidence level.

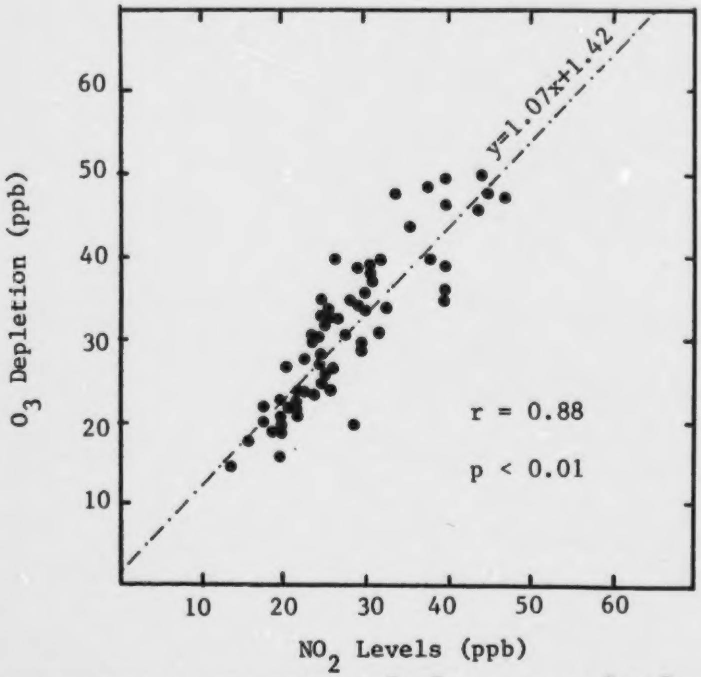

Figure 48. Scattergram of instantaneous $[O_3]_{dep}$ versus [NO_2]. The 64 observations have a significant linear correlation with r = 0.88 at the 99% confidence level.

The amount of O_3 depletion is demonstrated to have a one-to-one relationship with NO levels due to the plant. This correlation is the most convenient method of determining O_3 depletion since the NO_2 concentration due to the plant is the lone independent variable.

SECTION 7

TOPOGRAPHIC INFLUENCE ON SURFACE WINDS

INTRODUCTION

To determine the transport of atmospheric pollutants on a scale of 10 to 100 km, the horizontal variation of the wind field should be taken into account. Slade (1968) noted the lack of study of the horizontal variation of the surface wind. Wendall (1972) found that the local wind field was apparently disturbed by local topography. Anderson (1972), who obtained mesoscale (10 to 100-km) wind fields by modeling topographic anomalies, concluded that topography is a major cause of horizontal wind variations.

This section focuses on the effect of the Baraboo Bluff on the local wind field. Specifically, the horizontal variation of the wind field will be examined as a function of wind direction and speed. First-order differential properties of the wind field--viz., divergence and vorticity--are also examined as a function of wind direction and speed in an effort to determine the effect of topography on the wind field.

INSTRUMENTATION AND DATA REDUCTION

The type and quantity of instrumentation varied from site to site. Table 7 lists the atmospheric parameters measured, the measuring height, and the equipment used. The instrumentation and strip-chart data reduction are described in Section 3.

Individual anemometers are assumed accurate to ±0.5 m/sec, but no further assumptions were made concerning the comparison of anemometers between sites. When possible, the two anemometers at each site were compared, with the results showing that they differed by < 0.5 m/sec, the assumed absolute accuracy of each anemometer. The system error for the potentiometer-recorder system was about 7.5 deg assuming 2% accuracy for the recorder. The alignment error was of the order of ±10 deg.

From the 2 yr of data available from the four sites, eight data sets were selected using five criteria. The first was that there be a complete set of data from each site over the length of time of that particular data set, which was not less than 4 days. Secondly, data sets were chosen such that data reduction could be accomplished from the chart of either a north-oriented or a south-oriented vane. This eliminated the necessity of jumping

TABLE 7. PARAMETERS AND INSTRUMENTATION USED AT EACH OF THE FOUR SITES IN THE METEOROLOGICAL NETWORK

Site Recorder	Parameter	Height (m)	Sensor	System
Messer	Wind direction	32	Beckman-Whitley	Esterline-Angus
	Wind speed	2,32	Stewart anemometer	Esterline-Angus
Whitley	Air temperature	2	Thermocouples	Brown Angus
	Temperature differences	0.2-2 2-32	Thermocouples	Brown Angus
Wyocena	Wind direction	9	Wind vane system	Esterline-Angus
Dekorra	Wind speed	9	Stewart anemometer	Esterline-Angus
	Wind direction	9	Wind vane system	Esterline-Angus
	Wind speed	9	Stewart anemometer	Esterline-Angus
	Air temperature	2	Thermocouples	Brown Angus
	Temperature differences	0.2-2	Thermocouples	Brown Angus
Cemetery	Wind direction	9	Wind vane system	Esterline-Angus
	Wind speed	9	Stewart anemometer	

from one chart to the other. Thirdly, periods of precipitation were avoided since they often resulted in questionable readings at one or more of the sites. This was especially true during the summer when precipitation tended to be more localized. Fourth, wind speeds of < 1 m/sec for extended periods were avoided because this was near the response threshold of the wind systems and the data may be in error. Finally, data from December 1975 through March 1976 were not analyzed because the extreme weather conditions frequently caused instrument problems which were not obvious from the chart records.

Table 8 lists the eight data sets used and gives the number of days included in each. Data sets from 1975 did not include wind directions from approximately 330° to 030° since only one vane-anemometer system was in operation at each site. In order to compensate for this selection, more of the data sets were taken from the additional vane-anemometer system in 1976.

TABLE 8. LIST OF THE DATA SETS USED, GIVING THE NUMBER OF DAYS IN EACH DATA SET AND THE ORIENTATION OF THE WIND VANE ZERO WHERE NORTH REFERS TO ZERO ALIGNMENT TOWARDS NORTH AND SOUTH REFERS TO ALIGNMENT TOWARDS SOUTH

Period	No. of days[a]	Vane orientation
16-21 May 1975	5	North
6-10 Aug. 1975	5	North
11-16 Oct. 1975	5	North
6-10 Nov. 1975	5	North
14-18 Apr. 1976	4	South
1-5 May 1976	5	South
8-14 June 1976	6	North
29-31 May 1976	3	South
1-5 June 1976	5	South

[a] A total of 43 days.

Since the wind speed and direction at the Messer site were measured at 32 m rather than 9 m as was the case with the three valley sites, a 9-m wind speed was computed for the Messer site based on the wind speed at 32 m. The wind direction was taken to be the same at the two levels, so that wind direction data from the valley sites were compared directly with the 32-m direction from the Messer site. The 32-m wind speed was extrapolated to 9 m under the assumption of a logarithmic profile (Lettau 1959),

$$V(z) = (V^*/k)\log(1+z/z_0) \qquad (40)$$

where V^* is the friction velocity, k is the von Karman constant, z_o is the aerodynamic surface roughness, and $V(z)$ is the wind speed at a height z above the surface.

Although the assumption of a logarithmic profile is usually rather poor for any specific time, it is reasonable for time-averaged data (Lettau 1962). Under the assumption of the logarithmic profile, the wind speed at 9 m is given by:

$$V(9) = V(32)\log(1+9/z_o/\log(1+32/z_o), \tag{41}$$

where the value of the aerodynamic roughness (z_o) in this open forest region was tentatively set at 10 cm (Lettau 1969, Sellers 1965).

CALCULATIONS OF DIVERGENCE AND VORTICITY

The first-order differential properties--divergence and vorticity--are computed by considering the two velocity components, u and v, as functions of x and y for some arbitrary origin (Petterssen 1956). The horizontal divergence (DIV) and vorticity (VOR) can then be given by the following relations:

$$\begin{aligned} DIV &= du/dx + dv/dy \\ VOR &= dv/dx - du/dy. \end{aligned} \tag{42}$$

Since wind data were available for only three points, the above expressions were not used directly. Instead, the "Bellamy Triangle Technique" was used to obtain estimates of divergence and vorticity over the area of the network (Bellamy 1949, Poulter 1949, Bennett 1955, Frederick 1969).

The wind vector at each of the three sites is resolved into components that are parallel and normal to the opposite sides of the triangle formed by the three sites, where each site can be thought of as a vertex of the triangle. The sign conventions for the normal component are positive when directed outward and negative when directed inward. The parallel component is taken as positive when directed counterclockwise about the centroid of the triangle and negative when clockwise.

The equations given by Bellamy (1949) were used to compute the normal and parallel components of the wind velocity at a particular site (vertex) of the triangle. These expressions are given as:

$$DIV_i = (V_i/h_i)\sin(\beta_{jk}) - \alpha_i)$$

$$VOR_i = -\,(V_i/h_i)\cos(\beta_{jk} - \alpha_i)$$

where β_{jk} is the azimuthal angle of the side of the triangle opposite to the vertex i, α_i is the wind direction at the vertex i, V_i is the wind speed at vertex i, and DIV_i and VOR_i are the partial divergences and vorticities, respectively, at the vertex i.

As pointed out by Frederick (1969), an ambiguity is involved in computing the azimuthal angles (β_{jk},s) for the sides of the triangle. This arises from the fact that the azimuth can be computed for a particular side at either of the two vertices which it connects. Only one of the measured angles is correct so that it is important to choose the correct vertex from which to measure the azimuthal angle. For a particular vertex and the associated opposite side, the correct vertex is the one that is to the left of the height from the vertex of interest to the opposite side when the vertex of interest is directed towards the observer. The correct azimuthal angles for the triangle formed by the three valley sites are given in Figure 49 along with distances between sites and the resulting heights of the triangle.

The distances between the sites were estimated to the nearest 100 m from topographic maps. However, the derived triangle heights and azimuthal angles were calculated to a considerably higher degree of accuracy (10 m for the heights and ±0.0001 rad for the azimuthal angles). This was necessary to prevent biasing the computed divergences and vorticities when summing the partial terms. The bias results from the fact that terms of equal magnitude but of opposite sign are being summed, which is sometimes referred to as "cancellation of terms" (Dahlquist and Bjorck 1974). Thus, even a very small error (resulting from rounding off an angle) will introduce an error that could be of the same magnitude as the divergence or vorticity. The triangle dimensions and angles must satisfy the Law of Sines:

$$\frac{\sin \alpha}{a} = \frac{\sin \beta}{b} = \frac{\sin \gamma}{c} \tag{43}$$

which relates the interior angles of the triangle to the lengths of the opposite sides. The resulting bias from the dimensions given in Figure 49 is four orders of magnitude below the results and is a function of wind direction (through the sine and cosine terms). This indicates that if cruder estimates of angles had been used the resulting divergence and vorticity would have seemed to be a strong function of direction. This might explain why the use of this method gives the impression that the orientation of the triangle with respect to the wind is important (Schmidt 1965).

The major problem with using the "Bellamy Triangle Method" is its assumption of a linearly varying wind field. The influence of topography on the surface wind field is non-linear. This means that the method described will at best give only a first-order approximation to the true divergence and vorticity over the area of the triangle. More than three sites would be needed if an attempt were made to determine higher order variations.

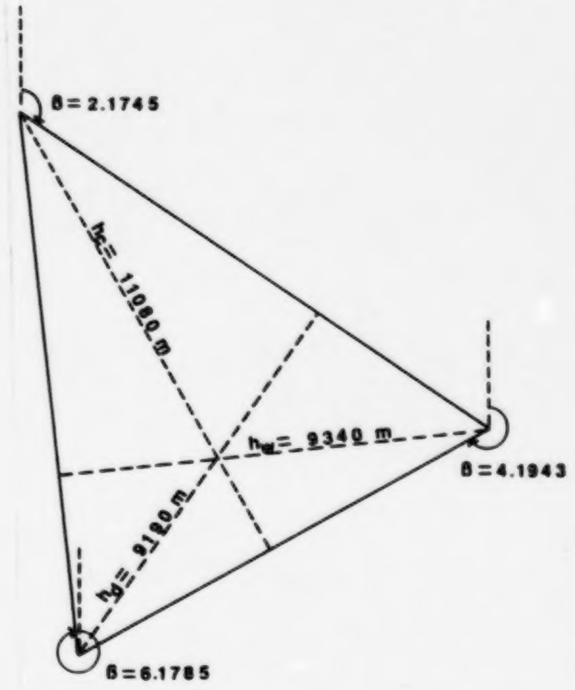
θ = 2.1745
h_c = 11080 m
h_e = 9340 m
θ = 4.1943
h_g = 9120 m
θ = 6.1785

Figure 49. The dimensions of the triangle formed by the meteorological network near Portage, Wisconsin. The angles are in radians.

COMPARATIVE ANALYSIS

In order to determine the influence of the Baraboo Bluff on the wind field in the region of the Columbia Generating Station, an initial analysis was carried out under the assumption that the influence would be a strong function of wind direction. Therefore, all quantities were considered strictly as functions of wind direction. This dependence on wind direction was determined by forming 20° sector averages of each quantity, and then assigning this value to the mid-point of the sector. In this way 18 mean values were obtained at directions of 10°, 30°, 50° etc.

The averaging process consisted of summing a particular 30-min mean quantity every time the wind direction fell within the 20° sector of interest. The mean value was obtained by dividing the total sum by the number of times the wind direction fell within that particular sector. This averaging was done for wind direction and speed, and for the divergence and vorticity computed over the triangle formed by the three valley sites. In order to eliminate low wind conditions (i.e., wind speeds below the response thresholds of the wind instruments) wind speeds of <1.5 m/sec were not considered and the averaging process did not include that particular time period. The total number of data values used in forming each of the sector mean values is given in Table 9. The low number of observations in the 00° to 20° and 340° to 360° sectors made analysis impossible in these sectors.

TABLE 9. NUMBER OF DATA VALUES USED TO COMPUTE THE SECTOR MEANS. EACH DATA VALUE IS A 30-MIN MEAN FOR A SECTOR 20° WIDE

Sector	Data point	Sector	Data point
1	13	10	201
2	37	11	195
3	52	12	95
4	55	13	91
5	59	14	71
6	79	15	67
7	89	16	57
8	68	17	37
9	98	18	21

Initially the wind direction at the Messer site was assumed to be representative of the mean wind field in this region. However, the results of the sector-averaging process proved unsatisfactory since it was obvious that the wind direction at the Messer site was influenced by the Baraboo Bluff. It was then assumed that the wind data at the Wyocena site would be representative since this site was farthest from the Baraboo Hills and in generally uniform terrain. The wind direction differences were computed by subtracting wind direction at the Wyocena site and performing the sector averaging process (Figure 50).

Immediately obvious is the fact that wind directions differ quite significantly from those at Wyocena. The first anomaly occurs when the wind direction is between 100° and 180° at the Wyocena site and is characterized by a veering of wind direction, particularly at Messer. This implies that some mechanism is operating to force the wind at the Messer site to acquire a greater westerly component relative to the Wyocena wind direction. An obvious mechanism would be a channeling of the wind along the southern bluffs. This is supported by the fact that the wind direction at the Dekorra site exhibits a similar variation in these sectors. Thus, the wind direction at the Messer site is not always representative of the wind direction in the region surrounding the Columbia Generating Station, varying as much as 20° from the wind direction at the Wyocena site.

The influence of the Baraboo Hills on the wind direction appears quite significant, especially for winds blowing perpendicular to the hills. Dekorra, the site closest to the eastern edge of the hills, exhibits the strongest variation as would be expected. However, variations at the Cemetery site also appear to be correlated with the orientation of the flow relative to the Baraboo Hills.

Wind speed differences were formed by subtracting the wind speed at a particular site from the wind speed at the Wyocena site. Sector-averaged values were computed in the same way as for the wind direction differences. The computed 9-m wind speed at the Messer site was used in determining the Messer site wind speed differences (Figure 51).

The Messer wind speed appears to average 1 m/sec higher than the Wyocena wind speed for wind directions < 300° and was often higher than the Wyocena wind speeds during the night. For wind directions between 140° and 240°, the wind speed difference is quite constant while wind direction differences were significant.

The wind speed differences of the Cemetery site show a marked variation with wind direction. For wind directions between 20° to 80°, the Cemetery wind speed is nearly 1 m/sec greater than that at Wyocena. This may be due in part to the fact that the Cemetery site is better exposed to the wind from these directions. For wind directions between 100° and 200°, the Cemetery wind speed becomes approximately 1 m/sec less than the Wyocena speed, indicating that the previous values were not due to a calibration error. These directions correspond to flow over the city of Portage, implying that the city may act to retard flow. The wind speed varies only slightly from the Wyocena values for wind directions between 200° and 340°.

For wind directions between 120° and 160°, speed is slightly higher at the Dekorra site. This is surprising since the surface is much rougher in the vicinity of the Dekorra site, leading one to expect lower wind speeds. It is possible that the channeling of the wind for these directions is

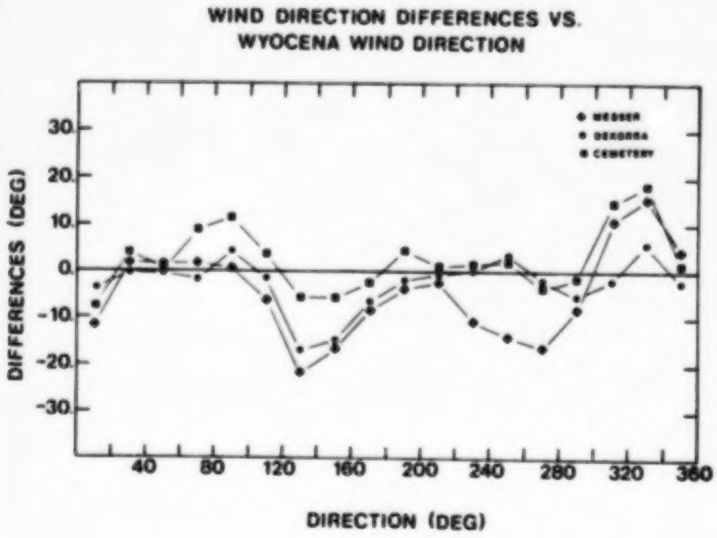

Figure 50. Wind direction differences at three sites with respect to wind direction at the Wyocena site. A wind direction of 130 deg is perpendicular to the southern bluff and about 330 deg for the less clearly defined northern bluff of the Baraboo Hills.

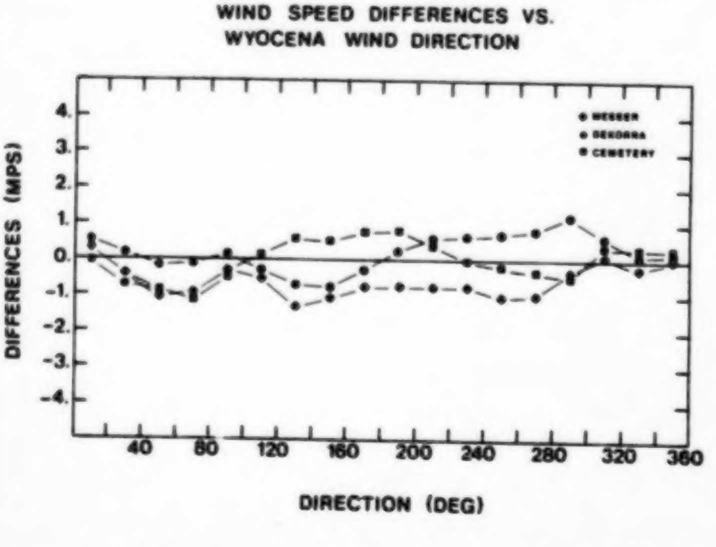

Figure 51. Wind speed differences for each site from the Wyocena wind speed as a function of Wyocena wind direction.

contributing to the higher winds. For wind directions between 200° and 300° the Dekorra wind speed is about 1 m/sec less than that at Wyocena. This is due most likely to the large stand of trees west of the site.

The local surface at each site strongly influences wind speed between sites because wind speed was measured only at 9-m height. The only case where the wind speed variations did not correspond to an increase in surface roughness was at Dekorra. If a sector has a higher mean wind speed, then the difference for that sector will also tend to be higher. This probably accounts for the larger values at the Dekorra site for directions from 260° to 300°. The mean wind speeds tended to be higher for directions between 220° and 340°. Wind direction and speed differences change sign at each site at approximately the same wind directions, indicating that the causes are probably similar.

The vorticity computed over the area defined by the three valley sites was averaged over 20° sectors (Figure 52). As was the case for the wind direction and speed, the Wyocena wind direction was assumed representative of the region. This was shown to be a much better assumption than was the Messer wind direction (Weidner 1976). The significant features in Figure 52 are the double oscillation and the prominent shift from positive to negative in the 220° to 240° sector. The double oscillation appears symmetric about the direction of a wind blowing perpendicular to the southern bluffs, i.e., 130°. Contributions to the total vorticity from the Dekorra and Cemetery sites are nearly equal in magnitude and sign except for wind direction > 240° where the Dekorra site predominates.

The overall analysis seems to point to a strong correlation between the values of vorticity and the direction of the wind relative to the Baraboo Hills. The maximum values which occur for flow perpendicular to the hills and the vorticity sign change as the wind direction shifts through the azimuth of the southern hills support the above statement.

The results of the divergence analysis averaged over 20° sectors are given in Figure 53. Three interesting features are noted. First are the large values of convergence for wind directions between 100° and 180°; second is the point at which the value becomes positive (divergent) at a wind direction of approximately 200°; and finally is the generally positive (divergent) values for wind directions between 220° and 320°. Unlike the plot of vorticity with wind direction, the divergence does not exhibit a double oscillation, but rather a more general trend from negative (convergent) to positive (divergent) values.

The divergence and vorticity are not solely a function of wind direction, but also depend on wind speed. To illustrate this multiple dependence, the divergence and vorticity values were averaged in 20° wind direction sectors and in 1 m/sec wind speed intervals centered on 1, 2, 3, ... m/sec. In this case wind speeds < 0.5 m/sec were excluded from the analysis, rather than wind speeds of 1.5 m/sec as was done previously. The actual number of data points for each average varied considerably with direction and speed as shown in Table 10. The data were smoothed using adjacent points with the following weighting function,

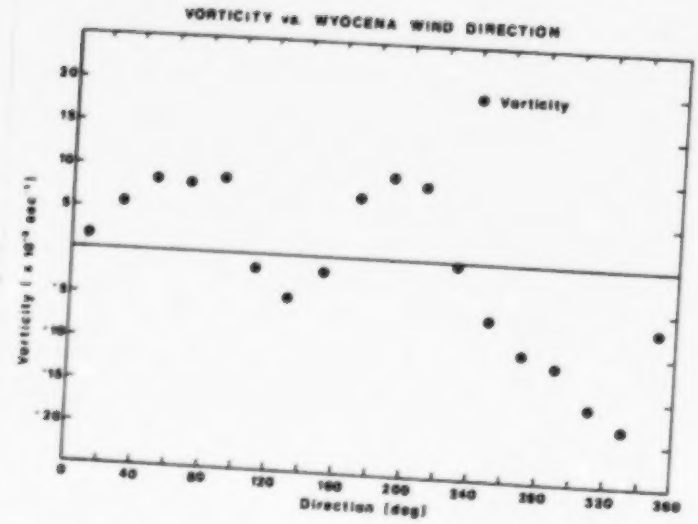

Figure 52. Mean vorticity determined from the Wyocena-Dekorra-Cemetery sites as a function of the Wyocena wind direction.

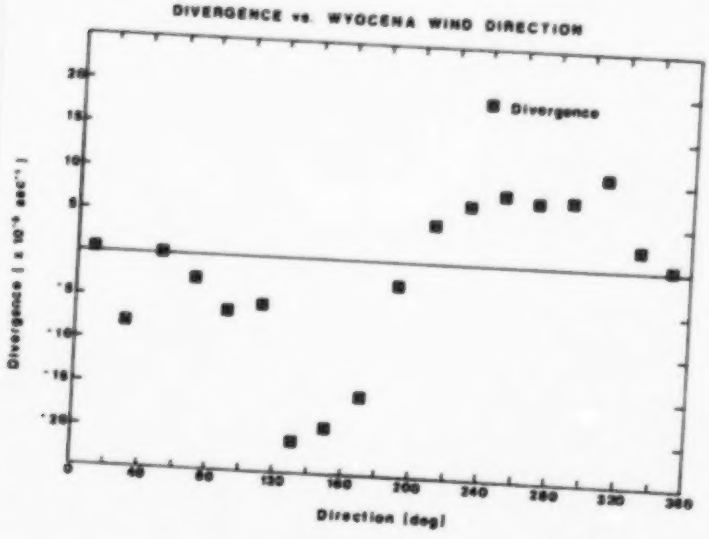

Figure 53. Mean divergence determined from the Wyocena-Dekorra-Cemetery sites as a function of Wyocena wind direction.

TABLE 10. NUMBER OF 30-MIN MEAN VALUES USED IN COMPUTING CONTOUR VALUES FOR DIVERGENCE AND VORTICITY. SPEED CLASS IS M/SEC AND SECTOR DIRECTION IS THE SECTOR NUMBER TIMES 20° MINUS 10°

Sector	Speed							
	1	2	3	4	5	6	7	8
1	10	9	7	4	4	2	-	-
2	20	31	10	4	3	1	-	-
3	22	14	9	7	2	-	-	-
4	12	18	28	13	7	4	-	-
5	20	11	16	14	12	7	-	-
6	23	10	12	11	13	5	-	-
7	24	13	9	11	14	10	7	-
8	11	23	22	20	14	12	6	-
9	12	28	43	15	13	29	4	-
10	10	56	64	41	29	15	9	4
11	15	48	34	29	28	10	10	6
12	20	37	19	22	15	11	5	4
13	17	22	30	16	12	7	7	-
14	18	14	22	15	10	9	8	2
15	18	19	16	17	25	15	8	-
16	11	28	17	11	10	9	6	-
17	10	11	6	6	4	-	-	-
18	6	7	4	-	-	-	-	-

$$V(I,J) = (V(I-1,J)*P(I-1,J)+V(I+1,J)*P(I+1,J) + V(I,J-1)*P(I,J-1)+V(I,J+1)*P(I,J+1) + 2*V(I,J)*P(I,J)/P_t, \quad (44)$$

where:

$V(I,J)$ is computed quantity for the wind sector I and wind speed interval J;

$P(I,J)$ is number of data points used to compute the quantity V;

P_t is total number of data points used in the weighting function given by

$$P_t = P(I-1,J)+P(I+1,J)+P(I,J-1)+P(I,J+1)+2P(I,J). \quad (45)$$

The results are shown as contours for the vorticity and divergence in Figures 54 and 55, respectively. The vorticity shows two maxima, one in the 40° to 60° sector and the other in the 200° to 220° sector for positive values, and a broad region of maximum negative values centered at 320° to 340°. A general increase in the magnitude of the vorticity with increasing wind speed for a particular wind sector would be expected. This appears to be the case, except for wind directions parallel to the southern bluffs where the sign of the vorticity term changes. However, the gradient of the vorticity isopleths increases with wind speed for these wind directions. It appears that the wind speed has its largest effect on the vorticity for speeds < 3 m/sec. Here there tends to be less organization of the vorticity field which is probably due to the higher variability of the wind directions at low wind speeds.

The contours of divergence shown in Figure 55 indicate a similar increase in magnitude with wind speed. The maximum negative (convergent) values are centered in the 140° to 160° sector, while the maximum positive (divergent) values are centered over the 280° to 300° sector. The "zero" line falls in the 220° to 240° sector once the wind speed is > 2 m/sec, again reflecting flow parallel to the southern bluffs. Notice that the maxima for the divergence values tend to fall in the regions of the largest gradient for the vorticity at high wind speeds. This is due to the fact that one is looking at components of the wind field that are approximately 90° out of phase with respect to each other. The divergence field shows little organization for wind directions away from the azimuthal direction of the southern bluffs which served to emphasize the influence of the bluffs on the divergence field in the vicinity of the Columbia Generating site.

In summary there appears to be strong evidence that the Baraboo Hills significantly influence the surface winds over the meteorological network. This is reflected in the linear wind field and the first-order properties of divergence and vorticity. For wind directions resulting in convergence,

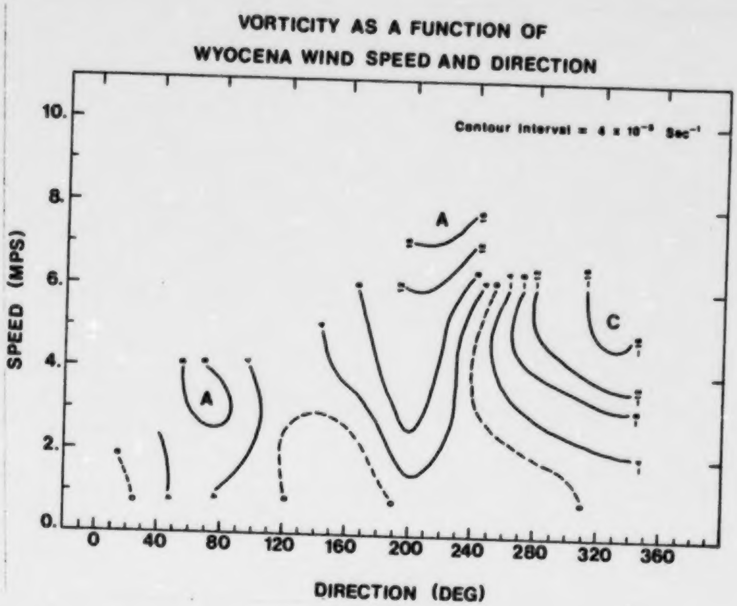

Figure 54. Vorticity as a function of the Wyocena wind speed and direction. A is the zone of maximum anticyclonic flow and C is the zone of maximum cyclonic flow.

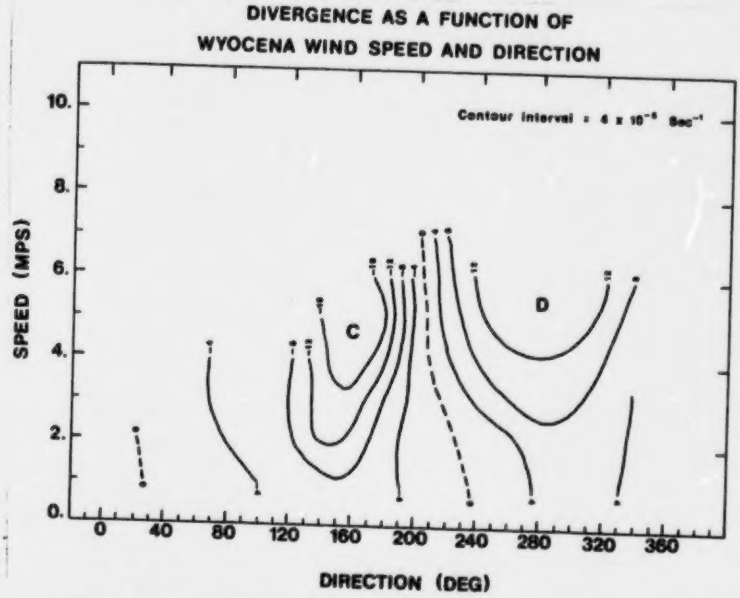

Figure 55. Divergence as a function of the Wyocena wind speed and direction. C is the zone of maximum convergence and D is the zone of maximum divergence.

continuity arguments imply a compensating upward vertical motion, while divergence would require downward motion. Such motions would be important in the transport and diffusion of atmospheric pollutants. It would appear that the Wyocena wind data provide a fairly good estimate of the mean wind field for the region, but the resulting deviations at the other sites must be considered if an accurate determination of pollutant transport is to be made.

The number of 30-min mean values with the same sign as the sector mean were used to determine the consistency of the results for each wind sector. The average consistency is 80%, being higher for large positive or negative sector mean values and approximately 50% for small values (Weidner 1976).

The effect of averaging time also was examined by taking the sector mean values of wind speed and direction, and determining an overall sector mean value of divergence and vorticity. The agreement is good for both cases (Wediner 1976). The largest difference occurs in the 120° to 140° sector, where the wind field is most likely to have greatest nonlinearity. In this sector it shows greatest deviations from the Wyocena data. The recomputed means tended to reduce the magnitudes of the vorticity and divergence, but the difference is small between the recomputed long-averaging time values and the original values computed from 30-min means.

CONCLUSIONS

There appears to be a definite organization of the wind field as functions of wind direction and speed around the Baraboo Bluffs. This was true especially when the wind blew perpendicular to the bluffs. The wind direction at the Dekorra site deviated approximately 15° from that measured at Wyocena. The symmetric variation of the divergence and vorticity fields about the azimuthal direction of the southern bluffs support the view that the Baraboo Bluffs play an important part in the kinematics of the wind field in the region of the meteorological network. The wind data at the Messer site was influenced by the direction of the wind relative to the bluffs and provided a poor representation of the mean wind field in the valley.

SECTION 8

A COMPARISON BETWEEN THE HINO AND WIND DIRECTION RANGE METHODS FOR ESTIMATING GROUND LEVEL SULFUR DIOXIDE CONCENTRATIONS FROM AN ELEVATED SOURCE

INTRODUCTION

Presently, Gaussian Plume computer models are not reliable predictors of mean hourly pollutant levels downwind from an elevated point source. Researchers are still seeking better methods for estimating these pollutants--one of which is SO_2--at ground level.

This section covers the period 27 April to 31 December 1976. σ_y and σ_z are the horizontal and vertical dispersion coefficients, respectively, used in the Gaussian Plume model in Eq. (14). Two different methods for calculating σ_y and σ_z are compared to determine which method produces results that are closest to observed concentrations. A total of 343 mean hourly ground-level SO_2 concentrations were calculated using the two different methods of estimating σ_y and σ_z when all other parameters in the model were the same.

To calculate σ_y and σ_z this study used the horizontal wind directional range and vertical wind speed range method, otherwise known as the range method. The comparison method, used by Ragland et al. (1980), employed a more traditional approach and estimated the dispersion coefficients by using the Mikio-Hino Stability classification system, or the stability method.

It has been shown (Nuclear Regulatory Guide 1972), and will be clarified later, that by using the actual wind statistics rather than a stability classification method, one will obtain results which are in closer agreement with observed data. The importance of using the actual wind statistics to determine the dispersing chracteristics of the atmosphere will be reemphasized in this section. It will also be shown that by using wind statistics rather than a classification scheme, the Gaussian Plume equation will yield better results.

THE GAUSSIAN MODEL

Gaussian diffusion theory was developed by Sutton (1932) and numerous variations of his derived equations have been used in air pollution studies. For example, the Wisconsin Environmental Protection Agency and

Department of Natural Resources use Gaussian-type diffusion models in their pollution studies.

By starting with the basic continuity equation (Eq. 1) for a scalar property, the necessary Gaussian equations needed for this pollution study (Ragland et al. 1980) can be derived. Using the Gaussian distribution assumes the pollutant is normally distributed perpendicular to the advecting horizontal wind. The center line value represents the maximum concentration in the plane perpendicular to the plume line. Statistically it is assumed that the concentration falls off to 10% of the center line value two standard deviations on either side of the center line (Slade 1968). This appears to be a good first approximation for long averaging times (hours, etc.), although atmospheric pollutants rarely achieve a normal distribution for the 1 hr periods considered in this study. "In practice, deviations from a Gaussian distribution are common but in an apparently nonsystematic way. The concentration profile through a plume may be too peaked, too flat, or too skewed to be classified as Gaussian curves. However, since no single class of functions adequately describes all the possibilities, it appears practical to maintain the Gaussian interpolation formula and inquire into the magnitude of possible resulting errors" (Slade 1968).

DISPERSION COEFFICIENTS

In the Gaussian Plume equation, (Eq. 14) σ_y and σ_z represent the horizontal and vertical spread of the plume as it is advected downwind of the point source. Much work has been done to achieve a good estimate for σ_y and σ_z (Cramer 1957, Pasquill 1962, Hino 1968, Slade 1968). Heretofore, no one method has been proven to be superior to the others.

Methods to Determine σ_y and σ_z

The stability method used the Mikio-Hino stability classification system. This classification system attempts to estimate a net radiation budget for the lower atmosphere and from this determine the dispersing characteristics of the lower atmosphere (Hino 1968). Ragland et al. (1980) describes the results obtained from using this classification method.

The range method was used in this study. The equations used for estimating σ_y and σ_z in this method were taken from Slade (1968). They estimate the turbulent structure of the atmosphere, directly from the wind field. The equations are:

$$\sigma_y = \frac{\text{Range } \Theta \cdot x}{4.28}$$

$$\sigma_z = \frac{\text{Range } \phi \cdot x}{4.28} \qquad (46)$$

$$\text{Range } \phi = \frac{\text{Range } w}{u}$$

where

σ_y is standard deviation of the cross wind direction

σ_z is standard deviation of the vertical wind speed

Range θ is the range of the horizontal wind direction

Range w is the range of the vertical wind speed

Φ is vertical wind direction

x is downward distance from the smoke stack to the monitoring site

$\bar{u}$ is mean wind speed of the advecting wind field for the point source.

The range of the needed horizontal and vertical wind components were obtained by using a horizontal wind vane and a vertical anemometer.

The stability method is not a direct method of estimating dispersion coefficients which arise from the dynamics of the atmosphere. Using the horizontal and vertical wind ranges, which are based on the dynamics of the atmosphere, appears to be a much more appropriate means of estimating σ_y and σ_z (Environmental Research Laboratory, 1977).

Plume Rise

Before Eq. (14) can be used as a computer model one more aspect of the plume must be taken into account. That is, how high will the plume be allowed to rise into the atmosphere? This is handled by considering a mixing height which acts as a lid on atmospheric pollutants and limits the vertical extent of the plume between the ground and itself. In this study there were no means by which to measure the actual mixing height, therefore a value of 1500 m was used.

Csanady (1973) presents the basic equation needed for this validation study:

$$C = \frac{Q}{2\pi\sigma_y\sigma_z\bar{u}} \text{Exp}\left(\frac{-y^2}{2\sigma_y^2}\right) \sum_{n=-\infty}^{\infty} \text{Exp}\left\{\frac{(-h-2nH)^2}{2\sigma_z^2}\right\} \qquad (47)$$

h is stack height

H is mixing height

n is number of reflections

The infinite series must be written in a more usable form before it can be implemented in a computer model. Ragland et al. (1980) works through the mathematical derivation and arrives at the form:

$$C = \frac{Q}{2\pi\sigma_y\sigma_z\,\overline{u}} \quad \exp\left(\frac{-h^2}{2\sigma_y^2}\right) \quad \exp\left(\frac{-h^2}{2\sigma_z^2}\right)$$

$$\left\{1 + \sum_{n=1}^{\infty} \left[\exp\left(\frac{2nh\ H - 2n^2H^2}{\sigma_z^2}\right) - \exp\left(\frac{-2nhH - 2n^2H^2}{\sigma_z^2}\right)\right]\right\}$$

Using an upper limit of $n = 10$ is sufficient because the exponented terms become too small to affect the rest of the equation for $n > 10$.

When considering the spreading of the plume from the stack the initial rise of the plume as it is released from the stack must be considered. To simplify the treatment of this initial plume rise, an imaginary height called the "effective stack height" is used in the model. This imaginary height is the sum of the actual stack height (h_s) plus the initial rise of the plume (Δh) after emission. Variable h in Eq. (14) represents the "effective stack height."

Briggs (1971, 1972) has done extensive work in the area of plume rise. His relationships based on the stack height, wind velocity, stack heat flux, and turbulence are used in this study.

There are a number of non-meteorological variables required by the Gaussian plume equation. Two are the amount of coal burned per hour and the temperature of the gas mixture leaving the stack, or the heat flux up the stack and a number of other parameters. Empirical formulae that depend on the design of the boiler used in burning the coal have been written to deal with these needed model inputs. A discussion on the boiler at the Columbia Generating Station, along with a complete set of empirical formulae that were used for that particular boiler, can be found in a report by Wisconsin Power and Light (1976).

The Gaussian Plume computer model used for the range method was basically the same as the model used in the stability method (Ragland et al. 1980). The only difference in the mechanics of the model is the manner in which σ_y and σ_z are calculated. All other variables and model inputs are identical. This was done to insure that any difference in the SO_2 concentrations calculated for the two methods would be due solely to differences in the dispersing schemes employed by each method.

The coal-fired generating station, located near Portage, Wisconsin, 50 miles north of Madison, Wisconsin, burns a low sulfur Montana coal. Since the start up of the generating station on 15 July 1975, the plant has proven to be a very "clean" generating station. This coal-fired generating station has consistently emitted SO_2 concentrations well below the limit established by the federal government (Wisconsin Power and Light 1976).

A network of seven SO_2 monitoring sites was set up around the generating station for Wisconsin Power and Light Co. by the Dames and Moore consulting firm. Figure 43 shows the area and sites surrounding the power plant, and Table 11 gives the distance and direction of each monitoring site from the station.

TABLE 11. DISTANCES AND DIRECTIONS OF SO_2 MONITORING SITES FROM THE COLUMBIA GENERATING STATION

Site	Distance (km)	Direction
Portage, Cemetery	9.9	NNW, 332°
Lake George	5.9	ENE, 69°
Dekorra	4.4	SW, 227°
Messer	7.3	W, 267°
Genrich	8.3	N, 7°
Bernander	14.6	E, 97°
Russell	15.5	NE, 37°

Determining Observed Sulfur Dioxide Concentrations

In order to determine exactly how much SO_2 the generating station was adding to the atmosphere, the procedure described as follows was used (Ragland et al. 1980). If the plume was determined to be over one of the seven monitoring sites, the averaged SO_2 concentrations for the other six sites was calculated. This average was then subtracted from the SO_2 reading at the site within the plume. The remaining value was thought to be contributed exclusively by the power plant. The assumption used here is that the SO_2 concentrations at the other sites are caused by a background level of SO_2. This background concentration is considered to be contributed by sources other than the Columbia Generating Station. If a site direction from the Columbia Generating Station was within 22.5° of a line downwind of the Messer site and had a reading of at least 10 μ g.m^{-3}, then it was assumed to be under the plume.

A study by Dames and Moore (1976), shows that at times the background concentrations of SO_2 were of the same order of magnitude as those observed at the downwind monitoring sites. This occurred mainly when the prevailing wind was from the south, making the Madison and Chicago areas possible contributors to the background concentration level.

Instrumentation and Meteorological Recording

Dames and Moore used the Phillips SO_2 monitor PW 9700 to measure the ground level SO_2 concentrations. The monitor was considered accurate for readings $\geq$ 10 μg.m^{-3}, which was the lower limit of accuracy for the Phillips SO_2 monitor. During the study period, the monitors were calibrated quarterly by Dames and Moore. The observed SO_2 hourly values were punched on computer cards and sent to a central data base. The meteorological variables recorded for this study were made at the Messer site (Figure 13).

The range method required the horizontal wind directional range and vertical wind speed range. One other variable needed was the horizontal wind speed. This along with the other wind variables mentioned were recorded continuously on top of the 32-m tower at the Messer site.

Messer was the only site equipped with a vertical anemometer, and therefore had to be used for the vertical wind measurements. One question that arises when considering the Messer site is what effect the sloping terrain east of the site has on the vertical wind speed when the wind is from the east. Since the range of the vertical wind speed is required, while the absolute value of the vertical wind speed is not, the sloping terrain should have only a negligible effect on the absolute value of the vertical wind speed. The degree to which the wind field was affected by the Baraboo Bluffs is unknown, but local terrain may have had some influence on the wind field at the Messer site.

Calculated Sulfur Dioxide Data

The Dames and Moore consulting firm recorded and provided the ground-level SO_2 concentrations used in this study. The calculated SO_2 values for the stability method were obtained from Goodell (1977).

The meteorological data had to be translated from a continuous strip chart trace into hourly averaged numerical values. The recorders were run continuously for the study period, but due to maintenance problems with the recorders or the instrument systems themselves, some of the desired time periods had to be disregarded. The stability method had a total of 492 hours in which to compare calculated SO_2 concentrations to actual SO_2 data. The hours that were selected were chosen for two reasons:

(1) Because they represented times when the plume was suspected of being over one of the SO_2 monitoring stations, and (2) because these hours contained a complete set of input data that was required for the stability method.

Of the 492 cases that the stability method considered, the range method used 343 cases to compare calculated to actual concentrations. Vertical wind measurement is required by the range method, but this was not available for the remaining cases.

The horizontal wind speed, which represented the advecting wind for the plume, was processed directly onto punch cards (Section 3). The horizontal wind directional range and the vertical wind speed range were processed by hand, rather than using the digitizing chart reader.

To determine the needed wind range components the following method was used: (1) Each hour was broken down into six 10-min intervals, (2) for each interval two markers were drawn so that 90% of the trace fell within these markers (the 10% that fell outside the markers represented the brief extreme eddies which were not considered here because they acted for such a short time period) (3) after the 10-min traces had been processed, a representative hourly value was computed by giving equal weight to each interval and finding the arithmetic mean for the sample. The above procedure was done in an attempt to better represent a normally distributed plume.

The strip charts were divided across the papers into 50 intervals. For the wind directional range each interval represented 6.9° of azimuth angle, and for the vertical anemometer range each interval represented 0.5 m/sec. The ranges were computed by multiplying the number of intervals used on a chart for a particular hour by the appropriate scale factor.

Averaging Procedure

The SO_2 ground level monitors are sensitive to wind direction changes, so to relieve some of this sensitivity an averaging scheme was used to desensitize the model output to wind direction (Ragland et al. 1980). The process that was used calculated an average concentration over some arc length. The size of the arc was dependent on the turbulent structure of the atmosphere and was given by

$$\text{Arc length} = 4\ \sigma_y \cdot x \qquad (48)$$

where σ_y depends on the range of the horizontal wind direction and x is the distance to the monitoring site.

The averaging procedure proved to be of great benefit in calculating the ground level SO_2 concentrations. It reduced the overall error between the range method and the actual observed concentration by as much as 10 standard deviation points. The reason for the success of this method lies in the fact that it is virtually impossible to pinpoint the mean hourly wind direction. Therefore, by calculating an average concentration for a variable arc length it is not necessary to know precise wind direction. The averaging procedure does add some error, but it eliminates errors in the measuring and processing of data which may be 10 degrees or more.

RESULTS

In an attempt to obtain better results from the Gaussian Plume Equation, an alternate method was used to determine the turbulent structure of the atmosphere. This method used the range of the wind statistics (Eqs. 15 and 16) rather than employing the more traditional approach of employing stability class indices. Once the turbulent structure had been determined, this information was used in the Gaussian Plume equation to estimate ground level SO_2 concentrations. Concentrations determined for the range method, along with those obtained from the stability class method, were compared to actual SO_2 data.

Model Results Compared

Overall, the range method showed some improvement over the stability method. Compared to the observed SO_2 data, the overall standard deviation for the range method was 45 $\mu g.m^{-3}$ while for the stability method the standard deviation was 48 $\mu g.m^{-3}$. The average concentration for the observed SO_2 data over the 343 hourly values was 52 $\mu g.m^{-3}$, which implies that both methods have errors of the same order of magnitude as the mean concentration. At first glance, these seem to be poor results. A more in-depth review of the results, however, show more of an improvement than the standard deviations indicate.

Figure 56 is a bar graph of the stability method results versus the results obtained by using the range method. Both methods have been normalized by the observed SO_2 values for the corresponding hours. The most striking portion of the graph is the region between 00.0 and 0.10 units, where the stability method has underestimated 18.5% of the concentrations by 90% or more. In the same region of the graph, the range method underestimated 4.6% of the data by a corresponding amount. Most of the exaggerated underestimations of the stability method occurred during hours that were characterized by light winds. It is during these situations that the range method offers a definite improvement over the stability method. These hours correspond to the D and E Mikio-Hino stability classes. Table 12 represents the variability of σ_y and σ_z for both methods within the D and E stability classes. By nature σ_y and σ_z were constant in the stability method for a given stability and site. However, in the range method σ_y and σ_z are allowed to vary with time. The magnitude of the standard deviations of σ_y

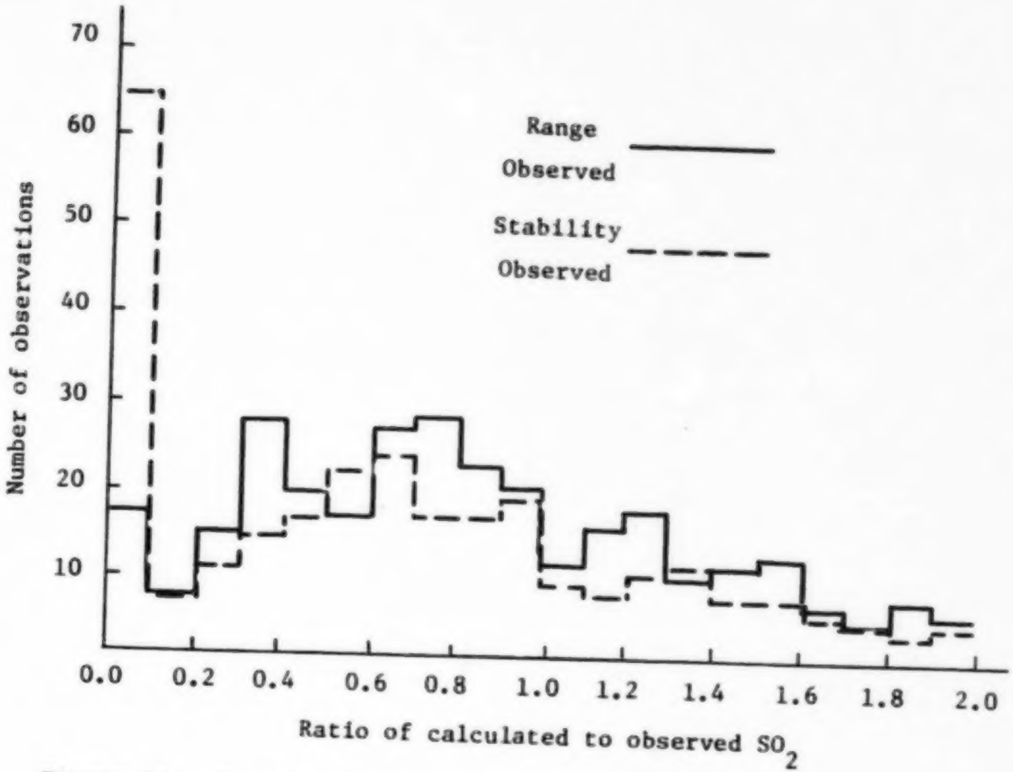

Figure 56. The SO_2 ground-level concentrations obtained by using two different dispersing characteristic methods in the Gaussian Plume equation.

TABLE 12. VARIABILITY OF σ_y AND σ_z

		σ_y[a]		Standard Deviation of σ_y		σ_z[a]		Standard Deviation of σ_z	
Stability	Site	Range	Stability	Range	Stability	Range	Stability	Range	Stability
D	Lake George	817	330	441	0	355	98	187	0
D	Genrich	825	450	246	0	1645	124	1903	0
D	Bernander	1342	749	407	0	1119	168	599	0
D	Russell	1134	790	404	0	716	174	285	0
E	Genrich	759	339	289	0	589	76	322	0
E	Bernander	1567	564	603	0	883	506	615	0
E	Russell	1271	595	622	0	660	552	314	0

[a] Units are in meters.

and σ_z in the range method is evidence that the atmosphere can exhibit extreme turbulent variability even in supposedly classifiable situations.

In general, the curve for the range method seems to be skewed towards underestimating the SO_2 concentrations. Even though the curve appears to be weighted towards underestimating the SO_2 concentrations, more of the range method's results lie within a factor of two of the observed values than results of the stability method. Of the 343 hours used in the study, 64% of the range method's values lie within a factor of two of the observed data, while 53% of the stability method's estimations fell within these limits. Although a factor of two may represent a sizable error in some cases, it still represents a fairly good estimation when the present state of the art is considered.

Erratic Sulfur Dioxide Behavior

It appears that not all of the model's underpredictions or overpredictions can be contributed solely to model inadequacies. During a number of time series (5 consecutive hours or more), the actual SO_2 data exhibited "erratic" behavior. The SO_2 concentrations, as measured by the monitors, seemed to jump from low concentrations to high concentrations, or vice versa, without any justification by the model input data.

Table 13 shows a representative time series for 6 May from 0700Z to 1600Z, one of the periods when the observed SO_2 concentrations seemed to vary around for no apparent reason. Table 13 also includes the model input parameters. An examination of Table 13 reveals that the input parameters do not support the "erratic" behavior exhibited by the observed SO_2 data. Between the hours of 0900Z and 1000Z, the model and the observed SO_2 concentrations not only disagree in the amount of effluent at the surface, but the model predicts a slight increase while the data shows a sizable decrease in ground level SO_2 concentrations. This is rather disconcerting because the model and the data drastically disagree and because the observed data has tended to exhibit this inexplicable behavior a number of times within the study.

Nearly all of these cases occured at the Dekorra site. This site is the closest monitoring station to the power plant, therefore, such behavior should not be totally unexpected. The most predictable stations were the Bernander and Russell sites. They also happen to be the stations farthest from the SO_2 source. The site names and standard deviations calculated between the model and the data for both models is given in Table 14. Table 14 shows that the highest standard deviations correspond to the closest stations, while the smallest deviations between the model and the data correspond to the stations farthest from the power plant. One explanation for this apparent inverse relationship is that the plume approaches a normal distribution as distance from the generating station increases.

TABLE 13. A TIME SERIES REPRESENTING SOME OF THE "ERRATIC" BEHAVIOR OBSERVED AT DEKORRA. THE GROSS MEGAWATT LOAD (GMW) IS A MEASURE OF THE AMOUNT OF COAL USED IN 1 HR

									Predicted SO_2	
		Horizontal		Range Method		Stability Method				
Hour	Wind Direction	Wind Speed	GMW	σ_y	σ_z	σ_y	σ_z	SO_2 Observed	Range Method	Stability Method
7	56.5	3.0	385	782	550	390	231	45	48	200
8	55.0	3.0	469	715	796	390	231	178	63	212
9	66.5	2.5	501	901	634	232	542	178	51	116
10	53.0	2.5	506	795	638	232	542	88	56	114
11	64.0	2.0	506	1007	696	232	542	66	44	125
12	67.0	2.0	508	1020	700	232	542	44	40	122
13	62.0	2.0	507	874	726	232	542	130	48	123
14	65.0	2.0	510	980	745	232	542	130	45	127
15	74.0	2.0	508	1086	894	232	542	130	43	126
16	81.0	2.0	510	967	747	232	542	64	50	126

TABLE 14. OVERALL STANDARD DEVIATIONS[a] USING RANGE AND STABILITY METHODS RANKED ACCORDING TO SITE

Site Name	Standard Deviation Range	Standard Deviation Stability	Distance from Columbia Generating Station (km)
Dekorra	61	66	4.4
Lake George	49	57	5.9
Messer	37	32	7.3
Genrich	43	43	8.3
Bernander	17	18	14.6
Russell	27	21	15.5

[a] Units are in $\mu g/m^3$.

Conclusions and Recommendations

The vertical and horizontal wind range method was shown to provide a more accurate description of the turbulent structure of the atmosphere than that given by the stability classification method. The validity of the range method was tested in the Gaussian Plume Equation for predicting ground level SO_2 concentrations. The range method's strength lies in its ability to obtain far better results during light wind situations. During neutral and unstable situations both models perform approximtely the same. Besides offering better results, the range method requires a minimal set of meteorological variables. It depends only on wind statistics; other parameters--lapse rate or cloud cover--are not required.

There is much room for improvement in the study of air pollution and the results of this investigation are indicative of the potential to improve existing air pollution models. The input parameters that afford the greatest amount of variability in the results obtained from the Gaussian Plume Equation are those that describe the dispersing characteristics of the atmosphere--σ_y and σ_z. Most of the current research in air pollution relies on using stability classification systems to estimate σ_y and σ_z. However, if substantial advances are to be made in the field, direct methods must be used to represent the atmosphere.

As previously mentioned in Section 7, the Wyocena site affords the best representation of the wind in the valley around the power plant. This may be a more attractive site than the Messer site since the effect of the Baraboo bluffs on the wind is not completely understood. The fact that the top of the smoke stack is 152.5 m above the valley floor presents a problem when wind regime in the valley is measured. Some type of Ekman solution could possibly be used to account for the wind speed and directional change within the boundary layer.

The unexplainable fluctuations at the Dekorra site presented the greatest problem in the study. This site should be studied in more detail to explain the behavior of the plume close to the source. The placement of a bivane or vertical anemometer at the site would help explain the correlation between vertical motions and ground level concentrations close to the source. It appears that the plume requires some time before it assumes a normal distribution in the atmosphere.

The Columbia Generating Station and the area surrounding the power plant offer a fine opportunity for air pollution research. Most of the area is flat and the surrounding land offers a broad study region. The proper location of the meteorological monitoring equipment around the station is extremely important. A few of the suggestions at the end of this report might be used in future research.

SUMMARY

There are two different methods for estimating the dispersion coefficients σ_y and σ_z. These coefficients are used in the Gaussian Plume equation to estimate hourly averages of ground level SO_2 concentrations downwind of an elevated point source. The estimated SO_2 concentrations obtained from the Gaussian equation for each method were compared to actual observed data.

One method for estimating σ_y and σ_z uses the horizontal wind directional range and the vertical wind speed range. The other makes use of the Mikio-Hino stability classification system. All other parameters used in the Gaussian equation are the same for both methods.

The vertical and horizontal wind range method offered two significant improvements over the stability classification method. First, during light wind situations the horizontal and vertical wind range method was superior to the stability classification method. Second, the horizontal and vertical wind range method employs fewer atmospheric variables while offering a more direct approach to estimating the dispersing characteristics of the atmosphere.

SECTION 9

POSSIBLE INFLUENCE OF THE COOLING POND ON THE LOCAL ENVIRONMENT

INTRODUCTION

The Columbia Generating Station, with one 527-megawatt unit, dissipates waste heat from the condensor with recirculated water from a 162-ha (400-acre) cooling pond. The cooling pond dissipates the waste heat largely by the fluxes of latent and sensible heat from the pond surface to the air. These additions of latent and sensible heat to the air may in turn alter the local environment. The addition of water vapor to the air increases water vapor content of the air above the ambient, which may result in the formation of fog downwind from the cooling pond. Water vapor in the fog may then condense on surfaces which could affect the local environment. The sensible heat fluxes, however, may warm the air moving over the cooling pond, increasing air tempreatures downwind and reducing the likelihood of fog.

Extensive studies on the fluxes of latent and sensible heat have been and are being carried out by Argonne National Laboratory using a cooling pond at Dresden, Illinois (Hicks et al. 1973). One goal of the Argonne studies at Dresden is to accurately evaluate the bulk transfer approach to the fluxes of latent and sensible heat by using eddy correlation techniques (Hicks 1974, Hicks and Wesely 1974, Hicks et al. 1974)

Yamada (1978) modeled the mesoscale circulation associated with the Dresden cooling pond in an attempt to assess the environmental effects of the cooling pond. The model has been used to simulate the formation of fog and clouds over a cooling pond. The model's pond area is about 4 km^2, while the area of the Columbia Generating Station's cooling pond is about 1.6 km^2.

The Argonne group has studied the Dresden pond for approximately 8 yr. The evaluation of how the Columbia Generating Station's cooling pond has influenced the local environment cannot be compared to the work done by the Argonne group at this time.

LATENT AND SENSIBLE HEAT FLUXES

The sensible and latent heat fluxes from the Columbia Generating Station cooling pond are estimated by the bulk aerodynamic method (Hicks and Wesely 1974). The relationships used are:

$$E_o = f(V)(e_a - e_s) \tag{49}$$

where

E_o is latent heat flux to the air (W m^{-2})

e_a is vapor pressure of the air above the pond (mb)

e_s is vapor pressure of the pond surface determined from the saturation vapor pressure at the pond temperature (mb)

f(v) is a wind speed dependent function

f is 6.1 + 3.0 V

V is wind speed over pond (m sec^{-1})

The relationship for f(V) above is based on Rimsha and Donshenko as tested by Hicks et al. (1974), resulting in the smallest mean and RMS error.

The sensible heat flux from the cooling pond to the air is estimated as:

$$Q_o = 0.47\ f(V)(T_a - T_s) \tag{50}$$

where

Q_o is sensible heat flux to the air (W m^{-2})

T_a is air temperature over pond (°C)

T_s is pond temperature (°C)

Measurements over the pond of T_a, e_a, and V were missing, so T_a and e_a at Truax Field, Wisconsin were used and V was measured at the Dekorra site about 1 mile south of the cooling pond. Mean daily values were used for all items because cooling pond temperatures and other items were only available as daily averages. The estimated values of E_o and Q_o are daily averages. The cooling pond temperatures were measured at the consenser inlet and outlet so the cooling pond average temperature was calculated as the geometric average of the inlet and outlet temperature. The average daily values of E_o and Q_o were averaged over the month to obtain monthly averages. E_o was also converted to the average daily water loss from the cooling pond in units of m^3 day^{-1}. The monthly average values of Q_o and E_o are given in Table 15.

TABLE 15. MONTHLY AVERAGE HEAT BUDGET FOR THE COLUMBIA GENERATING STATION COOLING POND FROM 1 JULY 1975 TO 30 JULY 1976. UNITS ARE W m^{-2}. THE HEAT BUDGET EQUATION[a] IS $SW\downarrow(1-a) + LW\downarrow - \sigma T_o^4 + P_o = S_o + Q_o + E_o$

Month	$SW\downarrow(1-a)$	$LW\downarrow - \sigma T_o^4$	P_o	S_o	Q_o	E_o	Rem
July	284.	-63.	169	24	71	337	2
Aug.	195.	-83.	338	-7	90	392	61
Sept.	161.	-87.	368	-44	107	327	-36
Oct.	125.	-34.	114	-13	57	161	-26
Nov.	63.	-55.	391	-46	104	164	85
Dec.	44.	-80.	328	3	137	147	11
Jan.	71.	-91.	345	0	184	162	-21
Feb.	96.	-93.	348	31	160	207	15
Mar.	139.	-79.	415	2	162	256	57
Apr.	230.	-86.	395	33	145	365	-4
May	247.	-70.	234	-18	104	285	140
June	283.	-52.	115	63	74	345	-136
July	279.	-88.	355	13	102	542	-101
Average	170	-74	309	20	115	284	4

[a] $SW\downarrow$ is global radiation; a is pond albedo; $LW\downarrow$ is longwave radiation from the sky; σT_o^4 is longwave radiation from the pond; T_o is pond surface temperature; P_o is Columbia Generating Station output to the cooling pond; S_o is heat storage in the pond water; Q_o is sensible heat loss to the air; E_o is latent heat loss to the air; Rem is calculated so that if the left side of the equation is greater, Rem is positive.

HEAT BUDGET

It would be advantageous to confirm the estimates of Q_o and E_o with independent methods. The heat budget approach for the cooling pond was based on the following relationship:

$$SW\downarrow(1-a) + LW\downarrow - \sigma T_o^4 + P_o = S_o + Q_o + E_o \qquad (51)$$

where

$SW\downarrow$ is solar radiation incident on the cooling pond

a is pond albedo

$LW\downarrow$ is longwave radiation down

σT_o^4 is longwave radiation up from pond

σ is Stefan-Boltzmann constant

P_o is condenser output per m^2

S_o is heat storage in pond water per m^2

The units are Wm^{-2}. $SW\downarrow$ was measured at the Messer site and was within 3% of monthly values estimated from Truax Field using percent possible sunshine. For convenience, the Truax Field data was used to compute the average daily $SW\downarrow$ (Stearns 1978). The albedo of water used was 0.05. $LW\downarrow$ was determined as σT_a^4, where T_a is the average daily temperature at Truax Field. This will provide an overestimation of $LW\downarrow$. The heat discharged to the cooling pond from the condenser was initially calculated as the flow rate of the pump per m^2 of pond area times the water temperature difference across the condenser. This method proved erratic when compared to the average monthly power generated. Therefore, the average monthly power generated divided by 0.65 (Andrews and Anderson 1979) was used to determine the average power discharge to the cooling pond by the generating station. The heat storage in the pond was determined from the day-to-day change in average temperature and the average pond depth. Monthly averages were calculated from the daily averages for all values in the heat budget equation and are presented in Table 15. Positive values of Rem indicate that the heat inputs of $SW\downarrow$ and P_o are greater than the losses. P_o may be in error due to the assumption of 0.65 as the ratio of the power generated to the power discharged to the cooling pond. The average monthly difference for the 13-month period is 4 $W\ m^{-2}$ even though an individual month such as May is off by 140 $W\ m^{-2}$. As a result, the estimated latent heat loss will be assumed correct.

The water budget in Table 16 shows a remainder which is assumed to be leakage from the cooling pond. Inflow, outflow, and precipitation are based on Andrews and Anderson (1976). Evaporation is calculated from the latent heat flux values given in Table 15. The change in pond water level from month to month should give the storage change, but missing data prevented this from being fully applied. The monthly changes were small compared to the remainder. The 13-month average remainder was $2.76 \times 10^4\ m^3\ day^{-1}$. The value obtained by Andrews (1977) was $2.1 \times 10^4\ m^3\ day^{-1}$ for an annual average. Increasing the evaporation by $0.66 \times 10^4\ m^3\ day^{-1}$ would increase the average latent heat flux by 119 $W\ m^{-2}$ and would seriously upset the average heat budget. A source for this much heat input would be difficult to find.

TABLE 16. MONTHLY AVERAGE WATER BUDGET FOR THE COLUMBIA GENERATING STATION COOLING POND FOR 1 JULY 1975 TO 31 JULY 1976. THE UNITS ARE 10^4 m^3 DAY^{-1}. THE BUDGET EQUATION IS INFLOW OUTFLOW + PRECIPITATION - EVAPORATION EQUALS REMAINDER

Month	Inflow	Outflow	Precipitation	Evaporation	Remainder	Storage change
July	5.46	-0.87	0.21	-1.87	2.93	
Aug.	5.52	-0.95	0.61	-2.18	3.00	0
Sept.	5.44	-1.07	0.11	-1.82	2.66	0
Oct.	5.28	-0.51	0.04	-0.90	3.91	+0.49
Nov.	5.46	-1.20	0.53	-0.91	3.88	-0.49
Dec.	5.46	-1.19	0.07	-0.82	3.52	+1.60
Jan.	5.28	-1.61	0.14	-0.90	2.91	0
Feb.	5.95	-1.44	0.32	-1.15	3.65	0
Mar.	4.28	-1.38	0.50	-1.42	1.98	-0.38
Apr.	5.05	-1.01	0.60	-2.03	2.61	+0.38
May	5.26	-1.04	0.28	-1.58	2.92	+0.38
June	2.36	-0.64	0.20	-1.92	0.01	—
July	5.42	-1.07	0.55	-3.01	1.89	—
Total	66.23	-13.98	4.16	-20.51	35.88	
Average	5.09	-1.07	0.32	-1.57	2.76	

INFLUENCE ON THE LOCAL ENVIRONMENT

The addition of water vapor to the atmosphere by the cooling pond can result in fog and possible condensation downwind of the cooling pond. Hicks and Shannon (1976) developed a cooling pond fog index defined as:

$$e_c - e_c' > 0.7 \text{ mb} \tag{52}$$

where

e_c is $1/2\ (e_s + e_a)$

e_c' is saturation vapor pressure at $T_c = (T_a + T_s)/2$.

The index indicates the presence of fog over the cooling pond.

The fog index was applied to the Columbia Generating Station cooling pond with fog indicated on the dates in Table 17. Air temperature and vapor pressure were daily averages from Truax Field.

TABLE 17. DAILY AVERAGES OF TEMPERATURE AND VAPOR PRESSURE ON DAYS WITH A HIGH LIKELIHOOD OF RIME FORMING DOWNWIND OF THE COLUMBIA GENERATING STATION COOLING POND

Date	T_a[a] (°C)	T_s[b] (°C)	e_a[c] (mb)	e_s[d] (mb)	$e_c - e'_c$[e] (mb)	Δe[f] (mb)	ΔT[g] (°C)
17 Dec. 1975	−14.7	12.7	1.51	14.58	2.36	−0.20	1.1
18 Dec. 1975	−14.2	12.8	1.15	14.77	2.12	−0.35	1.1
4 Jan. 1976	−15.6	11.0	1.15	13.11	1.94	−0.18	1.1
8 Jan. 1976	−19.4	9.0	0.76	11.47	1.96	−0.12	1.1
16 Jan. 1976	−11.9	9.1	2.10	11.56	1.27	+0.03	0.8
17 Jan. 1976	−17.5	9.4	1.09	11.78	1.90	−0.01	1.1
18 Jan. 1976	−14.7	9.6	1.25	11.95	1.55	−0.25	1.0
27 Jan. 1976	−17.8	11.8	0.98	13.83	2.51	0.00	1.2
2 Feb. 1976	−21.4	13.2	0.69	15.17	3.39	+0.14	1.4
5 Feb. 1976	−12.8	13.9	1.59	15.77	2.30	−0.15	1.1

[a] T_a is Truax Field average air temperature.

[b] T_s is Columbia Generating Station cooling pond temperature.

[c] e_a is Truax Field average vapor pressure.

[d] e_s is Columbia Generating Station cooling pond vapor pressure.

[e] $ec^{-e'}c$ is cooling pond fog index fog if > 0.7 mb.

[f] Δe is vapor pressure deficit downwind of the Columbia Generating Station cooling pond. Positive values indicate possible rime deposits.

[g] ΔT is air temperature rise downwind of cooling pond.

Fog over the cooling pond is not a problem unless the water is conveyed downwind from the cooling pond. The vertical near-surface air layer over the pond is highly unstable because the pond temperature in winter exceeds the air temperature by 20°C or more. Using the assumption that the ratio of the rise of the uniformly mixed layer over the pond to the fetch is 0.05, and Eq. (49) the vapor pressure of the air downwind of the cooling pond is:

$$e_d = 0.0410\ e_s + 0.96\ e_a \qquad (53)$$

where e_d is vapor pressure of air at downwind edge of cooling pond. If e_d is greater than the saturation vapor pressure of the air at the air temperature, then condensation could occur on surfaces away from the cooling pond assuming they are at air temperature. Table 16 indicates that this could occur on 16 December 1975 and 2 February 1976--since Δe is positive on these dates. Hennen (1976) reported that condensation occurred on the instrument mast located at the dike end south of the generating station on 2 February 1976 during the 1975-76 winter.

Everett and Zerbe (1976) report on fog and downwind rime icing associated with the Dresden cooling pond. In winter fog usually extended several hundred meters downwind from the warmest pond and caused rime icing. Their report does not include data on the pond temperature. The latent and sensible heat fluxes reported by Hicks and Wesely (1974) over the Dresden cooling pond are ≥ 400 W m^{-2} and are comparable to the estimates at the Columbia Generating Station cooling pond. The generating capacity of the Dresden Generating Station is not known so that direct comparison to the Columbia station cannot be made.

The possible warming of the air due to passage over the cooling pond can be estimated from an expression similar to Eq. (33). This equation gives temperature increases on the order of 1°C downwind from the cooling pond. This temperature increase is not considered significant enough to influence local climate.

Increasing the waste heat discharge by adding another 527-MW unit to the Columbia Generating Station will increase the likelihood of fog and rime occurring downwind from the cooling pond.

SECTION 10

INTRA- AND INTER-SITE CORRELATION OF WIND DATA

The U.S. Weather Service data at Truax Field, Madison, Wisconsin is frequently used to estimate wind conditions at other locations. Truax Field data were used to make the initial environmental impact statements regarding the ground level concentration of emissions for the Columbia Generating Station. Truax Field wind data are also used to estimate the local wind energy potential.

Data from sites at the generating station and from Truax Field were compared using mean values and correlation coefficients to determine the conditions under which measurements at one point are valid at another point. The data are from the 2-yr period 1 January 1976 to 31 December 1977. Correlation coefficients were determined between two sets of simultaneous observations. The correlation coefficient is described as:

$$r = \frac{1}{n} \sum_{i=1}^{n} xy_i/(\sigma_x\sigma_y) \qquad (54)$$

where

r is correlation coefficient

x_i is value of first wind speed or direction

y_i is value of second wind speed or direction

n is number of observations

σ_x is standard deviation of x

σ_y is standard deviation of y.

To calculate the correlation coefficient there must be a valid data point at each site. If the wind speed is zero the Truax Field, then the wind direction is given as zero; however, this is not a valid observation and must be removed from the data set. Erroneous data points are discarded and do not enter into the correlation coefficients or mean values.

To improve recording reliability, the Messer Site was equipped with two anemometers and wind vanes at the 32-m level. Table 18 gives the monthly

TABLE 18. MONTHLY MEAN WIND SPEEDS AND CORRELATION BETWEEN MESSER[a]-MESSER[b], MESSER[b]-TRUAX AND WYOCENA-TRUAX FOR 1976 AND 1977. THE MEAN AND CORRELATIONS BETWEEN SITES ARE CALCULATED USING VALID DATA AT EACH SITE FOR THE SAME TIMES. WYOCENA RECORDING STOPPED 1 OCTOBER 1977. WIND SPEED UNIT IS M/SEC

	Sites								
	Messer-Messer			Messer-Truax			Wyocena-Truax		
Month	32[a]	34[b]	Correlation	34[b]	28[c]	Correlation	43[b]	28[c]	Correlation
				1976					
Jan.	7.6	7.8	0.85	7.9	4.9	0.68			
Feb.	7.6	7.2	0.83	7.6	4.4	0.58	4.1	4.5	0.74
Mar.	10.3	9.1	0.96	8.0	5.6	0.76	5.2	5.5	0.82
Apr.	6.3	6.4	0.92	6.8	4.4	0.65	3.7	4.4	0.63
May	5.3	5.5	0.86	5.6	4.0	0.62	3.5	4.0	0.79
June	5.9	6.3	0.90	6.3	4.1	0.59	3.5	4.1	0.81
July	5.3	5.5	0.95	5.3	3.8	0.52	2.8	3.8	0.75
Aug.	5.8	5.3	0.89	6.1	3.5	0.29	2.4	3.6	0.73
Sept.	5.9	5.7	0.57	6.0	3.6	0.50	3.1	3.6	0.81
Oct.	7.0	6.4	0.84	6.3	4.0	0.68	3.1	4.0	0.85
Nov.	8.1	7.7	0.87	7.7	4.8	0.53	4.5	4.9	0.41
Dec.	9.3	8.8	0.97	7.7	4.5	0.63	4.3	4.5	0.82
Average	7.03	6.81		6.77	4.30		3.69	4.26	
				1977					
Jan.	9.5	8.9	0.98	8.0	4.7	0.69	4.0	4.7	0.84
Feb.	8.9	8.1	0.89	8.0	4.7	0.62	4.0	4.5	0.85
Mar.	7.7	6.9	0.94	7.3	4.8	0.70	4.4	4.8	0.84
Apr.	8.3	7.2	0.98	7.9	4.7	0.59	4.1	4.7	0.78
May	6.4	5.7	0.95	5.7	3.9	0.43	3.1	3.8	0.73
June	6.9	5.9	0.97	5.6	4.0	0.55	3.3	4.0	0.74
July	7.1	5.9	0.96	5.7	3.9	0.42	3.3	3.9	0.66
Aug.	5.3	4.8	0.94	5.7	3.5	0.56	2.8	3.3	0.77
Sept.	7.1	5.9	0.96	6.7	3.8	0.49	3.2	3.9	0.79
Oct.	7.9	6.7	0.95	8.3	4.6	0.54			
Nov.	7.7	7.2	0.98	7.7	5.1	0.76			
Dec.	8.1	7.7	0.97	7.7	4.8	0.64			
Average	7.58	6.74		7.03	4.13		3.24	4.20	

[a] Instantaneous anemometer averaged visually for 1 hr.

[b] Contact anemometer totaled for 1 hr.

[c] Three-minute average every 3 hr.

correlation between the two wind speeds and the mean values for 1976 and 1977. The correlation is usually >0.90, with 1977 showing a better correlation than 1976, although the mean values differed more in 1977.

The Messer-Truax comparison shows differences in mean value. This is expected because the local height of the Truax Field anemometer is 6.3 m, while the Messer anemometer is at 32 m. The correlation coefficient is never more than 0.76 for the 2 yr, with a low value of 0.29 in August 1976. The Wyocena anemometer at 10 m is comparable in location to the anemometer at Truax Field. Surface roughness could account for the difference in mean wind speed between Wyocena and Truax Field. At Wyocena surface roughness--attributed to rough grass--was between 7 and 10 cm, while at Truax Field values are about 2 cm for rough-cut grass. The correlation coefficient ranges from 0.85 to 0.41, which is a better correlation than that between the Messer site and Truax Field.

Table 19 gives wind direction mean values, differences and correlations between several instrument locations. The two wind vanes at the Messer site correlated well (the lowest correlation was 0.88) and were higher than the wind speed correlations for the same site. The consistent difference in the mean values of the two wind vanes after September 1976 indicates an orientation error. The advantage of the two wind vanes should provide the most reliable value.

Messer-Truax Field shows a high correlation coefficient and small differences in mean value. The Truax Field data is recorded only to the nearest 10°. The Wyocena-Truax Field show a similar high correlation but after July 1976 the orientation of the Wyocena wind vane appears to be in error.

Correlation coefficients were calculated as a function of hour of day between the Messer Site and Truax Field. As can be seen in Table 20 the wind direction correlation was uniform with the time of day, but wind speed was not. The wind speed correlation is about 0.8 at 1500 CST dropping to 0.4 at 0000 CST. It is concluded that the Truax Field wind speed data would be valid from 0900 CST to 1800 CST but not at other times of the day. The times 1800 to 0900 CST are times when inversion is usually present and the wind speed increases more strongly with height.

The above has implications for generation of electrical power from wind. Figure 57 shows annual average wind speed at the two sites as a function of hour of day. The Truax Field data shows the expected decrease of the wind speed at night. The Messer site wind speed slightly decreases near sunrise and sunset, but the day-night variation is small. The exatrapolation of Truax Field data to 32 m using the power law underestimates the observed values at the Messer site, except at 1200 and 1500. This same effect is observed at Washington Island and Edgewater, Wisconsin (Stearns and Kuffell 1981) where the lower anemometer is at the same site as the one or more higher anemometers. This has serious implications for wind energy. The extrapolation of Truax Field wind speeds to 32 m using the 1/7 power law would have underestimated the actual

TABLE 19. MONTHLY MEAN WIND DIRECTIONS AND CORRELATION BETWEEN MESSER^{a}-MESSER^{b}, MESSER^{b}-TRUAX AND WYOCENA-TRUAX FOR 1976 AND 1977. THE MEAN AND CORRELATIONS BETWEEN SITES ARE CALCULATED USING VALID DATA AT EACH SITE FOR THE SAME TIMES. WYOCENA RECORDING STOPPED 1 OCTOBER 1977. WIND DIRECTION UNITS ARE DEGREES FROM NORTH

	Sites								
	Messer-Messer			Messer-Truax			Wyocena-Truax		
Month	31^{a}	33^{a}	Correlation	31^{a}	28^{b}	Correlation	41^{a}	28^{b}	Correlation
				1976					
Jan.	231	233	0.99	239	253	0.91			
Feb.	240	242	0.92	179	180	0.89	255	243	0.91
Mar.	—	—	—	206	197	0.93	239	225	0.91
Apr.	176	179	0.97	179	180	0.92	214	182	0.92
May	181	177	0.97	182	182	0.94	191	184	0.94
June	182	185	0.96	199	204	0.86	198	201	0.89
July	204	209	0.96	223	224	0.84	210	214	0.83
Aug.	185	174	0.94	201	195	0.84	179	209	0.86
Sept.	208	194	0.97	223	221	0.91	197	221	0.87
Oct.	241	221	0.96	247	247	0.92	224	256	0.91
Nov.	264	244	0.96	259	264	0.91	237	267	0.85
Dec.	249	250	0.94	250	255	0.88	230	259	0.88
				1977					
Jan.	256	240	0.77	253	261	0.78	238	268	0.83
Feb.	252	234	0.91	244	246	0.88	233	250	0.86
Mar.	195	176	0.88	189	207	0.92	184	203	0.94
Apr.	187	175	0.96	184	191	0.90	198	187	0.91
May	173	156	0.95	169	177	0.81	159	174	0.86
June	217	194	0.97	210	223	0.88	206	215	0.89
July	214	193	0.93	211	209	0.90	197	213	0.90
Aug.	220	205	0.88	226	223	0.82	207	222	0.81
Sept.	209	186	0.97	203	192	0.89	175	197	0.86
Oct.	221	199	0.99	217	216	0.93			
Nov.	217	198	0.98	200	212	0.93			
Dec.	213	202	0.97	205	231	0.94			

[a] Visually averaged for 1 hr.

[b] Three-minute average every hr.

TABLE 20. MONTHLY MEAN WIND SPEEDS AND DIRECTION CORRELATIONS BETWEEN THE MESSER SITE AND TRUAX FIELD AS A FUNCTION OF TIME OF DAY FOR 1976 AND 1977

	Wind speed correlation for hour								Wind direction correlation for hour							
Month	00	03	06	09	12	15	18	21	00	03	06	09	12	15	18	21
1976																
Jan.	0.67	0.72	0.55	0.60	0.77	0.71	0.72	0.75	0.87	0.93	0.90	0.86	0.85	0.91	0.86	0.85
Feb.	0.59	0.48	0.69	0.76	0.65	0.68	0.51	0.43	0.78	0.85	0.67	0.91	0.91	0.91	0.90	0.85
Mar.	0.81	0.60	0.71	0.75	0.75	0.78	0.86	0.82	0.83	0.86	0.91	0.91	0.88	0.81	0.92	0.70
Apr.	0.73	0.49	0.68	0.71	0.72	0.65	0.76	0.72	0.88	0.91	0.87	0.92	0.87	0.94	0.93	0.90
May	0.59	0.50	0.57	0.74	0.76	0.82	0.77	0.55	0.87	0.87	0.92	0.95	0.93	0.92	0.91	0.88
June	0.42	0.35	0.37	0.66	0.75	0.88	0.80	0.73	0.76	0.76	0.89	0.88	0.85	0.88	0.90	0.83
July	0.51	0.51	0.59	0.79	0.71	0.84	0.52	0.66	0.82	0.82	0.83	0.86	0.82	0.75	0.82	0.85
Aug.	0.30	0.23	0.39	0.62	0.61	0.58	0.51	0.36	0.71	0.78	0.81	0.85	0.86	0.82	0.88	0.86
Sept.	0.44	0.49	0.42	0.65	0.72	0.81	0.68	0.40	0.82	0.85	0.76	0.94	0.92	0.90	0.92	0.90
Oct.	0.45	0.51	0.53	0.84	0.85	0.83	0.81	0.73	0.86	0.85	0.80	0.95	0.91	0.88	0.91	0.92
Nov.	0.55	0.65	0.48	0.66	0.67	0.73	0.46	0.62	0.79	0.68	0.69	0.87	0.94	0.93	0.84	0.86
Dec.	0.71	0.62	0.66	0.75	0.68	0.79	0.64	0.54	0.89	0.90	0.84	0.91	0.82	0.91	0.90	0.79
1977																
Jan.	0.61	0.70	0.66	0.79	0.86	0.85	0.64	0.63	0.86	0.64	0.72	0.65	0.81	0.80	0.81	0.76
Feb.	0.46	0.53	0.66	0.83	0.77	0.76	0.75	0.39	0.84	0.92	0.78	0.80	0.87	0.80	0.94	0.84
Mar.	0.62	0.40	0.54	0.70	0.84	0.78	0.81	0.64	0.89	0.88	0.88	0.92	0.85	0.94	0.91	0.90
Apr.	0.47	0.54	0.46	0.81	0.86	0.78	0.80	0.42	0.90	0.91	0.87	0.89	0.84	0.83	0.88	0.79
May	0.08	0.11	0.16	0.82	0.82	0.73	0.76	0.37	0.77	0.79	0.67	0.86	0.87	0.77	0.81	0.83
June	0.34	0.54	0.47	0.82	0.75	0.87	0.60	0.42	0.80	0.82	0.77	0.88	0.90	0.91	0.86	0.90
July	0.46	0.63	0.47	0.52	0.53	0.49	0.43	0.12	0.88	0.87	0.79	0.93	0.90	0.88	0.87	0.86
Aug.	0.64	0.66	0.50	0.58	0.77	0.75	0.79	0.70	0.79	0.90	0.83	0.92	0.79	0.78	0.71	0.80
Sept.	0.34	0.49	0.31	0.69	0.79	0.80	0.63	0.54	0.77	0.89	0.90	0.93	0.94	0.90	0.84	0.81
Oct.	0.46	0.31	0.27	0.55	0.75	0.87	0.71	0.74	0.86	0.90	0.92	0.96	0.93	0.92	0.88	0.88
Nov.	0.70	0.76	0.64	0.75	0.85	0.83	0.73	0.83	0.94	0.88	0.85	0.94	0.92	0.92	0.85	0.93
Dec.	0.43	0.71	0.68	0.48	0.80	0.71	0.70	0.45	0.90	0.93	0.85	0.89	0.88	0.93	0.90	0.93

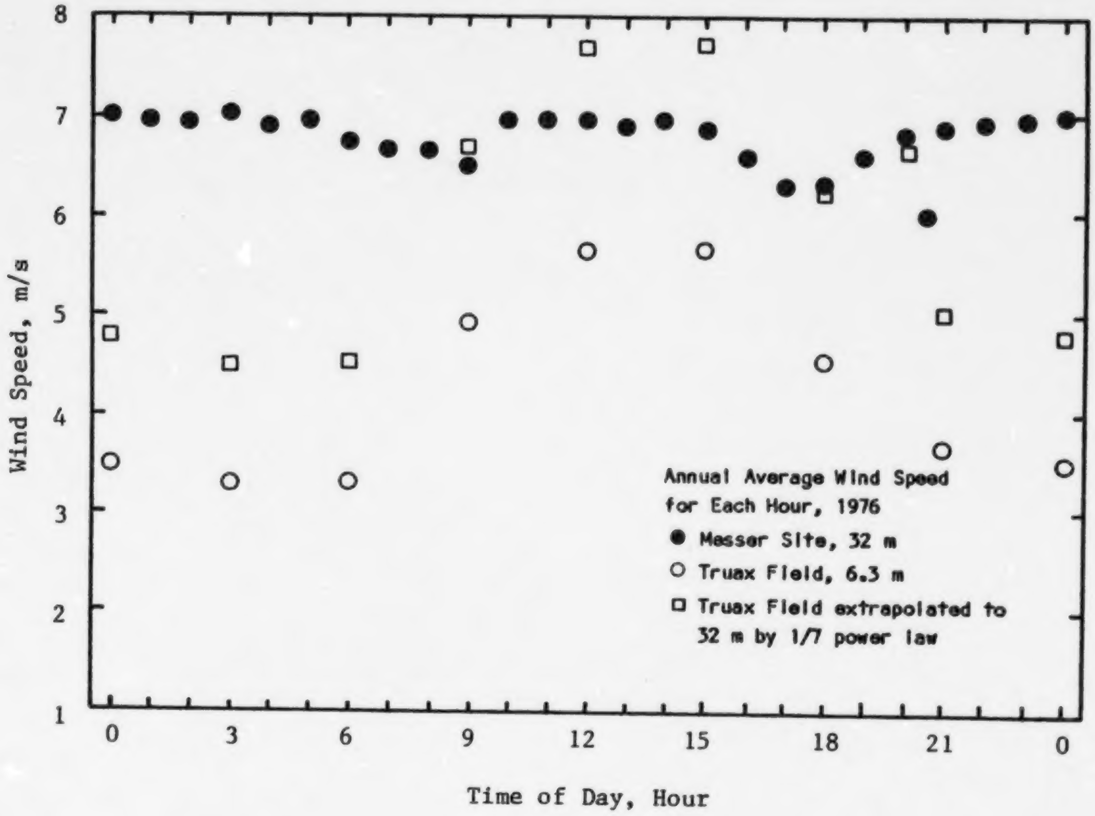

Figure 57. Average annual wind speed as a function of time of day for Messer site and Truax Field for 1976. The anemometer heights are 32 m at Messer and 6.3 m at Truax. The Truax Field data is also extrapolated to 32 m using the relationship $v(32\text{ m})/V(6.3\text{m}) = (32\text{ m}/6.3\text{ m})^{1/7}$ which is the power law relationship commonly used to extrapolate a low level wind speed to greater height.

available wind energy at 32 m by 33%. This difference may be sufficient to determine the economic feasibility of using wind energy.

The correlation between two wind speed systems at one location as performed at the Messer site leaves a great deal to be desired. The two systems were different and the data reduction method was different but even so better agreement was expected. Sites such as Wyocena, Dekorra and Cemetery also had two anemometers which were of the same type. Occasional checks showed that the two separate systems were in agreement within one cosent on the contact anemometer for 1 hr so only one anemometer was actually processed. Thus, correlations between two similar anemometers were not made but should not be expected to give a correlation of 1.0 since at 5 m/sec one contact difference is a speed difference of 0.31 m/sec or about 6%.

The use of two anemometers at one site increases the amount of data collected and the average of the two gives the most nearly correct value for wind speed. If two anemometers had not been installed the relatively low correlation would not have been discovered. The best methodology is to install two rather than one anemometer and wind vane at each location where measurements are made.

The monthly average wind speed for the two anemometers at the Messer site was in reasonable agreement during the first 9 months of 1976. It then shifted in October 1976, from a 3% difference, to an 11% difference because of a change in the electronics in September 1976.

REFERENCES

Alley, F. C., and L. A. Ripperton. 1961. The effect of temperature on photochemical oxidant production in a bench scale reaction system. J. Air Pollut. Control Assoc. 11(19):581-584.

Allwine, K. J., and K. J. Westberg. 1977. Potential impact of coal-fired power plants on ground level ozone concentrations in Wisconsin. Report to the Wisconsin Public Service Commission. Wisconsin Public Service Commission, Madison, Wisconsin.

Angell, J. K., D. H. Pack, L. Machta, C. R. Dickson, and W. H. Hoecker. 1972. Three dimensional air trajectories determined from tetroom flights in the planetary boundary layer of the Los Angles Basin. J. Appl. Meteorol. 11:451-471.

Anderson, G.E. 1972. Mesoscale influences on wind fields. J. Appl. Meteorol. 10:377-386.

Andrews, C., and M. Anderson. 1976. Hydrogeology. Documentation of environmental change related to the Columbia Electric Generating Station. Tenth Semiannual Report, Fall-Winter 1976. Institute for Environmental Studies, University of Wisconsin, Madison, Wisconsin. pp. 83-109.

Andrews, C., and M. Anderson. 1980. Impacts of coal-fired power plants on local ground water systems. EPA-600/3-80-079. U.S. Environmental Protection Agency, Duluth, Minnesota. 202 p.

Beals, G. A. 1971. Guide to local diffusion of air pollutants. Air-Weather Service Tech. Report 214. Air-Weather Service, U.S. Air Force, Washington, D.C.

Bellamy, J. C. 1949. Objective calculations of divergence, vertical velocity, and vorticity. Bull. Am. Meteorol. Soc. 30: 45-49.

Bennett, G. T. 1955. Calculation of the dilation of area from simultaneous wind records at three neighboring stations. In: Selected Meteorological Papers of Sir Napier-Shaw. MacDonald, London. pp. 130-131.

Bowie, E., and R. Weightman. 1914. Types of storms of the United States and their average movements. Monthly Weather Review Supplement No. 1. U.S. National Weather Service, Washington, D.C. p. 147.

Briggs, G. A. 1971. Plume rise: A recent critical review. Nucl. Safety 2(1):15-24.

Briggs, G. A. 1972. Chimney plumes in neutral and stable surroundings. Atmos. Environ. 6:507-510.

Briggs, G. 1969. Plume rise. A.E.C. Critical Review Series. Air Resources Atmospheric Turbulence and Diffusion Laboratory, Oak Ridge, Tennessee.

Bufalini, J. J., and A. P. Altshuller. 1963. The effect of temperature on photochemical smog reactions. Int. J. Air Water Pollut. 7(8):769-771.

Coffey, P. E., and W. N. Stasiuk. 1975. Evidence of atmospheric transport of ozone into urban areas. Environ. Sci. Technol. 9:59-62.

Cramer, H. E. 1957. A practical method for estimating the dispersal of atmospheric contaminants. Proceedings of the First National Conference on Applied Meteorology. American Meteorological Society, Hartford, Connecticut. pp. C-33-C-55.

Csanady, G. T. 1973. Turbulent diffusion in the environment. D. Reidel Publishing Co., Boston, Massachusetts.

Dahlquist, G., and A. Bjork. 1974. Numerical methods. Prentice-Hall, New Jersey. 573 p.

Dames and Moore. 1976. Dames and Moore quarterly reports I-IV. 1976. Air quality and monitoring program, Columbia Generating Station. Dames and Moore, Chicago, Illinois.

Davis, D. D., G. Smith, and G. Klauber. 1974. Trace gas analysis of power plant plumes via aircraft measurement: O_3, NO_x, and SO_2 chemistry. Science 186:733-736.

Everett, R. G., and G. A. Zerbe. Winter field program at the Dresden cooling pond. Argonne National Laboratory radiological and environmental research division annual report. ANL-76-88. Argonne National Laboratory, Argonne, Illinois.

Falconer, P. D. 1973. A pilot diffusion climatology survey for a power generating site near Portage, Wisconsin. M.S. Thesis, Department of Meteorology, University of Wisconsin, Madison, Wisconsin.

Fankhauser, R. K. 1976. Ozone levels in the vicinity of 33 cities. J. Air Pollut. Control Assoc. 26(8):771-777.

Flohn, H., and P. Hess. 1952. Singularities of large-scale synoptic patterns over the course of the year in the trend of weather conditions for central Europe. Meteorol. Rundschau. Air-Weather Service Technical Report. Air-Weather Service, U.S. Air Force, Washington, D.C.

Frederick, G. L. 1969. Estimates of vorticity, divergence, and vertical velocity in a surface layer. M.S. Thesis, University of Wisconsin, Madison, Wisconsin. 65 p.

Friedlander, S. K., and J. H. Seinfeld. 1969. A dynamic model for photochemical smog. Environ. Sci. Technol. 3:1175.

Galbally, I. 1969. An evaluation of the Ehmert technique for measuring ozone profiles in the atmospheric surface layer. J. Geophys. Res. 74(28):6869-6872.

Galbally, I. 1968. Some measurements of ozone variation and destruction in the atmospheric surface layer. Nature 218:456-457.

Geiger, R. 1966. The climate near the ground. Harvard University Press, Cambridge, Massachusetts.

Gold, E. 1920. Aids to forecasting: Types of pressure distribution with notes and tables for the 14 years, 1905-1918. Geophys. Memoirs 2:149-174.

Goodell, B. D. 1977. A validation study of the Gaussian Plume Model as applied to an elevated point source. M.S. Thesis, Department of Mechanical Engineering, University of Wisconsin, Madison, Wisconsin.

Heffter, J. L., and A. D. Taylor. 1975. A regional-continental scale transport, diffusion, and deposition model. Technical Memorandum ERL ARL-50. Environmental Research Laboratories, National Oceanic and Atmospheric Administration, Washington, D.C.

Hennen, E. 1965. Personal Communication.

Hicks, B. B. 1974. Cooling pond studies at Dresden: An introduction. ANL-8060, Part IV. Argonne National Laboratory Radiological and Environmental Research Division Annual Report. Argonne National Laboratory, Argonne, Illinois. pp. 1-3.

Hicks, B. B., and J. D. Shannon. 1976. A new cooling pond index. Argonne National Laboratory Radiological and Environmental Resaerch Division Annual Report. ANL-76-88, Part IV. Argonne National Laboratory, Argonne, Illinois. pp. 19-28.

Hicks, B. B., and M. L. Wesely. 1974. Some errors that can result from the use of industrial techniques for assessing the thermal performance at cooling ponds. ANL-8060 Part IV. Argonne National Laboratory Radiological and Environmental Research Division Annual Report. Argonne National Laboratory, Argonne, Illinois. pp. 19-28.

Hicks, B. B., M. L. Wesely, and R. Hart. 1973. Field studies at the Dresden cooling pond: An introduction. ANL-8060 Part IV. Argonne National Laboratory Radiological and Environmental Research Division Annual Report. Argonne National Laboratory, Argonne, Illinois. pp. 1-7.

Hicks, B. B., M. L. Wesely, and C. M. Sheih. 1974. Eddy correlation measurements over a pond with limited fetch. ANL-8060 Part IV. Argonne National Laboratory Radiological and Environmental Reserach Division Annual Report. Argonne National Laboratory, Argonne, Illinois. p. 4-18.

Hino-Mikio. 1968. Maximum ground level concentration and sampling time. Atmos. Environ. 2:149-165.

Junge, C. E. 1963. Air chemistry and radioactivity. In: J. Mieghem (ed.). International Geophysics Series, Volume 4. Academic Press, New York. 382 p.

Kauper, E. K. 1960. The ozone of discontinuity between land and sea breezes and its importance to southern California air pollution studies. Bull. Am. Meteorol. Soc. 41:410-422.

Kroening, J. L., and E. P. Ney. 1962. Atmospheric ozone. J. Geophys. Res. 67(5):1867-1875.

Leighton, P. A. 1961. Photochemistry of air pollution. Academic Press, New York. 300 p.

Lettau, H. H. 1959. Wind profile, surface stress and geostrophic drag coefficients. Adv. Geophys. 6:241-256.

Lettau, H. H. 1962. Theoretical wind spirals in the boundary layer of a barotropic atmosphere. Beitr. Phys. Atmos. 35:195-212.

Lettau, H. H. 1969. Note on aerodynamic roughness-parameter estimation on the basis of roughness-element description. J. Appl. Meteorol. 8: 831.

Lund, I. 1963. Map-pattern classification by statistical methods. J. Appl. Meteorol. 2:56-65.

Lyons, W. A. 1973. Fumigation and plume trapping on the shores of Lake Michigan during stable onshore flow. J. Appl. Meteorol. 12:494-510.

Meteorology Research, Inc. 1975. The chemistry dispersion and transport of air pollutants emitted from fossil fuel power plants in California - airborne pollutant measurement and analysis. MRI 75 FR-1382, Technical Report. Meteorology Research, Inc., Altadena, California.

Miller, M. E. 1967. Forecasting afternoon mixing depths and transport wind speeds. Monthly Weather Review 95:35-43.

Miller, P. K., M. H. McCutchan, and H. D. Milligan. 1972. Oxidant air pollution in the Central Valley, Sierra Nevada Foothills, and Mineral King Valley of California. Atmos. Environ. 6:623-633.

Munn, R. E. 1964. Turbulence statistics at Douglas Point. J. Appl. Meteorol. 3:771-779.

National Air Pollution Control Administration. 1970. Air quality criteria for photochemical oxidants. Publication Number AP-63. National Air Pollution Control Administration, Washington, D.C. 178 p.

National Oceanic and Atmospheric Administration. 1976. U.S. standard atmosphere--1976. Department of Commerce, National Oceanic and Atmospheric Administration, U.S. Government Printing Office, Washington, D.C.

Pack, D. H. 1962. Air trajectories and turbulence statistics from weather radar using tetroons and radar transponders. Monthly Weather Review 91:583-604.

Panofsky, H. A., and B. Prasad. 1967. The effect of meteorological factors on air pollution in a narrow valley. J. Appl. Meteorol. 6:493-499.

Pasquill, F. 1974. Atmospheric diffusion. Ellis Harwood Limited, Chichester, England.

Perkins, H. C. 1974. Air pollution. McGraw-Hill, Inc., New York. 407 p.

Petterssen, S. 1956. Weather analysis and forecasting, Volume 1. McGraw-Hill, New York. pp. 32-43.

Pitts, J. N., Jr., J. H. Sharp, and S. I. Chan. 1964. Effects of wavelength and temperature on primary processes in the photolysis of nitrogen dioxide and a spectroscopic-photochemical determination of the dissassociation energy. J. Chem. Phys. 40(12):3655-3662.

Poulter, R.M. 1949. Correspondence. Bull. Am. Meteorol. 30:297.

Ragland, K. W., B. D. Goodell, and T. L. Coughlin. 1980. Air pollution studies near a coal-fired power plant. EPA-600/3-80-048. U.S. Environmental Protection Agency, Duluth, Minnesota.

Research Triangle Institute. 1973. Investigation of high ozone concentration in the vicinity of Garrett County, Maryland and Preston County, West Virginia. NTIS PB-218 540-3BE. Research Triangle Institute, Research Triangle Park, Maryland. 103 p.

Ripperton, L. A., H. Jeffries, and J. J. B. Worth. 1971. Natural synthesis of ozone in the troposphere. Environ. Sci. Technol. 5:246.

Samson, P. J., and K. W. Ragland. 1977. Ozone and visibility reduction in the Midwest: The evidence for large-scale transport. J. Appl. Meteorol. 16(10):1101-1106.

Sandberg, J. S., and R. H. Thuiller. 1970. Oxidant levels over San Francisco Bay and adjacent land stations. J. Air Pollut. Control Assoc. 20(9):599-602.

Schmidt, F. B. 1965. The role of wind shear in horizontal diffusion of ambient particles. Q. J. R. Meteorol. Soc. 91:318-329.

Schuck, E. A., and E. R. Stephens. 1969. Oxides of nitrogen. Adv. Environ. Sci. 1:73-118.

Sellers, W. D. 1965. Physical climatology. University of Chicago Press, Chicago, Illinois. 272 pp.

Shaw, N. 1972. Acoustic sounding of the atmosphere. Ph.D. Thesis, Department of Physics, University of Melbourne, Australia.

Singer, I. A. 1967. Steadiness of the wind. J. Appl. Meteorol. 6:1033-1038.

Singer, I. A., and M. E. Smith. 1953. Relation of gustiness to other meteorological parameters. J. Meteorol. 10:121-126.

Slade, D. H. (ed.). 1968. Meteorology and atomic energy. Atomic Energy Commission, Air Resources Laboratory, Oak Ridge, Tennessee.

Smith, M. E. 1951. The forecasting of micrometeorological variables. Meteorol. Monogr. 4:50-55.

Stasiuk, W. N., and P. E. Coffey. 1974. Rural and urban ozone relationships in New York State. J. Air Pollut. Control Assoc. 24(6):564-568.

Stearns, C. R. 1978. A method for estimating available solar energy for dwelling heat. Department of Meteorology, University of Wisconsin, Madison, Wisconsin.

Stearns, C. R. 1967. Micrometeorological studies in the coastal desert of southern Peru. Ph.D. Thesis, University of Wisconsin, Madison, Wisconsin.

Stearns, C. R. and L. Kuffell. 1981. Height variation in diurnal wind patterns. Proceedings of the Wind Energy Technology Conference, Engineering Extension, University of Missouri-Columbia, Kansas City, Missouri.

Stephens, E. R. 1969. Chemistry of atmospheric oxidants. J. Air Pollut. Control Assoc. 19(3):181-185.

Stephens, E. R. 1968. The marine layer and its relation to a smog episode in Riverside, California. Atmos. Environ. 2(4):393-396.

Suomi, V. E., M. Fransilla, and N. F. Islitzer. 1954. An economical net radiometer. J. Meteorol. 11:276-282.

Sutton, O. G. 1953. Micrometeorology. McGraw-Hill Book Company, Inc., New York.

Sutton, O. G. 1932. A theory of eddy diffusion in the atmosphere. Proc. R. Soc. (London), Series A, 135:143-165.

U.S. Environmental Protection Agency. 1977. Turbulent classification schemes for stable and unstable conditions. Environmental Research Laboratories, U.S. Environmental Protection Agency, Cincinatti, Ohio.

U.S. Nuclear Regulatory Commission. 1972. On site meteorological programs. Nuclear Regulatory Guide 1.23. U.S. Nuclear Regulatory Commission, Washington, D.C. 6 p.

U.S. Standard Atmosphere. 1976. ESSA, NASA, and U.S. Air Force, U.S. Government Printing Office, Washington, D.C.

Van Dop, H., R. Guicherit, and R. W. Lanting. 1977. Some measurements of the vertical distribution of ozone in the atmosphere boundary layer. Atmos. Environ. 11:65-71.

Weidner, G. 1976. Topographical influence on surface winds near Portage, Wisconsin. M.S. Thesis, University of Wisconsin, Madison, Wisconsin.

Wendell, L. L. 1972. Mesoscale wind fields and transport estimates determined from a network of wind towers. Monthly Weather Rev. 100:565-578.

Williamson, S. J. 1973. Fundamentals of air pollution. Addison-Wesley Publ. Co., Reading, Massachusetts. 472 p.

Wisconsin Department of Natural Resources. 1974. A report to the board concerning high oxidant levels in Wisconsin, summer, 1973. Unpublished report. Wisconsin Department of Natural Reosurces, Madison, Wisconsin.

Wisconsin Department of Natural Resources. 1974-1976. Aerial monitoring data. Wisconsin Department of Natural Resources, Madison, Wisconsin.

Wisconsin Power and Light Co. Undated. Wisconsin Power and Light Stack Test Results. Internal Report of Wisconsin Power and Light Co., Wisconsin Power and Light Co., Madison, Wisconsin.

Wolff, G. T., P. J. Lioy, G. D. Wright, R. E. Meyers, and R. T. Cederwall. 1977. An investigation of long-range transport of ozone across the midwestern and eastern United States. Atmos. Environ. 11:797-802.

Yamada, T. 1978. Three-dimensional second-order closure numerical model of mesoscale circulation in the lower atmosphere. Argonne National Laboratory Radiological and Environmental Research Division Report. ANL/RER-78-1. Argonne National Laboratory, Argonne, Illinois. 67 pp.